ASH DEPOSITION AND ASH AEROSOL FORMATION MECHANISMS DURING OXY-COAL COMBUSTION

by

Zhonghua Zhan

A dissertation submitted to the faculty of
The University of Utah
in partial fulfillment of the requirements for the degree of

Doctor of Philosophy

Department of Chemical Engineering

The University of Utah

August 2015

The University of Utah Graduate School

STATEMENT OF DISSERTATION APPROVAL

The dissertation of **Zhonghua Zhan**

has been approved by the following supervisory committee members:

Jost O.L. Wendt	, Chair	**4/14/2015** Date Approved
Andrew R. Fry	, Member	**3/25/2015** Date Approved
Eric G. Eddings	, Member	**3/25/2015** Date Approved
Kevin J. Whitty	, Member	**3/25/2015** Date Approved
Lawrence E. Bool	, Member	**3/25/2015** Date Approved

and by **Milind Deo** , Chair of the Department of **Chemical Engineering**

and by David B. Kieda, Dean of The Graduate School.

ABSTRACT

Oxy-coal combustion has been considered a promising technology for CO_2 capture for existing coal-fired power plants. This work is concerned with the effects of retrofit on both the fly ash and the deposits. The research targets include: 1) To find out the difference between ash aerosol and ash deposit formation between oxy-coal combustion and air combustion. 2) To ascertain the relationships between deposits composition and size segregated ash aerosol composition. 3) To find out ash aerosol and ash deposit formation characteristics during oxy-coal combustion under various recycled flue gas (RFG) cleanup options and various RFG amounts. 4) To build up a model to predict ash deposition rate on a vertical surface.

Ash aerosol and ash deposits formation during oxy-coal combustion were explored through experiments in a self-sustained 100 kW rated down-fired oxy-fuel combustor, firing a Powder River Basin coal. The results showed that it was necessary to treat the deposits separately (inside, outside, vertical and side) other than in bulk, because the deposits from different locations of the probe showed different characteristics in both composition and particle size distribution. Deposits from the vertical and side surfaces were more similar to the inside deposits than to the bulk deposits. The main formation mechanism for vertical (inside) deposits was transportation of the vaporization mode ash aerosols through thermophoresis. Cases of oxy-coal combustion under various RFG cleanup options and various RFG amounts were also conducted to identify ash aerosols

and ash deposit formation characteristics. The results showed that the extent of RFG cleanup options had little effect on the ash aerosol compositions or size distributions. However, OXY50 cases produced more vaporization mode particles due to higher combustion temperature. Finally, a model was built up to predict ash deposition rate on a vertical surface within a laminar flow field. A dimensionless number, Thermophoresis number (Tp), was defined, which was the ratio of travel time by thermophoresis force and travel time by drag force. The criterion that a particle would be captured onto the vertical surface was $Tp < 1$. The predicted ash deposition rates showed high consistence with the experimental data.

To my wife, Na Wu

TABLE OF CONTENTS

LIST OF TABLES

LIST OF ABBREVIATIONS

Δ	delta or change
°	degree
℃	degree Celsius
μ_g	gas dynamic viscosity
μm	micrometer
3D	three-dimensional
AIR	air combustion case
Al	aluminum
Al_2O_3	aluminum oxide
APS	aerodynamic particle sizer
bcm	billion cubic meter
BLPI	Berner low pressure impactor
BTU	British thermal unit
C	carbon
Ca	calcium
CaO	calcium oxide
CCSEM	computer-controlled scanning electron microscopy
CFD	computational fluid dynamics
Cl	chlorine
cm	centimeter
cm^3	cubic centimeter
CO	carbon monoxide
CO_2	carbon dioxide
Cz	caption zone

d1	perpendicular distance of the particle to probe surface
d2	tangential distance to the downstream edge of the surface
d_c	tube diameter
d_p	particle diameter
dr	deposition rate
DTF	drop tube furnace
EDS	energy dispersive x-ray spectrometer
EERC	energy & environmental research center
et al.	and others
etc.	and the rest
FC	fixed carbon
Fe	iron
Fe_2O_3	ferric oxide
FGR	flue gas recycle
Ft	thermophoresis force
g	gram
h	hour
H	hydrogen or height
H_2	hydrogen gas
H_2O	water or moisture
HCl	hydrogen chloride
HHV	higher heating value
HSC	chemical reaction & equilibrium software
ICP-MS	inductively coupled plasma mass spectrometry
I.D.	inside diameter
IGCC	integrated gasification combined cycles
K	potassium or kelvin
K1	a constant associated with thermophoresis velocity
K_2O	potassium oxide
kg	kilogram

kPa	kilopascal
kW	kilo-watt
L	liter or length
lb	pound
LOD	loss of drying
LOI	loss of ignition
m	meter
mg	milligram
Mg	magnesium
MgO	magnesium oxide
min	minute
mm	millimeter
Mn	manganese
MnO	manganese oxide
MSD	mass size distribution
Mt	million ton
N_2	nitrogen
Na	sodium
Na_2O	sodium oxide
Nm^3/h	normal cubic meter per hour
NO_x	nitrogen oxide
NSD	number size distribution
O	oxygen
O_2	oxygen gas
O.D.	outside diameter
OFC	oxy-fuel combustor
OXY27	oxy-fuel combustion with 27% inlet oxygen
OXY30	oxy-fuel combustion with 30% inlet oxygen
OXY32	oxy-fuel combustion with 32% inlet oxygen
OXY50	oxy-fuel combustion with 50% inlet oxygen

P	phosphorus
PM	particulate matter
PM0.5	particulate matter with diameter smaller than 0.5 μm
PM0.5-2.5	particulate matter with diameter between 0.5 μm and 2.5 μm
PM10	particulate matter with diameter smaller than 10 μm
P_2O_5	phosphorus oxide
ppb	parts per billion
ppm	parts per million
PRB	powder river basin
PSD	particle size distribution
$\dot{q}_{PM1}$	flux of submicron ash particles
R^2	coefficient of determination
Re	Reynolds number
RFG	recycled flue gas
s	second
S	sulphur or area of two-dimensional deposition region
SEM	scanning electron microscopy
Si	silicon
SiO_2	silicon oxide
SMPS	scanning mobility particle sizer
SO_2	sulphur dioxide
SO_3	sulfur trioxide
S_{OFC}	area of OFC cross section
S_{probe}	area of probe vertical surface
Stk	stokes number
t	time
T	temperature
T_{gas}	gas temperature
Th	thermophoresis number
Ti	titanium

TiO_2	titanium oxide
T_{probe}	probe temperature
u_p	particle velocity
U_∞	upstream velocity
V	volatile matter
vol.	volume
Vt	thermophoresis velocity
Vx	vertical velocity
Vy	horizontal velocity
W	watt
wt.	weight
x	distance in the direction of flow
XPS	x-ray photoelectron spectroscopy
y	distance within the boundary layer
z	distance in z-direction or z-coordinate
Zn	zinc
δ	boundary layer depth
ρ	gas density
ρ_p	particle density
η_c	capture efficiency of impacted particles
ψ	correction factor in Stokes number
κ_g	conductivity of gas
κ_p	conductivity of particle

ACKNOWLEDGEMENTS

This thesis is based upon work supported by the Department of Energy under Award Number DE-NT0005015 and State of Wyoming under the Clean Coal Research Program, administered by the University of Wyoming under Awards 1100-20268 and 1001030. Praxair, Inc. contributed all the O_2 and CO_2 supply. I appreciate their support.

I would like to express sincere gratitude to my advisor, Prof. Jost O.L. Wendt, for his help, guidance, support and impact. He is a knowledgeable, rigorous and gracious mentor for both academics and life. He has taught me how to do research, including the attitude of doing scientific research, how to address an issue concisely and precisely, how to think scientifically, and how to write. He has also shared with me his viewpoint of life. He and his words will definitely have a life-long influence on me.

I greatly appreciate Prof. Andrew Fry for his contribution of the ash deposition probe system and his patient instruction in OPTO22 programming. Prof. Eric Eddings, Prof. Kevin Whitty, and Dr. Lawrence Bool are also acknowledged for their helpful discussion and advice.

I want to thank Prof. Minghou Xu and Prof. Dunxi Yu at Huazhong University of Science and Technology for their generous contribution on CCSEM analysis. In addition, I want to thank Prof. Weidong Fan at Shanghai Jiao Tong University, Prof. Yanwei Zhang at Zhejiang University, Dr. Sida Tian at North China Electric Power University and Prof. Yuxin Wu at Tsinghua University, for their assistance in experiments and discussion.

I would also like to express my thanks to the technical staff, Mr. Ryan Okerlund, Mr. David Wagner, Mr. Dana Overacker and Mr. Brian Nelson, for their help in the lab. The undergraduate research assistants, Mr. Michael Newton, Mr. Travis Legrande, Mr. Taylor Geisler, Mr. James Allen, Mr. Mbonisi Sibanda, Mr. Chris Coulter, Mr. Geoffrey Bodily and Mr. Marc Backman, are also sincerely appreciated for their wonderful help in conducting experiments and solving problems.

I will not forget the help from Dr. Brian Van Devener, Dr. Ignacio Preciado, Mrs. Yunlu Jia and Mrs. Huiqian Luo for their assistance in sample analysis.

I would also like to thank all the faculty and staff in the Department of Chemical Engineering, as well as all of my friends. They made my research and life in Utah wonderful and unforgettable.

I would take this chance to thank my father, uncle, brother and sister, for their persistent love, support and encouragement. Special thanks and memory to my mother. It has been ten years this March since you left us. I miss you. I hope there is no pain but happiness there. Your son always loves you.

Great appreciation to my wife Na Wu, who donates all her love to me. I appreciate her support and encouragement to fulfill this thesis and my dream. I will love you and protect you forever.

CHAPTER 1

INTRODUCTION

1.1 Oxy-coal Combustion

1.1.1 Climate Change

Currently, signs of climate change are being felt through temperature changes, in sea level rise, precipitation changes and other extreme events. As described in a recently published research article in National Geographic [1], "a massive glacier system in West Antarctica has started collapsing because of global warming and will contribute to significant worldwide sea-level rise …. The glaciers contain enough ice to raise global sea level by 4 feet (1.2 meters) and are melting faster than most scientists had expected …. If the entire West Antarctic Ice Sheet did melt, sea level would rise 11 feet (3.3 meters) …." This story sounds very scary, but it does remind us that global warming is a serious issue we have to confront and solve. With long-term monitoring and observation, scientists have provided convincing evidence of global warming [2]. They find that the global average surface temperature has already increased 0.7 ℃, the global average sea level has risen by 180 mm, and the northern hemisphere snow cover has been decreasing. These events have been occurring since the industrial revolution about 150 years ago, reminding us that our home planet has been becoming warmer. To find out the inducements that have been leading to global warming, scientists find a positive correlation between global warming

and changes in the atmospheric composition. In the past 150 years, the concentrations of carbon dioxide, methane and nitrous oxide in the atmosphere have increased from 280 ppm to 380 ppm, 800 ppb to 1800 ppb and 270 ppb to 320 ppb, respectively. These greenhouse gases act as insulation for the earth.

Combustion of fossil fuels contributes about 90% of the total CO_2 emission, and about 42% of fossil fuels are combusted for electricity and heat generation [3]. Therefore, fossil fuel combustion related industry, especially electricity and heat generation industry, should be obligated to employ CO_2 emission control.

1.1.2 Role of Coal in World Energy Supply

Due to the population growth and social development, the world energy demand will continue to grow rapidly. That is, the total primary energy supply would grow by 1.4% on average per year from 2007 to 2050 according to the Baseline scenario [4]. Although nuclear and renewable energy grow strongly, the total demand of fossil fuels remains reasonably constant, with coal becoming the predominant fuel, accounting for 34% of total primary energy use by 2050, while oil demand should drop from 34% in 2007 to 25% in 2050. The reasons why coal turns out to be the single most important fuel in the future are because, first, high oil prices would increase coal use in the coal to oil and coal to synfuels industries; second, high gas prices would lead to building more coal fired power plants; third, the rapid growth of energy intensive industries in some developing countries requires more energy supply, especially countries that are rich in coal reserves and limited in other energy supplies, such as China and India [4].

By 2050, coal demand will be 138% higher than that in 2007. Coal plays an important role in electricity generation worldwide. Currently, about 41% of global electricity is

supplied by coal-fired power plants. In some countries, this percentage would be even higher, for example, coal in electricity generation accounts for 93% for South Africa, 87% for Poland, 79% for China, 78% for Australia, 75% for Kazakhstan, 68% for India, 58% for Israel, 51% for Czech Rep, 51% Morocco, 54% for Greece, 41% for Germany and 45% for the United States [3].

Most of the energy consumed in the United States comes from fossil fuels. Coal is its most sufficient natural source, as shown in Table 1.1. The proven coal reserves in the US account for about 30% of the world's proven reserves, and its coal could still be used for another 224 years based on the production rate in 2008, while that number is 12.4 and 11.6 years for crude oil and natural gas, respectively [4].

1.1.3 Oxy-coal Combustion Technology

In order to reduce the CO_2 emission from pulverized coal-fired power plants, several technologies are proposed for CO_2 capture. These are normally described as precombustion capture, postcombustion capture and oxy-fuel combustion capture [5].

Precombustion capture involves removing CO_2 prior to combustion to produce pure hydrogen. This technology consists of three stages: firstly, the carbon contained fuels are either gasified or reformed into syngas (CO, H_2); secondly, the CO is converted into CO_2 via shift conversion which is a reaction between CO and water; finally, the CO_2 is separated from the hydrogen which can then be combusted cleanly. The CO_2 can then be compressed into liquid and transported to a storage site. A typical example of this technology is the Integrated Gasification Combined Cycles (IGCC).

In postcombustion capture CO_2 is captured after combustion. This technology does not change the traditional combustion process. However, it requires CO_2 capture medium

(solvents [6], sorbents [7-8], or membranes [9]) to separate the CO_2 from the flue gases.

Oxy-fuel combustion capture uses pure oxygen and recycled flue gas (RFG) instead of air to react with fuel. Consequently, this technology can produce a flue gas with high CO_2 concentration, making it easier for the subsequent CO_2 capture and storage. Chemical looping combustion is another oxy-fuel combustion technology [10-12], but it is not the focus of this work.

Oxy-fuel combustion was first proposed to produce CO_2 for enhanced oil recovery. It is now driven by the need for CO_2 sequestration. Oxy-fuel combustion differs from air combustion both chemically and physically. Due to higher thermal capacity of CO_2 than that of N_2, the inlet O_2 fraction for oxy-coal combustion is typically about 32% to obtain a similar adiabatic flame temperature as air combustion. On the other hand, CO_2 and H_2O have higher gas emissivity than N_2, which requires lower inlet O_2 proportion, typically 27%, and then lower adiabatic flame temperature to match a similar heat flux as air combustion. In oxy-coal combustion, the density of the flue gas increases due to the molecular weight difference between CO_2 and N_2.

To predict boiler performance during conversion from air-firing to oxy-firing, numerous studies on the effects of oxy-firing on heat transfer, ignition, combustion, flame stability, ash and pollutants formation have been conducted, and have been well summarized in several reviews [5,13-17].

Ash formation is an important concern in coal combustion, due to subsequent formation of slagging deposition, fouling deposition and particulate matter emission [18]. Slagging is the deposition process for ash that sticks on the furnace walls and heat transfer surface within the radiation zone, while fouling deposition is the deposition process for ash that sticks on the steam tubes located in the convection zone. These ash deposition processes

(slagging and fouling) on heat transfer surfaces produce resistances in heat transfer, and cause corrosion and accidents. Particulate matter emissions consist of the fine ash escaping from the ash removal system, and consist of hazardous air pollutants. Therefore, knowledge of the ash formation during oxy-coal combustion is essential to help evaluate this technology prior to retrofitting from air to oxy-firing.

1.2 Ash Formation during Coal Combustion

1.2.1 Minerals in Coal

Coal is formed from dead plant matter, the dead plant matter is first converted into peat, which in turn is converted into lignite, then subbituminous coal, after that bituminous coal, and lastly anthracite. This involves biological and geological processes that take place over a long time period.

The inorganic minerals in coal include clay, sulfide, sulfate, silicon oxide, carbonate and so on, of which the relative and absolute amount varies remarkably with coal mines and ranks. Na, Mg, Al, Si, P, S, Cl, K, Ca, Ti, Mn, Fe and Zn are the primary elements of which these minerals are composed [18]. For pulverized coal, minerals can be classified into excluded mineral and included mineral, as shown in Figure 1.1. Excluded mineral is composed of those minerals that have little or no association with carbonaceous materials, which come from either the mullock among the coal seam or the floor and roof rock of the coal seam in the mining process, e.g., pyrites are often excluded. In contrast, the included mineral is well associated with coal matrix, comprising both finely dispersed minerals and organically bound elements, which were originally within the coal plant or formed during the coal formation process. The fraction of organically bound elements increases when the coal rank decreases (H/C and O/C ratios increase).

1.2.2 Ash Aerosol Formation Mechanisms

During the combustion process, the minerals in coal form ash aerosols through different formation mechanisms, as discussed in various reviews [19-22] and summarized in Figure 1.2.

Both the included and excluded minerals can be transferred to large size residual ash aerosol through the process of no fragmentation followed by melting and full coalescence or solidification. They can also be transferred to medium size residual ash aerosol through the process of fragmentation followed by melting and partial coalescence or solidification. Coalescence [23-27] normally occurs between the included minerals within a single coal particle under high temperatures, during which the process is greatly affected by temperature, coal fragmentation, coal particle size, mineral fraction and mineral diameter [28]. Higher temperature would melt minerals and increase the chance of coalescence [29-30]. However, coal particle and excluded mineral fragmentation [31-32] would reduce the effects of mineral coalescence. Coal particle fragmentation is controlled by char macroporosity [32], environmental pressure [33-37], coal rank, coal particle size, mineral properties and combustion conditions, while the excluded mineral fragmentation is decided by thermal shock and gas evolution [18,38-41]. As a result of mineral coalescence, the average particle size of the coal ash after combustion is normally larger than the original coal minerals, although this trend is diminished and limited by coal and mineral particle fragmentation [38].

For the small size ash aerosol fraction, the widely recognized formation mechanism is vaporization, followed by different possible condensation processes, such as homogeneous nucleation, coagulation, agglomeration, heterogeneous condensation and chemical reaction [42-48]. During the combustion process of pulverized coal, a certain amount of minerals

will vaporize into gas phases, in which the process is affected by a number of parameters such as temperature, inherent volatility, coal type, coal particle size and combustion atmosphere. Combustion temperature is the dominant factor during mineral vaporization process. Higher temperature would greatly increase mineral vaporization. Some of the mineral elements in coal are highly evaporable, such as Na, K, S, while some of them have low volatility, such as Si, Al, Fe, Ca and Mg. The volatility of the elements also depends on the form of the elements in coal [19,43,45]: the included and organically-bounded minerals would be more easily vaporized compared to the excluded minerals. In addition, reducing environments in fuel-rich regions could also enhance mineral vaporization [45,49]. For example, reducing environments would help the formation of suboxides for refractory elements (Si, Al, Fe, Ca and Mg), which are more volatile than their oxidized forms.

The vaporized species will be reoxidized when diffusing away from the char particles [48]. Homogeneous nucleation will then occur to form numerous extremely small particles under the conditions of saturated mineral vapor in the boundary region of the char particles [50]. The thus formed nuclei would grow in size through coagulation when the particles collide [51]. Higher gas and particle temperature, as well as solid diffusivity increase or liquid viscosity reduction due to ash chemical composition change would enhance particle coagulation [48]. As the particle size increases, their diffusivity decreases. Hence, the chance of particle agglomeration contributing to larger particles becomes bigger [48]. Besides coagulation and agglomeration, heterogeneous condensation and chemical reaction could also increase the size of the nuclei formed from homogeneous nucleation.

Small size ash aerosols (typically referred as submicron size range aerosols) normally have greater health risk due to their small size and high enrichment of trace elements

[20,50,52-57]. Besides the above mentioned formation mechanisms for small size ash aerosol, there are still some other proposed formation mechanisms, such as surface ash shedding [40,42,45-46,58-60], bubble bursting [18,30,61-63], carryover of fine fuel particles [64-67] and convective transport for mineral matter [68-71]. Ash shedding is most possibly due to the volatiles release causing char particle rotation [72]. Bubble bursting happens when the liquid particles forming the cenosphere cannot hold the gases evolving inside. Carryover of fine fuel particles is due to the existence of submicron ash particles in raw coal. Convective transport of mineral matter produces submicron minerals through convective transport during devolatilization process.

The particle size distribution (PSD) of the ash aerosol is an important parameter to allow understanding of ash aerosol formation mechanisms and health risk assessments. A mode, normally shown as a peak in the PSDs, normally indicates that the particles therein were formed through similar formation mechanisms. There exist two theories for the ash aerosol PSDs, namely, biomodal and trimodal PSD. In the biomodal theory [19-20,50], the fine mode is centered at 0.1 μm, while the coarse mode is larger than 1 μm. In the tri-modal theory [23,73-80], the fine mode is similar to that in biomodal theory, with a central mode centered at 4 μm and a coarse mode centered at 8 μm. The difference in the two PSD modality theories might be caused by the instrument resolution difference at different times [51,74-80]. As discussed in the foregoing text, the formation mechanism for the fine mode ash aerosol is vaporization, followed by nucleation, condensation and coagulation. Sometimes, there are multiple modes within this fine mode region, where the extra-fine mode is normally formed in the sampling probe through nucleation. The formation mechanisms for the central and coarse modes are mineral coalescence and fragmentation. Presumably, the central mode should have more fragmentation compared to the coarse

mode. The modes are named differently by different authors in the literature. To avoid misunderstanding, this dissertation defines the modes according to their formation mechanisms, which are ultrafine vaporization mode, fine vaporization mode, fine fragmentation mode and coarse fragmentation mode.

Elemental size distributions were also used by some researchers to help explain formation mechanisms of the different mode ash aerosols [78-81]. Due to the health effects, trace elements in ash aerosol are also an important research area. The elemental size distribution of trace elements in ash aerosols depends on element type [82-86].

1.2.3 Ash Deposits Formation Mechanisms

When the minerals in coal are transferred to ash aerosol through the mechanisms discussed in last section, the ash aerosol will then end up with a different fate. For instance, the large size ash aerosol may drop to the bottom hopper underneath the combustion chamber, called bottom ash; some of the ash aerosol might stick to the heat exchanger surface, which is called slagging deposition if it occurs within the radiation zone, and fouling deposition if it occurs within the convection zone. Most of the ash aerosol would be captured by the dust removal system before entering the stack. However, there are still small amounts of small size ash aerosols able to escape from the dust removal system, which are normally denoted as particulate matter (PM) emission. PM has a serious negative effect on the environment and on human health, as discussed in a previous section.

Ash deposition on the heat-exchanger surface will decrease heat transfer efficiency and lead to increased corrosion, accidents, or even boiler shutdowns [87]. Ash deposition is the focus of this work, of which the formation mechanisms include inertial impaction, thermophoresis, condensation, chemical reaction and eddy impaction.

1.2.3.1 Inertial Impaction

Inertial impaction is a deposition process by which bulk deposits are transported to the heat exchanger surface by the fluid gas. This process is affected by target geometry, particle size and density, as well as gas flow field. Typically, it is important for particles with a size larger than 10 μm, because they have sufficient inertia to traverse the gas streamlines and impact onto the heat exchanger surface. However, not all the impacted particles could be captured by the surface because some may bounce off. This is related to capture efficiency, which strongly depends on target geometry, particle size and density, gas flow properties, particle composition and viscosity, as well as deposits surface composition, morphology and viscosity [88]. The inertial impaction rate is controlled by the Stokes number, which is defined as the ratio of the characteristic time of a particle to come to rest when injected into a stagnant fluid to a characteristic time of the flow to pass over a distance equal to the tube radius [89], as shown in (1.1)

$$Stk = \frac{\rho_p d_p^2 u_p}{9\mu_g d_c}\psi \tag{1.1}$$

where ρ_p, d_p and u_p are particle density, diameter and mean velocity, respectively, μ_g and d_c represent gas viscosity and tube diameter, respectively; Ψ is a correction factor that is only important when the particles do not obey Stokes' law.

The impaction rates are normally the highest at the cylinder stagnation point, and are decreasing fast with angular position measured from this stagnation point.

1.2.3.2 Thermophoresis

Thermophoresis is a phenomenon caused by temperature gradient. Particles suspended in the gas phase encountered strike from its surrounded gas molecules. Molecules on the high temperature side strike harder because of higher kinetic energy, comparing to these on the low temperature side. Therefore, the mechanically unbalanced particle will move towards the low temperature side if being put into an environment with temperature gradient. The temperature gradient can inherently exist in the gas phase, or it can be produced by the suspended particle itself if its surface temperature is not uniform [90]. The phenomenon of thermophoresis has been discovered experimentally since 1870 [91]. The relationship between the flow field of particle and the surrounding gas temperature was first proposed theoretically by Maxwell [92] and demonstrated experimentally by Reynolds [93]. Those relationships were then further developed and modified by other scientists as summarized by Bakanov [94]. Later, thermophoresis was also considered in the process of ash deposition during coal combustion [89,95].

Thermophoresis is an important formation mechanism for particles with a diameter less than 5 μm [96-100]. However, the role of thermophoresis would be weakened with the accumulation of the deposits, due to the decreasing of the temperature gradient in the thermal boundary layer.

1.2.3.3 Condensation

Condensation is a process in which mineral vapor deposits at a cooler probe surface, which is significant for low rank fuel because they will produce a large amount of condensable materials during combustion [42,101-102]. Deposits formed through condensation have a profound influence on the bulk strength and thermal conductivity, as

well as capture efficiency for inertial impacted particles.

1.2.3.4 Chemical Reaction

Chemical reaction is another principal mechanism for accumulating deposits from the gas phase vapor, where the important reactions include sulfation, alkali absorption and oxidation on the tube surface.

1.2.3.5 Eddy Impaction

Eddy impaction is a process helping the small particles arrive at the heat exchanger surface near the boundary layer. Those small particles are driven by turbulent eddies, as they are too light in weight for inertial impaction by the mean flow.

1.3 Literature Review of Ash Formation in Oxy-coal Combustion

1.3.1 Ash Aerosol

There exist, however, comparatively few studies focusing on ash aerosol formation during oxy-coal combustion, including both bench-scale [103-110] and pilot-scale experiments [111-114].

The bench-scale studies [103-107] are typically conducted on a drop tube furnace (DTF) under O_2/CO_2 environment to simulate fully cleaned RFG. The most common conclusions are: O_2/CO_2 combustion conditions with similar inlet O_2 concentration to air combustion produce smaller amounts of submicrometer ash aerosols compared to air combustion. However, increasing inlet O_2 concentration would diminish this difference. For instance, Suriyawong et al. [103] investigated submicrometer particle formation under O_2/CO_2 and air combustion conditions on a bench-scale facility. They concluded that oxy-

combustion of 20% inlet O_2 decreased the geometric mean size of ultrafine aerosol compared to air combustion. However, as the inlet O_2 increased from 20% to 50% the mean size of the ultrafine mode increased, probably due to increased metal vaporization and subsequent increased rate of coagulation at the higher flame temperatures. Sheng et al. [104] studied ash aerosol formation on a DTF burning three typical Chinese coals under various combustion conditions. They found that, compared to air combustion, oxy-combustion with the same O_2 concentration shifted the peak of ultrafine mode aerosol to a smaller size and decreased the fraction of ultrafine mode aerosol. However, this difference was diminished as the O_2 ratio increased. Increasing inlet O_2 also increased the formation of fine fragmentation mode particles. Jia et al. [105] studied ash particulate formation during oxy-coal combustion on a DTF operated at oxygen concentrations of 21% and 31.5% and with three coals. They found three particle modes below 20 μm and the mass concentrations of ultrafine mode aerosol (<0.1 μm) increased with increased temperature. Carbone et al. [106] investigated the factors influencing ultrafine particulate matter formation during pulverized coal combustion in oxy-firing conditions, and concluded that an enhanced oxygen concentration promoted ultrafine particle formation. Kazanc et al. [107] investigated submicrometer particulate matter formation during the combustion of coals of various ranks on a DTF, and concluded that the yields of the submicrometer particles from all three coals were lower when combustion occurred in O_2/CO_2 than in O_2/N_2 environments. Instead of simulating fully cleaned RFG, Jiao et al. [108] investigated the effect of HCl, SO_2 and moisture steam on ash aerosol formation during O_2/CO_2 combustion by injecting HCl, SO_2 and moisture steam into the combustion system to simulate real oxy-coal combustion with flue gas recycle (FGR). They concluded that HCl promoted the vaporization of metals via chlorination, not only limited to alkali metals, but

also the organically bound Al and Ti, while SO_2 promoted the sulfation of Na to condense into liquid droplets increasing fine ash yield. Co-existence of bulk HCl and SO_2 played a synergetic role in the sulfation of Na via an initial chlorination of the char-bound Na. In contrast, the coexistence of steam with HCl and SO_2 favored the formation of Na alumino-silicates, which were favorable for ash agglomeration. The above studies explored the formation of ash aerosols formed during the combustion process on DTF. Wen et al. [109] investigated the effect of the devolatilization process on PM10 formation during 29% inlet O_2/CO_2 and air combustion conditions on a DTF. They found that the combustion of CO_2-char generated more PM0.5 and PM0.5-2.5 than that of N_2-char. They argued that the gasification reaction between char and CO_2 that occurred during the devolatilization process increased the pore volume and BET surface area of the char produced in CO_2 environment. Those then led to a higher coal particle combustion temperature of CO_2-char compared to N_2-char, which increased vaporization of inorganic materials and fragmentation of char during CO_2-char combustion. Chen et al. [110] found a similar phenomenon.

Although the bench-scale research on ash aerosol formation during oxy-coal combustion [103-110] showed comparative similar results, the pilot-scale studies [111-114] showed some conflicts.

Yu et al. [111] investigated ash aerosol formation in a self-sustained 100 kW rated oxy-fuel combustor, investigating air combustion, as well as oxy-combustion with 27% and 32% O_2/CO_2 oxy-coal combustion, to match the radiation flux and the adiabatic flame temperature of air combustion, respectively. Their results suggested that oxy-coal combustion had no significant effects on either the trimodal PSD or the size segregated particle compositions. However, the study of Li and co-workers [112] on a self-sustained

one-dimensional down-fired coal combustor, burning a bituminous coal under air and oxy-coal conditions with RFG, suggested the production of increased amounts of fine ash aerosol under oxy-coal combustion conditions, than under air combustion conditions with similar furnace temperature profiles. Meanwhile, Morris et al. [113] conducted ultrafine particle emissions from air and O_2/CO_2 combustion on a pilot scale combustor, and concluded that ultrafine particles consist primarily of black carbon at low stoichiometric ratio, and oxy-coal combustion of a similar adiabatic flame temperature produced less amounts of black carbon comparing to air combustion. However, when switching to oxy-coal combustion with RFG [114], soot emissions can be significantly diminished due to "reburning." He [114] also suggested that ultrafine particle concentrations may increase within the boiler despite flue gas treatment with fabric filters, which may fail to remove the finest particles.

Therefore, to help predict the ash aerosol formation during oxy-coal combustion, it is still needed to put more effort working on this area due to the existence of the conflicts.

1.3.2 Ash Deposits

There exist, however, comparatively few studies [111-112,115-121] focusing on ash deposition formation mechanisms during oxy-coal combustion, where inconsistences exist for both ash deposition rate and deposits chemistry.

Jones et al. [115] investigated the impact of oxy-firing on impurities on the EERC's combustion test facility, and Weller et al. [116] conducted experimental evaluation of firing pulverized coal in a O_2/CO_2 atmosphere. They both reported no significant differences in ash deposition between air and oxy-coal combustion. However, other studies [111-112,117-121] reported some clear, but possibly inconsistent, differences between air and

oxy-coal combustion. For example, Yu et al. [111] explored ash deposition formation during oxy-coal combustion on a pilot-scale facility and Fryda et al. [117-118] investigated those on a bench-scale facility, and they both concluded higher deposition propensities under oxy-fuel conditions; Li et al. [112] conducted similar research on a pilot-scale facility but found the converse, namely that the ash deposition rate in the air combustion mode was larger than that in the oxy-coal combustion mode. It is not clear whether any of these differences were due to changes in deposition mechanisms or to changes in deposit chemistry or both. For deposit chemistry between the two combustion modes, using uncooled ceramic deposit probes, Yu et al. [111] reported that the content of Fe_2O_3 in the Illinois coal deposits and the content of SO_3 in the PRB coal deposits decreased in the order air-firing > oxy-firing with 27% O_2 > oxy-firing with 32% O_2. However, Stimpson et al. [119] collected coal ash deposits in a 160 kW, down-fired oxy-coal reactor under staged and unstaged conditions for four different coals at two locations. They concluded that the only major difference between the air and oxy-combustion deposits was the sulfur concentration, that is, deposits collected under oxy-coal combustion conditions contained higher concentrations of sulfur. Wu et al. [120] studied the ash deposition behaviors in a 3-MWth pilot-scale plant under both oxy-coal and air combustion conditions. They showed that characteristics of the deposit ash obtained from oxy-coal combustion were remarkably different from those of air combustion condition. Deposits from oxy-coal combustion had higher content of SO_3 and Fe_2O_3 and lower content of SiO_2 and Al_2O_3 compared to air combustion. In addition, the fusion temperature of fly ash from oxy-coal combustion was found to be around 200 °C lower than that of the air combustion case. Meanwhile, Fryda et al. [118] suggested that elemental compositions of the deposits did not differ significantly between air and oxy-coal combustion conditions. Furthermore, Wigley and

Goh [121] conducted characterization of rig deposits from oxy-coal combustion on a pilot-scale facility and found lower levels of coal mineral transformation and ash particle sintering, as well as denser packings and different shapes of deposits in oxy-coal combustion.

Therefore, to help predict ash deposit formation during oxy-coal combustion, it is still needed to put more effort into working on this area due to the existence of these conflicts. Furthermore, to understand the formation mechanisms of ash deposition, one would be expected to relate the ash aerosols and ash deposits, because the ash aerosol is the precursor of the deposit ash. This would be very helpful in developing proper deposition models, as well as technology of ash deposition control.

1.4 References

[1] Howard, B. C. *West Antarctica Glaciers Collapsing, Adding to Sea-Level Rise*, 2014.

[2] IPCC. *Contribution of Working Groups I, II and III to The Fourth Assessment Report of The Intergovernmental Panel on Climate Change*, 2007.

[3] IEA. Energy Technology Perspectives 2012, 2012.

[4] IEA. Energy Technology Perspectives 2010, 2010.

[5] Chen, L.; Yong, S. Z.; Ghoniem, A. F. *Progress in Energy and Combustion Science* **2012**, *38*, 156-214.

[6] Wang, M.; Lawal, A.; Stephenson, P.; Sidders, J.; Ramshaw, C. *Chemical Engineering Research and Design* **2011**, *89*, 1609-1624.

[7] Blamey, J.; Anthony, E. J.; Wang, J.; Fennell, P. S. *Progress in Energy and Combustion Science* **2010**, *36*, 260-279.

[8] Thiruvenkatachari, R.; Su, S.; An, H.; Yu, X. X. *Progress in Energy and Combustion Science* **2009**, *35*, 438-455.

[9] Merkel, T. C.; Lin, H.; Wei, X.; Baker, R. *Journal of Membrane Science* **2010**, *359*, 126-139.

[10] Fan, L. S. In *Chemical Looping Systems for Fossil Energy Conversions*; John Wiley & Sons, Inc.: 2010, p 1-56.

[11] Hossain, M. M.; DeLasa, H. I. *Chemical Engineering Science* **2008**, *63*, 4433-4451.

[12] Lyngfelt, A.; Leckner, B.; Mattisson, T. *Chemical Engineering Science* **2001**, *56*, 3101-3113.

[13] Buhre, B. J. P.; Elliott, L. K.; Sheng, C. D.; Gupta, R. P.; Wall, T. F. *Progress in Energy and Combustion Science* **2005**, *31*, 283-307.

[14] Wall, T.; Liu, Y.; Spero, C.; Elliott, L.; Khare, S.; Rathnam, R.; Zeenathal, F.; Moghtaderi, B.; Buhre, B.; Sheng, C.; Gupta, R.; Yamada, T.; Makino, K.; Yu, J. *Chemical Engineering Research and Design* **2009**, *87*, 1003-1016.

[15] Scheffknecht, G.; Al-Makhadmeh, L.; Schnell, U.; Maier, J. *International Journal of Greenhouse Gas Control* **2011**, *5, Supplement 1*, S16-S35.

[16] Wall, T. F. *Proceedings of the Combustion Institute* **2007**, *31*, 31-47.

[17] Toftegaard, M. B.; Brix, J.; Jensen, P. A.; Glarborg, P.; Jensen, A. D. *Progress in Energy and Combustion Science* **2010**, *36*, 581-625.

[18] Raask, E. *Mineral Impurities in Coal Combustion: Behavior, Problems, and Remedial Measures*; Hemisphere Publishing Corporation: New York, 1985.

[19] Damle, A. S.; Ensor, D. S.; Ranade, M. B. *Aerosol Science and Technology* **1981**, *1*, 119-133.

[20] Lighty, J. S.; Veranth, J. M.; Sarofim, A. F. *Journal of the Air & Waste Management Association* **2000**, *50*, 1565-1618.

[21] Yao, Q.; Li, S. Q.; Xu, H. W.; Zhuo, J. K.; Song, Q. *Energy* **2009**, *34*, 1296-1309.

[22] Xu, M.; Yu, D.; Yao, H.; Liu, X.; Qiao, Y. *Proceedings of the Combustion Institute* **2011**, *33*, 1681-1697.

[23] Kang, S. G. *Fundamental Studies of Mineral Matter Transformation during Pulverized Coal Combustion: Residual Ash Formation.* Massachusetts Institute of Technology, 1991.

[24] Yan, L.; Gupta, R. P.; Wall, T. F. *Fuel* **2001**, *80*, 1333-1340.

[25] Liu, G.; Wu, H.; Gupta, R. P.; Lucas, J. A.; Tate, A. G.; Wall, T. F. *Fuel* **2000**, *79*, 627-633.

[26] Liu, Y.; Gupta, R.; Sharma, A.; Wall, T.; Butcher, A.; Miller, G.; Gottlieb, P.; French, D. *Fuel* **2005**, *84*, 1259-1267.

[27] Wang, H.; Harb, J. N. *Progress in Energy and Combustion Science* **1997**, *23*, 267-282.

[28] Monroe, L. S. *An Experimental and Modeling Study of Residual Fly Ash Formation in Combustion of a Bituminous Coal*. Massachusetts Institute of Technology, 1989.

[29] Kang, S. G.; Sarofim, A. F.; Beér, J. M. *Symposium (International) on Combustion* **1992**, *24*, 1153-1159.

[30] Wibberley, L. J.; Wall, T. F. *Combustion Science and Technology* **1986**, *48*, 177-190.

[31] Baxter, L. L. *Combustion and Flame* **1992**, *90*, 174-184.

[32] Helble, J. J.; Sarofim, A. F. *Combustion and Flame* **1989**, *76*, 183-196.

[33] Wall, T. F.; Liu, G. S.; Wu, H. W.; Roberts, D. G.; Benfell, K. E.; Gupta, S.; Lucas, J. A.; Harris, D. J. *Progress in Energy and Combustion Science* **2002**, *28*, 405-433.

[34] Wu, H.; Bryant, G.; Benfell, K.; Wall, T. *Energy & Fuels* **2000**, *14*, 282-290.

[35] Wu, H.; Bryant, G.; Wall, T. *Energy & Fuels* **2000**, *14*, 745-750.

[36] Wu, H.; Zhang, D. K.; Kong, C.; Wall, T. F. *Developments in Chemical Engineering and Mineral Processing* **2005**, *13*, 415-422.

[37] Yu, J.; Harris, D.; Lucas, J.; Roberts, D.; Wu, H.; Wall, T. *Energy & Fuels* **2004**, *18*, 1346-1353.

[38] Kang, S. G.; Kerstein, A. R.; Helble, J. J.; Sarofim, A. F. *Aerosol Science and Technology* **1990**, *13*, 401-412.

[39] Srinivasachar, S.; Helble, J. J.; Boni, A. A. *Progress in Energy and Combustion Science* **1990**, *16*, 281-292.

[40] Srinivasachar, S.; Helble, J. J.; Boni, A. A.; Shah, N.; Huffman, G. P.; Huggins, F. E. *Progress in Energy and Combustion Science* **1990**, *16*, 293-302.

[41] Yan, L.; Gupta, R.; Wall, T. *Energy & Fuels* **2001**, *15*, 389-394.

[42] Helble, J.; Neville, M.; Sarofim, A. F. *Symposium (International) on Combustion* **1988**, *21*, 411-417.

[43] Quann, R. J. *Ash Vaporization under Simulated Pulverized Coal Combustion Conditions*. Massachusetts Institute of Technology, 1982.

[44] Zeng, T.; Sarofim, A. F.; Senior, C. L. *Combustion and Flame* **2001**, *126*, 1714-1724.

[45] Quann, R. J.; Sarofim, A. F. *Symposium (International) on Combustion* **1982**, *19*, 1429-1440.

[46] Quann, R. J.; Neville, M.; Janghorbani, M.; Mims, C. A.; Sarofim, A. F. *Environmental Science & Technology* **1982**, *16*, 776-781.

[47] Lee, C. M.; Davis, K. A.; Heap, M. P.; Eddings, E.; Sarofim, A. *Proceedings of the Combustion Institute* **2000**, *28*, 2375-2382.

[48] Helble, J. J.; Sarofim, A. F. *Journal of Colloid and Interface Science* **1989**, *128*, 348-362.

[49] Linak, W. P.; Peterson, T. W. *Symposium (International) on Combustion* **1988**, *21*, 399-410.

[50] Shaw, D. T. *Recent Developments in Aerosol Science*; Wiley, 1978.

[51] Neville, M.; Quann, R. J.; Haynes, B. S.; Sarofim, A. F. *Symposium (International) on Combustion* **1981**, *18*, 1267-1274.

[52] Helble, J. J. *Fuel Processing Technology* **2000**, *63*, 125-147.

[53] Linak, W. P.; Wendt, J. O. L. *Progress in Energy and Combustion Science* **1993**, *19*, 145-185.

[54] Xu, M.; Yan, R.; Zheng, C.; Qiao, Y.; Han, J.; Sheng, C. *Fuel Processing Technology* **2004**, *85*, 215-237.

[55] Ondov, J. M.; Ragaini, R. C.; Biermann, A. H. *Environmental Science & Technology* **1980**, *14*, 1534-1534.

[56] Linak, W. P.; Yoo, J. I.; Wasson, S. J.; Zhu, W.; Wendt, J. O. L.; Huggins, F. E.; Chen, Y.; Shah, N.; Huffman, G. P.; Gilmour, M. I. *Proceedings of the Combustion Institute* **2007**, *31*, 1929-1937.

[57] Davison, R. L.; Natusch, D. F. S.; Wallace, J. R.; Evans, C. A. *Environmental Science & Technology* **1974**, *8*, 1107-1113.

[58] Baxter, L. L. *Progress in Energy and Combustion Science* **1990**, *16*, 261-266.

[59] Kang, S. G.; Helble, J. J.; Sarofim, A. F.; Beér, J. M. *Symposium (International) on Combustion* **1989**, *22*, 231-238.

[60] Kramlich, J. C.; Newton, G. H. *Fuel Processing Technology* **1994**, *37*, 143-161.

[61] Sarofim, A. F.; Howard, J. B.; Padia, A. S. *Combustion Science and Technology* **1977**, *16*, 187-204.

[62] Smith, R. D.; Campbell, J. A.; Nielson, K. K. *Atmospheric Environment* **1979**, *13*,

607-617.

[63] Smith, R. D. *Progress in Energy and Combustion Science* **1980**, *6*, 53-119.

[64] Holve, D. J. *Combustion Science and Technology* **1986**, *44*, 269-288.

[65] Sadakata, M.; Mochizuki, M.; Sakai, T.; Okazaki, K.; Ono, M. *Combustion and Flame* **1988**, *74*, 71-80.

[66] Yu, D.; Xu, M.; Sui, J.; Liu, X.; Yu, Y.; Cao, Q. *Thermochimica Acta* **2005**, *439*, 103-109.

[67] Yu, D.; Xu, M.; Yao, H.; Liu, X.; Zhou, K.; Li, L.; Wen, C. *Proceedings of the Combustion Institute* **2009**, *32*, 2075-2082.

[68] Yu, D.; Xu, M.; Yu, Y.; Liu, X. *Energy & Fuels* **2005**, *19*, 2488-2494.

[69] Baxter, L. L.; Mitchell, R. E.; Fletcher, T. H. *Combustion and Flame* **1997**, *108*, 494-502.

[70] Zhang, L.; Ninomiya, Y.; Yamashita, T. *Energy & Fuels* **2006**, *20*, 1482-1489.

[71] Benson, S. A.; Sondreal, E. A.; Hurley, J. P. *Fuel Processing Technology* **1995**, *44*, 1-12.

[72] Kang, S. W.; Sarofim, A. F.; Beér, J. M. *Symposium (International) on Combustion* **1989**, *22*, 145-153.

[73] McElroy, M. W.; Carr, R. C.; Ensor, D. S.; Markowski, G. R. *Science* **1982**, *215*, 13-19.

[74] Linak, W. P.; Miller, C. A.; Seames, W. S.; Wendt, J. O. L.; Ishinomori, T.; Endo, Y.; Miyamae, S. *Proceedings of the Combustion Institute* **2002**, *29*, 441-447.

[75] Linak, W. P.; Miller, C. A.; Wendt, J. O. L. *Journal of the Air & Waste Management Association* **2000**, *50*, 1532-1544.

[76] Seames, W. S. *Fuel Processing Technology* **2003**, *81*, 109-125.

[77] Seames, W. S.; Wendt, J. O. L. *Fuel Processing Technology* **2000**, *63*, 179-196.

[78] Yu, D.; Xu, M.; Yao, H.; Liu, X.; Zhou, K. *Powder Technology* **2008**, *183*, 105-114.

[79] Yu, D.; Xu, M.; Yao, H.; Liu, X.; Zhou, K. *Chin. Sci. Bull.* **2008**, *53*, 1593-1602.

[80] Yu, D.; Xu, M.; Yao, H.; Sui, J.; Liu, X.; Yu, Y.; Cao, Q. *Proceedings of the Combustion Institute* **2007**, *31*, 1921-1928.

[81] Teramae, T.; Takarada, T. *Energy & Fuels* **2009**, *23*, 2018-2024.

[82] Ratafia, B. J. A. *Fuel Processing Technology* **1994**, *39*, 139-157.

[83] Davis, S. B.; Gale, T. K.; Wendt, J. O. L.; Linak, W. P. *Symposium (International) on Combustion* **1998**, *27*, 1785-1791.

[84] Xu, M.; Qiao, Y.; Liu, J.; Zheng, C. *Powder Technology* **2008**, *180*, 157-163.

[85] Xu, M.; Qiao, Y.; Zheng, C.; Li, L.; Liu, J. *Combustion and Flame* **2003**, *132*, 208-218.

[86] Zheng, C.; Liu, J.; Liu, Z.; Xu, M.; Liu, Y. *Fuel* **2005**, *84*, 1215-1220.

[87] Bryers, R. W. *Progress in Energy and Combustion Science* **1996**, *22*, 29-120.

[88] Srinivasachar, S.; Helble, J. J.; Boni, A. A. *Symposium (International) on Combustion* **1991**, *23*, 1305-1312.

[89] Baxter, L. L. *Ash Deposit Formation and Deposit Properties: A Comprehensive Summary of Research Conducted at Sandia's Combustion Research Facility*, 2000.

[90] Baxter, L. L.; DeSollar, R. W. *Fuel* **1993**, *72*, 1411-1418.

[91] Tyndall, J. *Journal and Proceedings of the Royal Institute of Chemistry of Great Britain and Ireland* **1870**, *6*, 189-199.

[92] Maxwell, J. C. *Philosophical Transactions of the Royal Society of London* **1879**, *B*, 170-231.

[93] Reynolds, O. *Philosophical Transactions of the Royal Society* **1880**, *170*, 727.

[94] Bakanov, S. P. *Soviet Physics Uspekhi* **1992**, *35*, 783.

[95] Li, B. *Modeling of Fireside Deposit Formation in Two Industrial Furnaces*. Abo Akademi University, 2013.

[96] GökoĞlu, S. A.; Rosner, D. E. *International Journal of Heat and Mass Transfer* **1984**, *27*, 639-646.

[97] Gokoglu, S. A.; Rosner, D. E. *Industrial & Engineering Chemistry Fundamentals* **1985**, *24*, 208-214.

[98] Fuchs, N. A. *The Mechanics of Aerosols*; Oxford: Pergamon Press, 1964.

[99] Byers, R. L.; Calvert, S. *Industrial & Engineering Chemistry Fundamentals* **1969**, *8*, 646-655.

[100] Beck, J. V.; Murio, D. A. *AIAA Journal* **1986**, *24*, 172-179.

[101] Rosner, D. E.; Nagarajan, R. *Chemical Engineering Science* **1985**, *40*, 177-186.

[102] Castillo, J. L.; Mackowski, D. W.; Rosner, D. E. *Progress in Energy and Combustion Science* **1990**, *16*, 253-260.

[103] Suriyawong, A.; Gamble, M.; Lee, M. H.; Axelbaum, R.; Biswas, P. *Energy & Fuels* **2006**, *20*, 2357-2363.

[104] Sheng, C.; Li, Y.; Liu, X.; Yao, H.; Xu, M. *Fuel Processing Technology* **2007**, *88*, 1021-1028.

[105] Jia, Y.; Lighty, J. S. *Environmental Science & Technology* **2012**, *46*, 5214-5221.

[106] Carbone, F.; Beretta, F.; D'Anna, A. *Energy & Fuels* **2010**, *24*, 6248-6256.

[107] Kazanc, F.; Levendis, Y. A.; Maffei, T. *Energy & Fuels* **2013**, *27*, 4984-4998.

[108] Jiao, F.; Chen, J.; Zhang, L.; Wei, Y.; Ninomiya, Y.; Bhattacharya, S.; Yao, H. *Fuel* **2011**, *90*, 2207-2216.

[109] Wen, C.; Yu, D.; Wang, J.; Wu, J.; Yao, H.; Xu, M. *Energy & Fuels* **2014**, *28*, 5682-5689.

[110] Chen, Y.; Wang, G.; Sheng, C. *Energy & Fuels* **2013**, *28*, 136-145.

[111] Yu, D.; Morris, W. J.; Erickson, R.; Wendt, J. O. L.; Fry, A.; Senior, C. L. *International Journal of Greenhouse Gas Control* **2011**, *5, Supplement 1*, S159-S167.

[112] Li, G.; Li, S.; Dong, M.; Yao, Q.; Guo, C. Y.; Axelbaum, R. L. *Fuel* **2013**, *106*, 544-551.

[113] Morris, W. J.; Yu, D.; Wendt, J. O. L. *Proceedings of the Combustion Institute* **2011**, *33*, 3415-3421.

[114] Morris, W. J.; Yu, D.; Wendt, J. O. L. *Proceedings of the Combustion Institute* **2013**, *34*, 3453-3461.

[115] Jones, M.; Pavlish, B.; Kay, J.; Laumb, J.; Downs, J. In *Air Quality VII Conference* Arlington, Virginia, USA, 2009.

[116] Weller, A. E.; Rising, B. W.; Boiarski, A. A.; Nordstrom, R. J.; Barrett, R. E.; Luce, R. G. *Experimental Evaluation of Firing Pulverized Coal in A CO_2/O_2 Atmosphere*, 1985.

[117] Fryda, L.; Sobrino, C.; Cieplik, M.; van de Kamp, W. L. *Fuel* **2010**, *89*, 1889-1902.

[118] Fryda, L.; Sobrino, C.; Glazer, M.; Bertrand, C.; Cieplik, M. *Fuel* **2012**, *92*, 308-317.

[119] Stimpson, C. K.; Chamberlain, S.; Tree, D. R. *Combustion Science and Technology*

2013, *185*, 1098-1117.

[120] Wu, X.; Dai, B.; Yan, K.; Zhang, J.; Zhang, X.; Zhang, J.; Zhang, L. In *Chemeca*, Adelaide, Australia, 2013.

[121] Wigley, F.; Goh, B. In *1st Oxyfuel Combustion Conference* Cottbus, Germany, 2009.

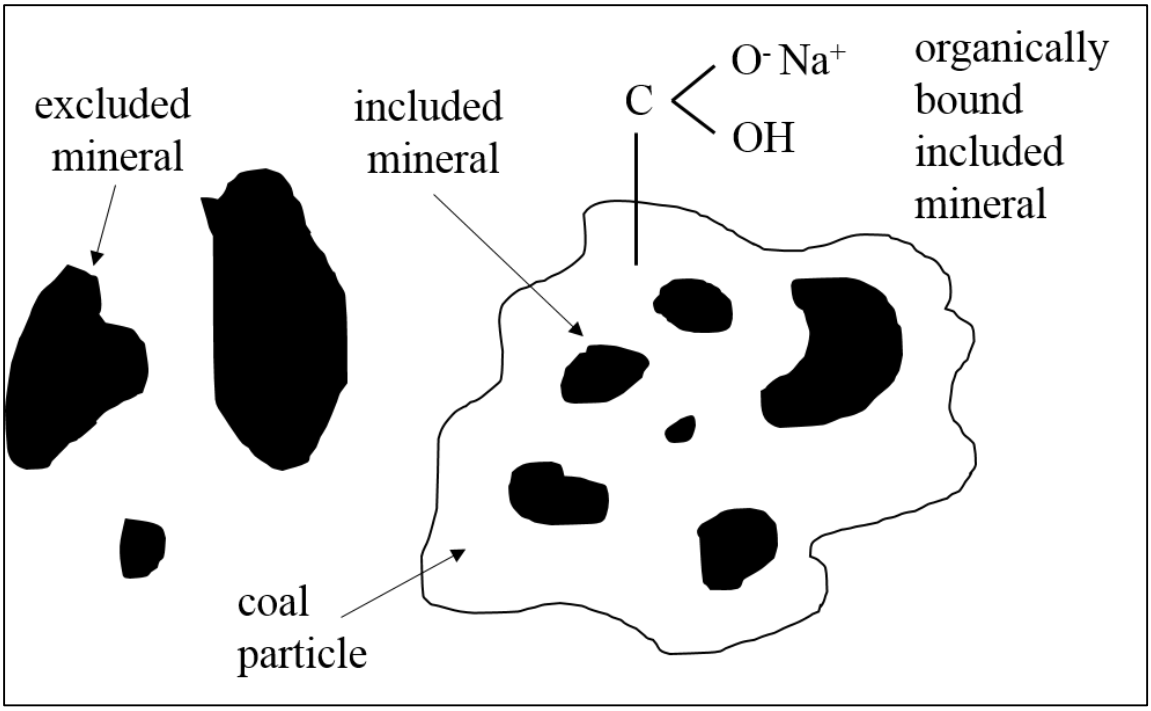

Figure 1.1 Included and excluded minerals in coal.

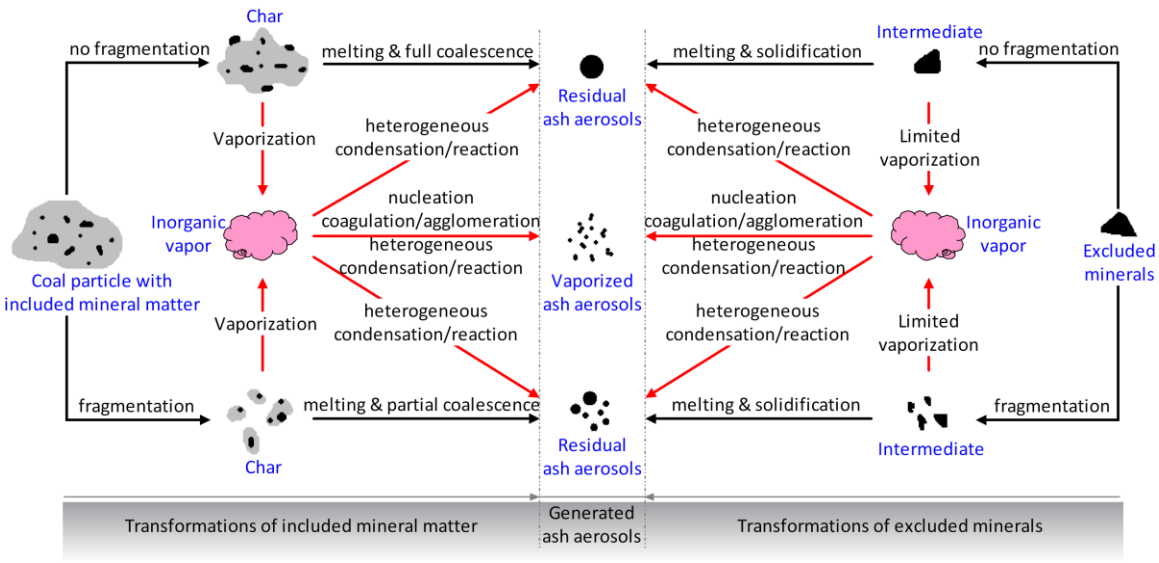

Figure 1.2 Ash aerosol formation during pulverized coal combustion [22].

Table 1.1 Proven energy reserves in the United States and in the world, 2008 [4].

	Coal (Mt)	Crude oil (Mt)	Natural gas (bcm)
Proven reserves: US	238 308	3 700	6 730
Proven reserves: World	826 000	170 800	185 020
Production in 2008: US	1 063	305.1	582.2
Reserve-to-production ratio: US	224	12.4	11.6

CHAPTER 2

SCOPE OF THIS WORK

2.1 Motivation and Objectives

As summarized in last chapter, ash formation is an important concern during oxy-coal combustion. However, there are currently few studies focusing on this area, among which conflicting results still exist. In addition, none of this research attempted to relate ash aerosols to ash deposits, and the effect of different RFG options are barely investigated. Therefore, to help predict ash transformation during oxy-coal combustion, there still remains a lot of unknown for researchers to explore.

In this work, we are targeting the following points:

1) To find out the difference of ash aerosol and ash deposit formation between oxy-coal combustion and air combustion.
2) To ascertain the relationships between deposit composition and size segregated ash aerosol composition.
3) To find out ash aerosol and ash deposit formation characteristics during oxy-coal combustion under a) various RFG stream cleanup options and b) various RFG amounts, as shown in Figure 2.1.

The innovative points of this work are summarized in Table 2.1, which compares the experimental facility, sampling probe, sampling method, sample treatment and

experimental conditions between this work and others' work.

1) For experimental facility, the pilot-scale OFC used in this work is more comparable to a full-scale plant than DTF.
2) The fouling deposition probe used here is temperature-controlled, which is more close to a realistic case than an uncooled probe.
3) This work has a complete set of ash samples including fouling deposition, slagging deposition, ash aerosols, and bulk ash, while others' work merely sampled part of these.
4) Instead of treating the fouling deposits as a bulk as in others' work, this work separates the fouling deposits into inside, outside, side, and vertical deposits.
5) The combustion conditions in this work include various RFG cleanup options and various RFG amounts, while others conducted simulated oxy-coal combustion cases with pure CO_2 or RFG with one recycle option. In addition, there is no pure CO_2 injection in this work, which means even the primary gas is RFG.

2.2 Experimental Apparatus and Analytical Techniques

The experimental work was conducted on a 100 kW rated down-fired self-sustained oxy-fuel combustor (OFC) in the Industrial Combustion and Gasification Research Facility, University of Utah. Necessary details about the OFC can be found in the corresponding chapters. Other details about the OFC can be found elsewhere [1-2].

For sampling or collection systems, a novel temperature-controlled ash deposition probe was used for fouling deposits collection; an uncooled ceramic probe was used for slagging deposits collection; a Berner low pressure impactor (BLPI), and a scanning mobility particle sizer (SMPS) coupled with an aerodynamic particle sizer (APS) were used

for ash aerosol sampling and measuring. A bulk ash sampling probe was used to sample bulk ash. Details about these sampling or collection systems can be found in the corresponding chapters.

Details about the analytical techniques can be found in the corresponding chapters.

2.3 Experimental Conditions

Powder River Basin (PRB) coal was combusted in the OFC. Ash aerosol and ash deposit data were obtained from cases of oxy-coal combustion with four different RFG cleanup options and two different RFG amounts.

The four different RFG cleanup options were:

1) RFG with ash removed, which means recycling the flue gas right after the bag house.
2) RFG with ash and moisture removed, which means recycling the flue gas right after the condenser.
3) RFG with ash, moisture and sulphur removed, which means recycling the flue gas right after the scrubber.
4) RFG with nothing removed, which means recycling totally dirty flue gas (dirty recycle).

The two different RFG amounts were:

1) 27 vol. % O_2 / 73 vol. % RFG (overall) in oxy-coal combustion.
2) 50 vol. % O_2 / 50 vol. % RFG (overall) in oxy-coal combustion (except dirty recycle).

Beyond that, cases of air combustion and oxy-coal combustion of 27 vol. % O_2/ 73 vol. % CO_2 and 50 vol. % O_2 / 50 vol. % CO_2 were also conducted. All these cases are given an abbreviation as shown in Table 2.2.

2.4 Structure of This Work

The following is the structure of this work.

Chapter 3 is mainly focused on the newly developed fouling deposition collection probe system and fouling deposit sample processing method, with an application to demonstrate the novel probe system and the sample processing method.

Chapter 4 is based on Chapter 3. With the application of the system and method developed in Chapter 3, Chapter 4 successfully relates the ash aerosol chemistry to the inside fouling deposit chemistry for the cases of air and oxy-coal combustion with once through CO_2.

Chapter 5 focuses on the ash aerosol and ash deposit formation during air and oxy-coal combustion with various RFG cleanup options and RFG amounts, with the system and methods developed in Chapter 3 and Chapter 4.

Chapter 6 includes modeling of ash deposition rate on vertical surface, based on the formation mechanism of thermophoresis. The predicted results are compared to experimental data as well.

Chapter 7 is the final conclusion of this work and suggestions for future work.

The appendices include A) carbonation of fly ash and ash deposits during oxy-coal combustion; B) data for oxy-coal combustion with dirty recycle case; C) ash deposition rates data for outside layer deposits. Those appendices are valuable, and therefore are supplied as a reference in case needed in future work.

2.5 References

[1] Zhang, J. *Oxy-coal Combustion: Stability of Coaxial Pulverized Coal Flames in O_2/CO_2 Environments*. University of Utah, 2010.

[2] Morris, W. J. *An Examination of Pulverized Coal Combustion Aerosols in Air and in Oxyfuel Combustion Environments*. University of Utah, 2011.

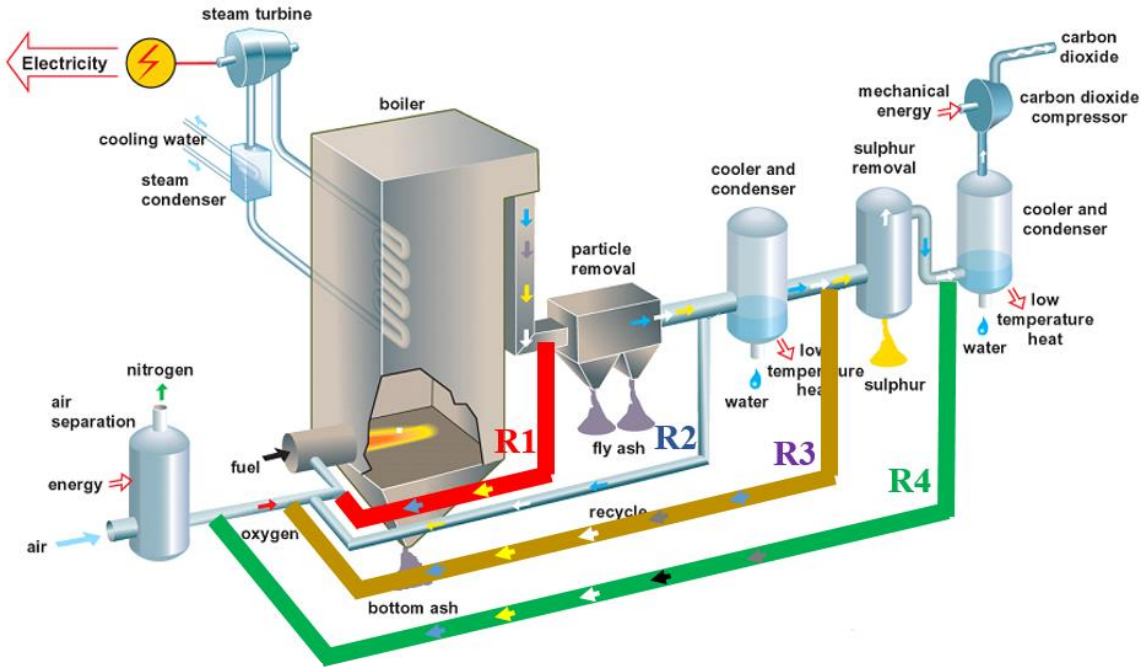

Figure 2.1 Oxy-coal combustion with various RFG cleanup options. R1 is the recycled flue gas including ash, H_2O, SO_2 and CO_2; R2 is the recycled flue gas including H_2O, SO_2 and CO_2; R3 is the recycled flue gas including SO_2 and CO_2; R4 is the recycled flue gas including only CO_2.

Table 2.1 Comparison between this work and others' studies.

	This Work	Others' Studies
Facility	OFC (well controlled pilot scale)	DTF or pilot scale
Probe	temperature controlled	temperature controlled or not
Sampling Method	deposition (fouling, slagging), aerosol (BLPI, SMPS/APS), bulk ash	some of these
Samples Treatment	separated (inside, outside, side, vertical)	treated as a bulk
Combustion Conditions	different RFG cleanup options different RFG recycle amounts OXY50 case no pure CO_2 injection	no recycle or recycle with one cleanup options and one recycle amounts OXY30

Table 2.2 Experimental cases abbreviation and description.

Case abbreviation	Description
Air	air combustion
OXY50 Once	oxy-coal combustion with 50% inlet O_2 and 50% once through CO_2
OXY27 Once	oxy-coal combustion with 27% inlet O_2 and 73% once through CO_2
OXY50-Ash	oxy-coal combustion with 50% inlet O_2 and 50% RFG after bag house
OXY27-Ash	oxy-coal combustion with 27% inlet O_2 and 73% RFG after bag house
OXY50-Ash-H_2O	oxy-coal combustion with 50% inlet O_2 and 50% RFG after condenser
OXY27-Ash-H_2O	oxy-coal combustion with 27% inlet O_2 and 73% RFG after condenser
OXY50-Ash-H_2O-S	oxy-coal combustion with 50% inlet O_2 and 50% RFG after scrubber
OXY27-Ash-H_2O-S	oxy-coal combustion with 27% inlet O_2 and 73% RFG after scrubber
OXY27-Dirty	oxy-coal combustion with 27% inlet O_2 and 73% dirty RFG

CHAPTER 3

NOVEL TEMPERATURE-CONTROLLED ASH DEPOSITION PROBE SYSTEM AND ITS APPLICATION TO OXY-COAL COMBUSTION WITH 50% INLET O_2[1]

3.1 Abstract

Prediction of ash deposition characteristics under oxy-firing conditions helps determine how retrofit to oxy-combustion might affect boiler performance. In order to obtain data to help achieve this end, a novel temperature controlled ash deposition probe was designed to collect temporally resolved deposit samples in a 100 kW rated down-flow test furnace system, firing a Powder River Basin coal. The rig was designed to represent practical units in terms of temperatures, and particle and gas concentrations, yet still be sufficiently well defined to allow controlled systematic studies. The deposit probe/furnace system, which is described in detail, was designed to segregate early "inside" deposits from the average deposits gathered over a period of time. Deposits were gathered under controlled conditions for oxidant input conditions of 50% O_2/50% CO_2 (once through, with no flue gas recycle)

---

[1] Reprinted with permission from Zhan, Z.; Bool, L. E.; Fry, A.; Fan, W.; Xu, M.; Yu, D.; Wendt, J. O. L., Novel Temperature-Controlled Ash Deposition Probe System and Its Application to Oxy-coal Combustion with 50% Inlet O_2. *Energy & Fuels* **2014**, *28*, 146-154. Copyright (2013) American Chemical Society.

and for air. Effects of deposit holding time, deposit probe temperature, and flue gas temperature at the probe location were investigated. Temporal segregation of deposits was achieved by physically separating deposits gathered on the horizontal probe surface into "inside" and "outside" deposits, where "inside" deposits approximated the initial deposit layers. Furthermore, results showed that deposits gathered over long times on the vertical surface of the probe were similar with respect to both composition and particle size distribution to the inside layer of the horizontal deposits, but different from the bulk horizontal deposits that have typically been reported in the literature. There were no significant effects of holding times greater than 1 hour on bulk deposit compositions, although particle size within the deposit did appear to increase with time. There were also no significant differences between compositions of "outside" deposits from oxy-firing (OXY50) and those from air firing. "Inside" deposits from OXY50, however, contained higher Si and Fe and lower S and Na compared to those from air combustion. These results are interpreted in the light of available mechanisms. Tests in which only the deposit surface temperature was changed showed that the mass of deposits on the vertical surface parallel to the flow, shown to be representative of the "inside" deposits on the horizontal surface, was proportional to the temperature difference between the flue gas and the surface. This supported the hypothesis that the early layer was deposited largely by thermophoresis of small particles, and not by Fickian or Brownian diffusion or impaction.

3.2 Introduction

Global warming due to increased CO_2 concentrations in the atmosphere is an issue of current concern [1], and in the foreseeable future, coal combustion in furnaces is still a major source of that pollutant [2]. Oxy-coal combustion, that is, the process of burning coal

with pure O_2 and recycled flue gas (RFG) rather than air, has been considered a promising technology for CO_2 capture for existing coal fired power plants. In order to predict boiler performance when it converted from air-firing to oxy-firing, numerous studies on the effects of oxy-firing on heat transfer, ignition, combustion, flame stability, ash and pollutants formation have been conducted, and have been well summarized in several reviews [3-8].

Ash deposition on boiler tubes plays a significant role in changing heat transfer, and in predicting boiler performance [9-10]. Therefore, knowledge of how oxy-firing might affect deposit characteristics would assist prediction of oxy-coal combustion performance after retrofit from air to oxy-firing. This work constitutes a first step towards obtaining the systematic data required to achieve this goal. It describes the design of a novel temperature controlled deposit probe, which is then applied to comparing the deposit characteristics from air firing to those from oxy-firing at high inlet O_2 conditions. The focus is on fouling deposits, usually found on steam super-heater tubes, rather than on slagging that occurs in the radiant zone near the burner.

There exist, however, relatively very few studies that focus on oxy-coal combustion deposits [11-17], and among these there still remain contradictions on whether deposits are altered during the transition from air firing to oxy-firing. For example, Jones et al.[17] and Weller et al.[13,17] reported no significant differences in ash deposition between air and oxy-coal combustion, while other studies [11-12,14-16] reported some clear, but possibly inconsistent differences between the two firing modes. Yu et al. [11] and Fryda et al. [15-16] found higher deposition propensities under oxy-fuel conditions, while Li et al. [12] found the converse, namely that the ash deposition rate in the air combustion mode was

larger than that in the oxy-coal mode. It is not clear whether any of these differences were due to changes in deposition mechanisms or to changes in deposit chemistry or both. Using uncooled ceramic deposit probes, Yu et al. [11] reported that the content of Fe_2O_3 in the Illinois coal deposits and the content of SO_3 in the PRB coal deposits decreased in the order air-firing > oxy-firing with 27% O_2 > oxy-firing with 32% O_2, while Fryda et al. [16] suggested that elemental compositions of the deposits did not differ significantly between air and oxy-coal conditions. Furthermore, Wigley and Goh [14] found lower levels of coal mineral transformation and ash particle sintering, as well as denser packings and different shapes of deposits in oxy-coal combustion.

Some of these discrepancies may be due to the differences in experimental facilities, deposit probe conditions, combustion conditions and coal types [10,18], all of which can affect ash deposition behavior. Combustion temperatures, combustion aerodynamics and mineral compositions, as well as deposit collection parameters all can play a role in measurements of deposition rates, and these are known to depend on deposition probe surface temperature, flue gas temperature at the collection port and collection holding time [18]. For example, a cooled probe, the surface temperature of which could be effectively controlled, will yield loose deposits, while an uncooled probe might yield sintered deposits. Collection at high flue gas temperatures might yield slagging deposits, while collection at lower flue gas temperatures yields fouling deposits. Clearly, ash deposition during coal combustion is a complex process, dependent on coal composition, combustion conditions, furnace operation, and burner and flame aerodynamics [10,18]. What is needed is an experimental system in which not only the combustion conditions but also the deposit gathering devices can be systematically controlled.

Mechanisms of fouling generally involve the following processes: first, a thin initial

sticky layer is formed on the heat transfer surface through vapor condensation, or molecular and/or Brownian diffusion, or thermophoresis and/or chemical reaction, or combinations of all these processes. Subsequently a thick loose outer layer containing larger ash particles rapidly accumulates through inertial impaction onto this sticky "inner layer." The loose outer deposit layer is not stable and may be removed by "soot blowing," or may even spontaneously drop off [12]. Since inertial impaction involves larger particles, it is thought to be the most important factor in controlling the total mass of ash deposits, if not the initiation or sticking of deposits. Sticking is related to the viscosity of the material on the collecting surface, and there exist several models to predict this [18-21]. Surface viscosity is affected by the composition of the initial deposit layer, and by the composition on the outside surface of the larger ash particles. Clearly, in order to unravel deposition mechanisms one must have both knowledge of the size segregated ash aerosol composition, and a systematic control of the collecting surface, in order to allow the study of both the initial and outside layers. One must, therefore, experimentally isolate this initial inner layer from the bulk of the material deposited on a heat transfer tube, and this issue is addressed in this work. In contrast to this approach, most literature studies [11-17] characterize only the bulk ash deposits during oxy-coal combustion, and this may miss important differences in how the initial deposit layer is formed.

In the research presented here, a novel wall temperature controlled deposit probe is described, and it is shown how, together with a prototype combustion system, it can be used to collect and isolate the "inside" and "outside" ash deposits for analysis and deposit mechanism development. The deposit probe is then tested and utilized to compare both "inside" and "outside" deposits for oxy-fired and air-fired combustion conditions. Oxy-coal combustion was at high inlet O_2 concentrations (50%), rather than at conditions to

match adiabatic flame temperature (O_2=32%) or gas radiation heat flux (O_2=27%) as was used in the previous investigation with an uncontrolled ceramic deposit probe [11]. This oxy-fuel condition was chosen for two reasons: first, high inlet O_2 conditions are of interest in practice since they represent oxy-firing conditions using minimum flue gas recirculation while still being usable in conventional boilers; second, these conditions are most likely to show (hopefully) greater differences in deposits from oxy- and air-firing, because of significant differences in both flame temperature and flue gas composition, and this should provide additional insight into ash deposition mechanisms. As in previous work, fresh, once through CO_2 is used to simulate perfectly cleaned recycled flue gas. Future work will focus on actual recirculated flue gas containing various amounts of contaminants.

3.3 Materials and Methods

3.3.1 Experimental Facility

Ash deposition experiments were conducted on a down-fired oxy-fuel combustor (OFC), which is sufficiently small to allow systematic control of inlet gas flow rates and wall temperatures, and yet large enough to simulate the self-sustaining combustion conditions of full scale units, especially in terms of temperatures, coal particle concentrations and mixing [22-23]. As shown in Figure 3.1a, the OFC is designed with three different zones: an ignition zone (0.61 m × 0.91 m × 1.22 m / I.D. × O.D. × H.), a radiation zone (0.27 m × 0.61 m × 2.60 m / I.D. × O.D. × H.) and a convection zone (0.15 m × 0.15 m × 3.66 m / I.D. × I.D. × L.). The ignition zone is surrounded by 3 × 8 × 840 W flanged ceramic plate electrical heaters to warm up the furnace and 3 thermocouples to monitor and control the furnace wall temperatures. The convection zone is installed with 8 heat exchangers to cool down the flue gas. Preheaters are used for heating up both primary

and secondary inlet gases to 480 K. Nine pairs of ports are positioned along the vertical section of the OFC for sampling and observation (marked as P1-P9 in Figure 3.1a). In this work deposit samples were obtained at Port 5, Port 6 and Port 7. Although the flame in the ignition zone is a pulverized coal turbulent diffusion flame, the flow laminarizes downstream (Reynolds Number is 743 for the OXY50 case and 1153 for the air case), so that by the time the flow reaches the deposit probe positions at Ports 5, 6 and 7, it is quite laminar with vertical streamlines and few turbulent eddies. This has important implications in collecting and segregating "outer" and "inner" deposits on the new deposit probe, as described below. Clearly, inertial deposition rates will be higher in the higher Reynolds Number flows (i.e., under air firing in this case). It should be noted that in this work, the focus is on deposition chemistry differences, rather than on deposition rate differences. The latter are clearly combustor and flow dependent and will be addressed in future work through a combination of experimentation and simulation. Additional details about OFC can be found elsewhere [22-23].

As noted above, combustion conditions examined involve oxy-combustion with 50% inlet O_2 oxy-coal combustion (referred as OXY50) case, and once through CO_2 to simulate the fully cleaned recycled flue gas (RFG), and air combustion. The burner was the same swirl burner used in previous work [11]. Measured flue gas temperature profiles for both OXY50 and air combustion cases are shown in Figure 3.1b. These temperatures were measured by Type K unshielded thermocouples inserted manually through a port up to the center axis of the furnace. These measured values would be expected to be significantly lower than the true values and are shown for comparison purposes only. It is recognized that in these experiments the residence time scales differ somewhat from those of full scale units. However, particle concentrations and other attributes are closer to full scale units

than those same quantities would be for drop tube furnaces, while the ability to conduct systematic studies and control experimental variables is still retained. As expected, the combustion temperature in the ignition zone was higher for the OXY50 case than in air case, but by Port 6, the most often used probe for the deposit probe, both temperatures have reached almost the same temperature. Axial temperature profiles decreased rapidly for both cases, with a steeper profile for the oxy-coal case because of the lower flue gas volumes and increased residence times.

3.3.2 Temperature Controlled Deposit Collection Probe

A novel temperature controlled deposits collection probe was designed, fabricated and demonstrated. It is constructed out of 8 parts, namely, an inner pipe, an outer pipe, a coupon, a spring cap, a manifold, a link, and an end cap (shown in Figure 3.2a) and thermocouple attached to the inside surface of the probe coupon (schematically depicted in Figure 3.2b). The probe is made of stainless steel. The outer pipe has inside/outside diameters of 52.5 mm / 60.3 mm, respectively, while the inner pipe inside/outside diameters are 27.9 mm / 33.4 mm. The length of the probe is 632 mm. The stainless steel coupon diameter is the same as that of the outer pipe and its length is 73.7 mm. The surface temperature was controlled for a fixed surface temperature in the range 473 K - 973 K with a fluctuation of <10 K. Although the probe was inserted into the furnace when it was cold, it always reached the set temperature within 5 minutes, and usually within 2 minutes, which is a short time compared to a typical holding time of ~7 hours. A schematic of the deposit probe system is shown in Figure 3.2b. A thermocouple is placed in a hole drilled into the inside surface of the coupon wall; its temperature (hereafter denoted as “skin temperature”) signal is transmitted to the control box which controls the flow of cooling air. Clearly, the

temperature difference between the surface exposed to the flue gas and that reported here as “skin temperature” would increase and the temperature gradient between the flue gas and the outer deposit surface would decrease, as the surface deposit layer grows. Compressed air is used as the cooling medium that enters at one end of the inner probe, flows from the small holes (part 4, manifold) into the hot end to the space between the inner pipe and outer pipe, to exit as shown. A photo of the collection probe prototype is shown in Figure 3.2c.

Deposit samples were obtained from both horizontal surface (coupon) and vertical surface (end cap) on the collection probe, as highlighted in Figure 3.2c. The horizontal surface is perpendicular to the flow, thus allowing particle deposition by impaction and diffusion, while the vertical surface is parallel to the gas streamlines in laminar flow, thus allowing deposition only by molecular processes. In this way it was hoped that horizontal and vertical surfaces would allow segregation of samples deposited by different mechanisms.

3.3.3 Coal Properties

Powder River Basin (PRB) is the largest coal mining region in the United States, and is used for this ash deposition research. PRB coal is a subbituminous coal, with a high moisture content (23.69 wt. %), low ash and low sulfur. Its proximate analysis, ultimate analysis and ash composition data are shown in Table 3.1 and Table 3.2. Loss on ignition values for the specific experiments reported here are not available, but similar experiments with similar measured temperature profiles and similar coal feeding rates have been reported elsewhere [24]. For air and oxy-firing (once through CO_2 with 27% and 32% inlet O_2) these LOI values ranged from 2.6% to 4.4% (for OXY32 and AIR, respectively) with

2% O_2 in the exhaust and from.4.6% to 5.6%, respectively, with 3% O_2 in the exhaust. The ash in all the experiments reported here was always light brown in appearance, indicating high carbon burnout.

In Table 3.1, percentages are Weight Percent of the coal as received, LOD denotes Loss on Drying or moisture content, V is the Volatile Matter (ASTM), FC is the Fixed Carbon (ASTM) and HHV is the Higher Heating Value.

3.3.4 Operating and Sample Collection Conditions and Analyses

In order to determine the deposition characteristics of PRB coal in oxy-coal combustion, experiments under high inlet O_2 (50%) concentrations (OXY50) with once through CO_2 were conducted on the OFC. The air combustion case was also investigated for comparison. O_2 and CO_2 were supplied by storage tanks outside the building. The furnace wall temperature at the ignition zone was set at 1283 K, the coal feeding rate was set at 4.54 kg/h and excess oxygen in the exhaust was fixed at 3 vol. % (dry). As in previous work [11], the exhaust vol.% O_2 was kept constant rather than the stoichiometric ratio. The OFC was always running with a slightly positive inside pressure to prevent air leaking in. CO_2 concentrations in the flue gas were around 95 vol. % (dry) in OXY50 case (the balance being O_2, H_2O- after water knock out, some N_2, and traces of SO_2, and NO_x). Deposit samples were obtained with temperature controlled deposits collection probe under different collection conditions, namely, 3 different collection ports (different flue gas temperatures: for OXY50, port 5, 1292 K; port 6, 1199 K; port 7, 1101 K), 3 different collection probe surface temperatures (723 K, 823 K and 923 K) and 4 different collection holding times (0.5 hour, 1 hour, 4 hours and 7 hours). Deposits from different positions of the collection probe (horizontal, vertical and side), as shown in Figure 3.3, were obtained,

and horizontal deposits were separated into “inside” and “outside” deposits, where “inside” deposits approximated the initial layer deposits. CCSEM (computer-controlled scanning electron microscopy), SEM (scanning electron microscopy) and ICP-MS were employed for elemental compositions, size distribution and morphology analysis. It is recognized that elemental analyses by SEM-EDS can vary in precision. However, they can be reasonably repeatable if results are obtained on the same instrument over a short period of time, which was the case in this work. For example, all the CCSEM data were obtained at the Huazhong University of Science and Technology in a single block of time spanning 4 weeks.

3.4 Results and Discussion

3.4.1 Deposit Probe Characterization

In the OFC the flow is laminar downstream of the combustion chamber. Deposition of airborne ash onto a horizontal deposit probe surface can occur by mechanisms of inertial impaction as well as diffusion. Diffusion may consist of Brownian and thermophoretic diffusion of small particles, and gaseous Fickian diffusion of volatile metal species followed by condensation or surface reaction. Deposition of airborne ash on a vertical surface, parallel to the streamline flow, must be dominated by diffusion without inertial impaction. Turbulent deposition is absent in this laminar flow situation. By using both horizontal and vertical surfaces to gather deposits, it was possible to segregate the total deposits involving both impaction and diffusion mechanisms from those deposited only by diffusion mechanisms. Furthermore, there are practical reasons for segregating horizontal and vertical deposits since some industrial applications may well have some heat exchanger pipes parallel to the flow of flue gas, and others at cross flow to the flue gas. The deposits collected from the combustor scale employed here arise from realistic airborne particle and

gas species concentrations, and realistic time temperature histories, while the segregation into horizontal and vertical deposits in the postcombustion laminar flow regime allows isolation of diffusion mechanisms alone from the combined inertial impaction and diffusion mechanisms.

Deposits were obtained from the vertical surface of the collection probe, identified as light grey shading in Figure 3.3, and are referred to as vertical deposits. Deposits were also obtained from the horizontal surface of the collection probe (coupon). Other than treating the horizontal deposits as a bulk as in the literature [11-17], we were able to scrape deposits on the surface with an angle to the flow at between 60 ° and 120 ° separately (Figure 3.3, referred as side deposits). More importantly, we were able to separate the horizontal deposits (defined by the surface subtended by the 120 ° angle shown on Figure 3.3) into "inside" deposits and "outside" deposits (Figure 3.3), where the "outside" deposits were the deposits that were loose and fell off easily from the probe when the probe was rotated, while the "inside" deposits remained stuck to the probe even after the probe was tapped or shaken with some vigor. We believe the "inside" deposits to be largely the initial layer of deposits that forms first on a heat transfer surface. Side deposits are also defined in Figure 3.3.

Elemental compositions, particle number size distribution (NSD) and particle mass size distribution (MSD) of these deposits as determined by CCSEM are shown in Figure 3.4; morphology analyses by SEM are shown in Figure 3.5, where Figure 3.5a-d are at a magnification of 600, Figure 3.5e-h are at a magnification of 5000, for deposits from side, vertical, inside and outside, respectively. These were for oxy-combustion conditions with an inlet O_2 of 50%.

Though all the deposits are rich in Si, Al and Ca, followed by Fe, S, Na and Mg,

deposits from the side and vertical surfaces and the "inside" deposits are rich in sulfur, alkali and alkaline earth metallic species, and depleted in Si and Fe compared to the "outside" layer. This suggests that deposits from the side and vertical surfaces and the "inside" deposits from the horizontal surface may share the same formation mechanism.

SEM results (Figure 3.5a, b, c) show that deposits from side, vertical and "inside" regions have similar fine particles (less than 2 μm), which are shown at greater magnification in Figure 3.5e, f, g. There is evidence of particle coalescence.

Notwithstanding that inertial impaction is the primary mechanism forming the bulk of the horizontal deposits, the inside and outside deposits show differences in both elemental compositions (Figure 3.4a) and MSDs (Figure 3.4c). Inside deposits are rich in sulfur, alkali and alkaline earth metallic species, while depleted in Si and Fe, compared to outside deposits. The MSD of inside deposits centers at around 10-20 μm, while that of outside deposits centers at around 46-100 μm. The difference could also be seen from SEM images (Figure 3.5c, d) showing that outside deposits have many more large particles (> 10 μm) than the inside deposits. Large irregular particles that might come from mineral fragmentation exist in outside deposits while not seen in inside deposits, which is consistent with the NSD (Figure 3.4b).

The results are that the main deposition mechanisms for inside and outside deposits are different, and that the outside deposits containing large number of large particles are formed through inertial impaction, while inside deposits are controlled by either condensation of mineral vapor or by Brownian diffusion or by thermophoresis or by a combination of all three. Also, although not identical, vertical and inside deposits were more similar to each other than to the outside or bulk deposits (see Figure 3.4 and Figure 3.5). The small differences between vertical and inside horizontal deposits in PSD's and

elemental compositions might be attributed to the fact that the inside horizontal deposits did in fact contain a few particles that arrived by inertial impaction, while the vertical deposits did not. The outside deposits, on the other hand, were rich in impacted particles.

3.4.2 Effect of Holding Time on Ash Deposition

Figure 3.6a shows elemental compositions of scraped bulk deposits (containing both inside and 1 deposits), that had been exposed to flue gases for various periods in excess of one hour. This was for oxy-combustion conditions at 50% inlet O_2. The data show no significant effects of holding time. However, apparent differences appear for holding times shorter than 1 hour (Figure 3.6b). Then, Si and Fe both increase, while Ca, S and Mg all decrease with increasing holding time, most likely because some Si-Fe enriched large particles are captured simultaneously with the formation of the initial deposits, as discussed in 3.4.1. Thus the elemental compositions of bulk horizontal deposits have a temporal dependence, but only at the very beginning of deposition (less than 1 hour). Figure 3.6c shows the effect of holding time on the elemental compositions of inside and outside deposits. No significant effects of holding time on elemental compositions of either inside or outside deposits are found. However, the particle sizes of both inside and outside deposits appear to increase with time (Figure 3.6d). For inside deposits, this might be due to slow reactions between alkali metals and sulfur compounds or some kind of sintering process of the formed deposits. For the outside deposits, this might suggest that ever larger particles are captured as time goes on, while at early times these might just bounce off. This conjecture is speculative, and more work is needed to understand exactly what is happening. Though the compositions of inside and outside deposits do not change significantly with time, the outside deposit layer increases in thickness, while the inside

deposit layer does not. Therefore, at long holding times, the overall composition of the deposit layer is dominated by that of the outside layer.

3.4.3 Effect of Flue Gas Temperature on Inside Deposits

The elemental compositions of the inside deposits, obtained at various ports at different flue gas temperatures (1292 K, 1199 K and 1101 K) show no significant variations (Figure 3.7a). However, their MSD (Figure 3.7c) peak shifts to a larger size for ports further down the furnace. Reasons for this are unclear, since coagulations rates would be expected to be low in this regime.

3.4.4 Effect of Collection Probe Surface Temperature on Vertical Deposits

Deposits were collected for the same holding times at a fixed port location but at different controlled deposit probe surface temperatures (723 K, 823 K and 923 K). Collection probe surface temperature does not affect the deposit rate of the horizontal (bulk) deposits in the studied temperature range and those data are not shown here. However, deposit surface temperature has remarkable effect on vertical deposition rate as shown on Figure 3.8. After 4 hours vertical deposit masses of 130.1 mg, 69.8 mg and 18.7 mg were collected for a collection probe surface temperatures of 723 K, 823 K and 923 K, respectively. A lower collection probe surface temperature causes a steeper temperature gradient between the flue gas and the probe surface, enhancing the driving force of particle diffusion by thermophoresis [25], as shown in equation (3.1) below:

$$F_t = 4.5\pi\left(\frac{d\mu^2}{\rho T}\right)\left(\frac{\kappa_g}{2\left(\kappa_g + \kappa_p\right)}\right)\frac{dT}{dx} \quad (3.1)$$

where F_t is the thermophoretic force for particles of diameter d, where μ, ρ, T are gas viscosity, density and temperature, respectively, κ_g and κ_p are thermal conductivity of gas and particle, respectively, and $\frac{dT}{dx}$ is temperature gradient in the gas to the surface. If thermophoresis dominates the formation of the vertical deposits the integral amount deposited should be proportional to $\frac{dT}{dx}$, that is approximately to delta T and this is in fact the case, as shown on Figure 3.8. Furthermore, since the vertical deposits are similar to the "inside" layer of the horizontal deposits, these data provide evidence that the initial "activating" step for horizontal deposition is mass transport by thermophoresis, rather than by Brownian or Fickian diffusion.

3.4.5 Comparison of Deposits from Oxy-coal Combustion and Air Combustion

Figure 3.9 shows the elemental compositions of "inside" and "outside" deposits, for a holding time of 1 hour and 7 hours, from both air and OXY50. It can be seen that, independent of holding times between 1 hour and 7 hours, inside deposits from OXY50 have higher Si and Fe and correspondingly lower S and Na compared to those from air combustion, while no significant differences are found for outside deposits. Higher Si and Fe, and correspondingly lower S and Na content for oxy-CO_2 combustion are expected because the peak particle combustion temperatures are higher. Therefore, more Si and Fe will vaporize in the combustion zone and be available to condense onto the probe surface,

to form the inside layer. Furthermore, higher temperatures allow more sodium to be scavenged by alumino-silicates, thus limiting the formation of sodium sulfates [26]. This result differs somewhat from the literature studies [12-13,15-17] where deposits are treated only in the bulk, and demonstrates again the importance of segregating bulk and early deposits. Previous research [11] also reported that S in bulk PRB coal deposits decreased in the order of AIR>OXY27>OXY32. Sheng et al. [27] found more iron melting into glass silicates in the oxy-coal ashes than in O_2/N_2 combustion. This might be because iron tends to decrease the melting temperature and increase the viscosity of the glass silicates [18].

3.5 Conclusions

A novel temperature controlled deposit collection probe was designed, tested and characterized under oxy-combustion conditions with inlet O_2 at 50%, as well as under air combustion.

Deposits from horizontal, vertical and side surfaces of the probe show different characteristics in both compositions and particle size distribution (MSD, NSD). Deposits from the vertical and side surfaces are more similar to the inside deposits on the horizontal surface than they are to the bulk deposits. They are rich in sulfur, alkali and alkaline earth metallic species, while depleted in Si and Fe, compared to the outside deposits on the horizontal surface, and consist chiefly of fine particles that are deposited through particle transport by thermophoresis. This deposit probe, therefore, when used in conjunction with deposit locations in which the flue gas is in laminar flow, allows segregation of deposit samples into bulk deposits (here denoted as bulk horizontal deposits) and initial early deposits (here denoted as inside and vertical deposits). This can provide validation data for future models that predict deposit rates.

There was no significant effect of holding time on compositions of both inside and outside deposits for holding times greater than 1 hour. However, holding time was important for horizontal deposits held for less than 1 hour, most probably because that is when inside deposits comprise a significant fraction of the bulk. Particle size in the bulk horizontal deposits increased as flue gas residence time to the deposit surface increased (and its temperature decreased). Reasons for this are not obvious, since one would expect coagulation of large particles to be too slow, and surface condensation to be too small to account for this. One might speculate that reactions on the probe surface might cause particles to increase in size, but future work is required to unravel this phenomenon.

In comparing deposits from oxy-combustion at high inlet O_2 (OXY50), and air combustion, there were no significant differences found for the outside deposits. Inside deposits, however, from OXY50 have higher Si and Fe and lower S and Na for the OXY50 case than for the air combustion case. The implications of this are that the OXY50 produces more small particles containing Fe and Si than the air case, probably because of the increased flame temperatures.

3.6 References

[1] IPCC. *Contribution of Working Groups I, II and III to The Fourth Assessment Report of The Intergovernmental Panel on Climate Change*, 2007.

[2] IEA. *Energy Technology Perspectives 2012*, 2010.

[3] Chen, L.; Yong, S. Z.; Ghoniem, A. F. *Progress in Energy and Combustion Science* **2012**, *38*, 156-214.

[4] Scheffknecht, G.; Al-Makhadmeh, L.; Schnell, U.; Maier, J. *International Journal of Greenhouse Gas Control* **2011**, *5, Supplement 1*, S16-S35.

[5] Toftegaard, M. B.; Brix, J.; Jensen, P. A.; Glarborg, P.; Jensen, A. D. *Progress in Energy and Combustion Science* **2010**, *36*, 581-625.

[6] Wall, T.; Liu, Y.; Spero, C.; Elliott, L.; Khare, S.; Rathnam, R.; Zeenathal, F.; Moghtaderi, B.; Buhre, B.; Sheng, C.; Gupta, R.; Yamada, T.; Makino, K.; Yu, J. *Chemical Engineering Research and Design* **2009**, *87*, 1003-1016.

[7] Wall, T. F. *Proceedings of the Combustion Institute* **2007**, *31*, 31-47.

[8] Buhre, B. J. P.; Elliott, L. K.; Sheng, C. D.; Gupta, R. P.; Wall, T. F. *Progress in Energy and Combustion Science* **2005**, *31*, 283-307.

[9] Baxter, L. L.; DeSollar, R. W. *Fuel* **1993**, *72*, 1411-1418.

[10] Bryers, R. W. *Progress in Energy and Combustion Science* **1996**, *22*, 29-120.

[11] Yu, D.; Morris, W. J.; Erickson, R.; Wendt, J. O. L.; Fry, A.; Senior, C. L. *International Journal of Greenhouse Gas Control* **2011**, *5, Supplement 1*, S159-S167.

[12] Li, G.; Li, S.; Dong, M.; Yao, Q.; Guo, C. Y.; Axelbaum, R. L. *Fuel* **2013**, *106*, 544-551.

[13] Weller, A. E.; Rising, B. W.; Boiarski, A. A.; Nordstrom, R. J.; Barrett, R. E.; Luce, R. G. *Experimental Evaluation of Firing Pulverized Coal in A CO_2/O_2 Atmosphere*, 1985.

[14] Wigley, F.; Goh, B. In *1st Oxyfuel Combustion Conference* Cottbus, Germany, 2009.

[15] Fryda, L.; Sobrino, C.; Cieplik, M.; van de Kamp, W. L. *Fuel* **2010**, *89*, 1889-1902.

[16] Fryda, L.; Sobrino, C.; Glazer, M.; Bertrand, C.; Cieplik, M. *Fuel* **2012**, *92*, 308-317.

[17] Jones, M.; Pavlish, B.; Kay, J.; Laumb, J.; Downs, J. In *Air Quality VII Conference* Arlington, Virginia, USA, 2009.

[18] Raask, E. *Mineral Impurities in Coal Combustion: Behavior, Problems, and Remedial Measures*; Hemisphere Publishing Corporation: New York, 1985.

[19] Smouse, S. M.; Wagoner, C. L. In *Conference on Inorganic Transformations and Ash Deposition During Combustion* Palm Coast, Florida, ASME, 1991.

[20] Wagoner, C. L.; Yan, X. X. In *Conference on Inorganic Transformations and Ash Deposition During Combustion* Palm Coast, Florida, ASME, 1991.

[21] Yong, S. Z.; Gazzino, M.; Ghoniem, A. *Fuel* **2012**, *92*, 162-170.

[22] Zhang, J.; Okerlund, R.; Eddings, E. G.; Wendt, J. O. L. In *6th International Symposium on Coal Combustion* Wuhan, China, 2007.

[23] Zhang, J.; Kelly, K. E.; Eddings, E. G.; Wendt, J. O. L. *Proceedings of the Combustion Institute* **2011**, *33*, 3375-3382.

[24] Morris, W. J. *An Examination of Pulverized Coal Combustion Aerosols in Air and in Oxyfuel Combustion Environments*. University of Utah, 2011.

[25] Epstein, P. *Zeitschrift Fur Physik* **1929**, *54*, 537.

[26] Gallagher, N. B.; Peterson, T. W.; Wendt, J. O. L. *Symposium (International) on Combustion* **1996**, *26*, 3197-3204.

[27] Sheng, C.; Li, Y. *Fuel* **2008**, *87*, 1297-1305.

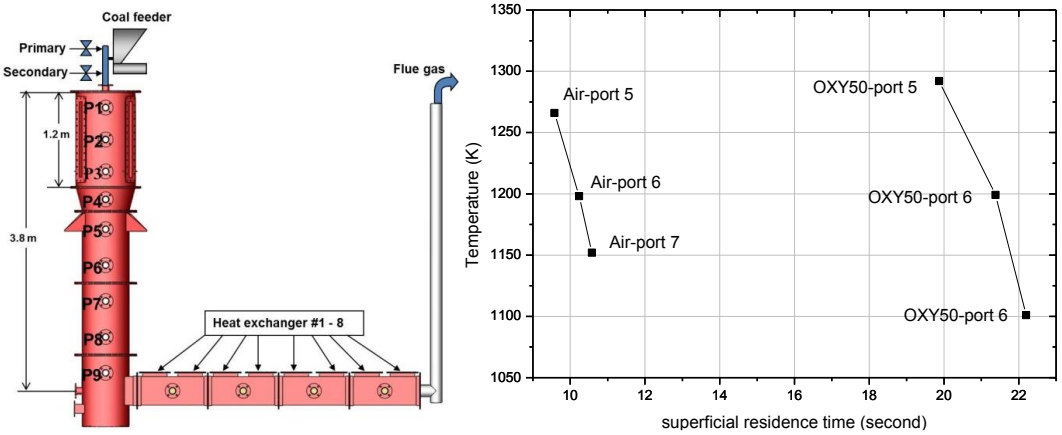

Figure 3.1 Structure of oxy-fuel combustor (OFC) and OFC flue gas temperature profile.

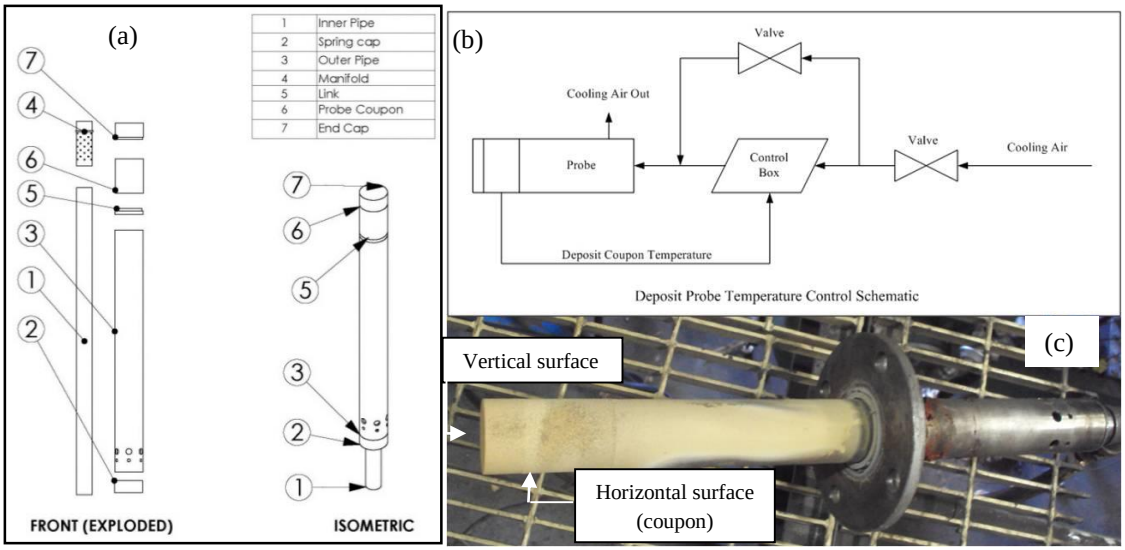

Figure 3.2 Structure of the temperature controlled deposit collection probe and collection system.

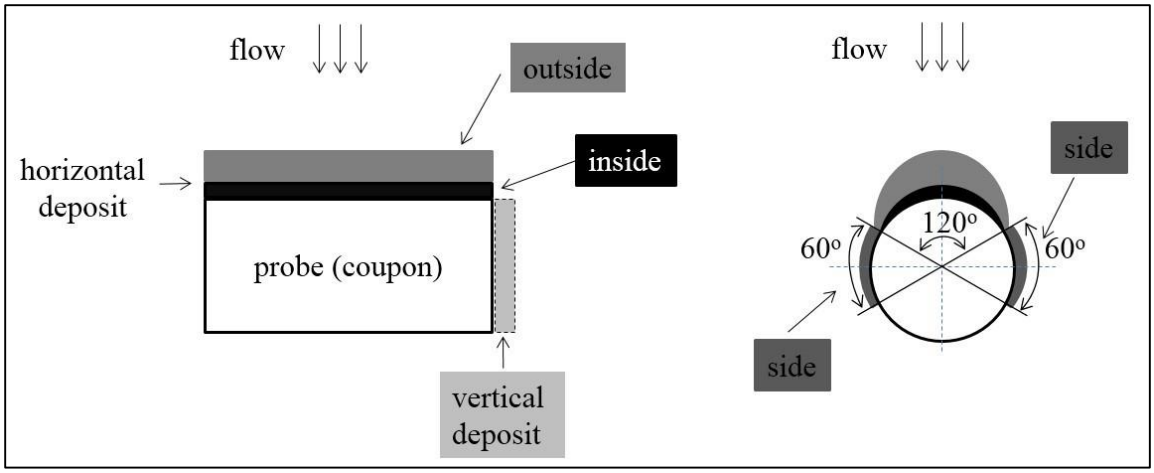

Figure 3.3 Deposits at different positions of the collection probe.

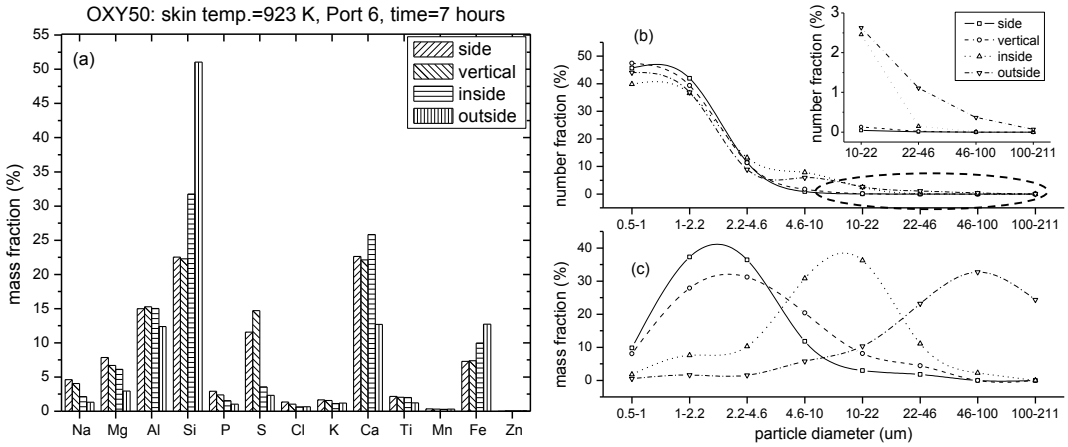

Figure 3.4 Elemental compositions, NSD and MSD of deposits from different positions of the probe. Oxy-combustion conditions, 50% inlet O_2; Port 6 skin temperature, 923 K; holding time 7 hours.

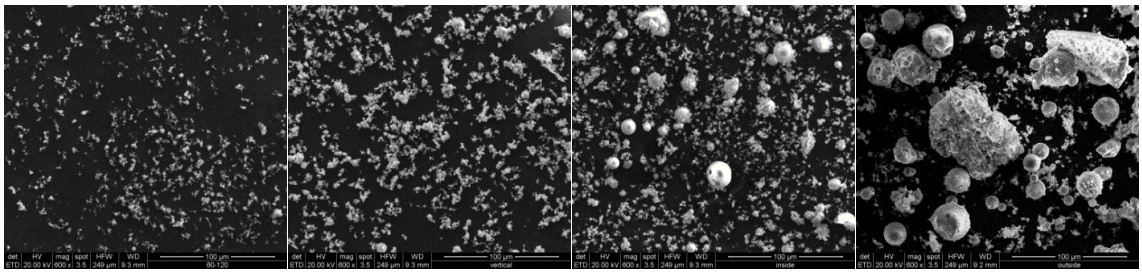

(a) side, ×500　(b) vertical, ×500　(c) inside, ×500　(d) outside, ×500

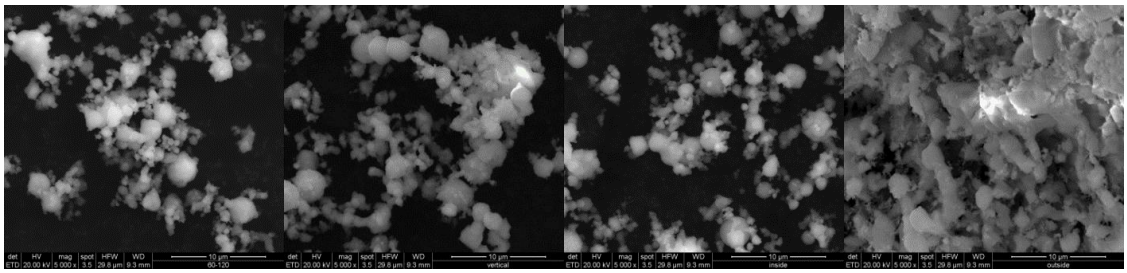

(e) side, ×5000　(f) vertical, ×5000　(g) inside, ×5000　(h) outside, ×5000

Figure 3.5 SEM image of deposits from different positions of the probe.

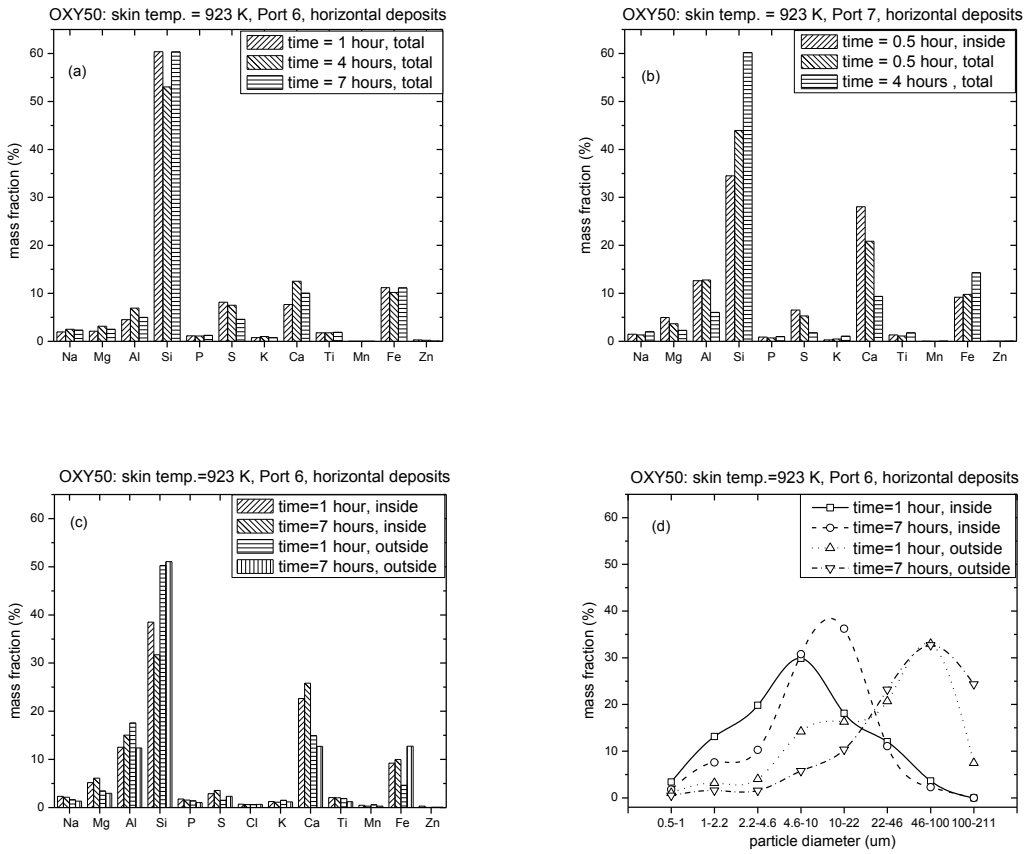

Figure 3.6 Elemental compositions and MSD of deposits collected after different holding times. Oxy-combustion conditions as for Figure 3.4.

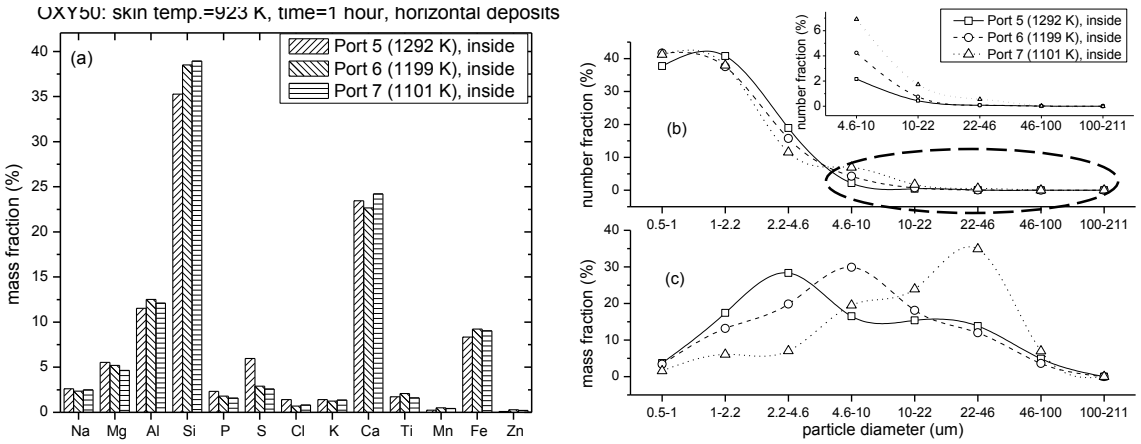

Figure 3.7 Elemental compositions, NSD and MSD of inside deposits from different flue gas temperature. Oxy-combustion conditions as for Figure 3.4.

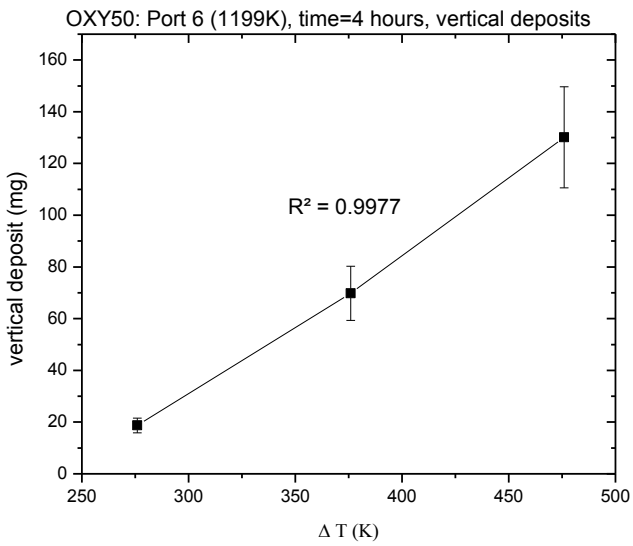

Figure 3.8 Relationship between vertical deposit and ΔT (flue gas and probe skin). Oxy-combustion conditions as in Figure 3.4.

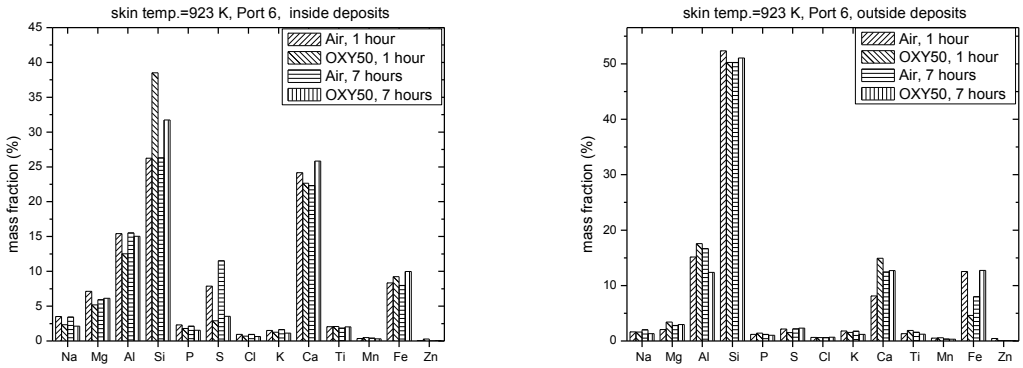

Figure 3.9 Elemental compositions of deposits from air and OXY50 combustion.

Table 3.1 PRB coal analysis (as-received basis).

C (%)	H (%)	N (%)	S (%)	O (diff) (%)	Ash (%)	LOD (%)	V (%)	FC (%)	HHV (BTU/lb)
53.72	6.22	0.78	0.23	34.11	4.94	23.69	33.36	38.01	9078

Table 3.2 PRB coal ash analysis.

Al_2O_3 (%)	CaO (%)	Fe_2O_3 (%)	MgO (%)	MnO (%)	P_2O_5 (%)	K_2O (%)	SiO_2 (%)	Na_2O (%)	SO_3 (%)	TiO_2 (%)
14.78	22.19	5.2	5.17	0.01	1.07	0.35	30.46	1.94	8.83	1.3

CHAPTER 4

ASH AEROSOL FORMATION FROM OXY-COAL COMBUSTION AND ITS RELATION TO ASH DEPOSIT[1]

4.1 Abstract

Ash aerosol and ash deposit formation during oxy-coal combustion were explored through experiments in a self-sustained 100 kW rated down-fired oxy-fuel combustor. Inlet oxidant conditions consisted of 50% inlet oxygen with CO_2 (hereafter denoted as OXY50 conditions). A Berner low pressure impactor (BLPI), a scanning mobility particle sizer (SMPS), and an aerodynamic particle sizer (APS) were used to obtain size segregated ash aerosol samples and to determine the particle size distributions (PSD). A novel surface temperature controlled ash deposition probe system that allowed inside and outside deposits to be separated was used to collect the ash deposits. The ash aerosol PSDs given by the BLPI and those produced by SMPS/APS were consistent with each other. Data suggested that oxy-coal combustion under these conditions did not change the formation mechanisms controlling the bulk ash aerosol composition, but it did increase the formation

[1] Reproduced by permission from Zhan, Z.; Fry, A.; Zhang, Y.; Wendt, J. O. L., Ash Aerosol Formation from Oxy-coal Combustion and Its Relation to Ash Deposit Chemistry. *Proc. Combust. Inst.* **2015**, 35(2), 2373-2380. Copyright (2014) The Combustion Institute.

of ultrafine particles initially formed through metal vaporization, due to increased vaporization of silicon at the higher combustion temperature. The smaller particles contained within the deposits had higher Si and lower Na and S concentrations under OXY50 conditions than for air combustion. Moreover, the ash aerosol composition for particle sizes less than 2.4 μm was related to the composition of the inside deposits. A higher Na in the ash aerosol resulted in higher Na in inside deposits with comparable absolute Na concentrations in both those aerosol particles and those inside deposit particles. The contribution of S and Si to the inside deposits showed that S in the vaporization modes together with Si in the ultrafine vaporization mode contributed significantly to the composition of the inside deposits. These results provided direct evidence that prediction of the chemistry of the initial deposit layer (but not of the bulk deposits) required knowledge of the size segregated chemistry of the ash aerosol.

4.2 Introduction

Climate change is a challenging issue for humans, eliciting much attention on CO_2 emission control from coal combustion sources [1-2]. Oxy-coal combustion, using pure oxygen and recycled flue gas (RFG) instead of air to react with coal is an auspicious technology to allow retrofit of existing coal combustion power plants to enable the capture and subsequent sequestration of the CO_2 produced. Numerous studies [3-5] have been conducted to evaluate furnace performance when converting from air combustion to oxy-coal combustion. This paper is concerned with the effects of retrofit on both the fly ash produced and the fouling deposits laid down on heat transfer surfaces.

The ash aerosol from coal combustion is an important issue because of the following aspects. First, it affects the performance of precipitators used to remove the larger particles

and also influences the emission of fine particulate matter (PM2.5), which contaminates the environment and harms the health of humans, animals, and plants [6]. Second, the ash aerosol is the precursor to forming ash deposits on heat transfer surfaces, thus determining the rates of deposit formation, as well as the chemical and physical properties of the deposits [7]. Ash deposition on heat-exchanger surface will cause problems with heat transfer, and lead to increased corrosion, accidents, or even boiler shutdowns [8]. Thus, in order to predict the impact of retrofit from air to oxy-coal combustion it is essential to predict how the ash aerosol may be altered and how the ash deposition characteristics may change. Furthermore, it would be valuable to determine the relationship between the airborne ash aerosol composition and that of the deposits created from that ash, since this would ultimately lead to models that follow the creation of the ash aerosol, the prediction of its size segregated composition, and its subsequent deposition and possible reaction on heat transfer surfaces. This work presented here follows our previous study [9] in which experimental methods were developed and tested, and is but an early step to achieve that goal. The focus is on deposits normally denoted as "fouling" (loosely bound deposits normally found on superheater tubes) rather than "slagging" (fused deposits formed near the burner in the radiant zone of the furnace).

Only a few studies [10-19] have focused on ash aerosol and ash deposition formation during oxy-coal combustion. Bench-scale experiments [10-12] on a drop tube furnace (DTF) have probed the effects of combustion conditions and oxygen proportions in O_2/CO_2 combustion on the ash aerosol. Suriyawong et al. [10] concluded that oxy-combustion decreased the geometric mean size of the ultrafine aerosol. However, as the inlet O_2 increased, the mean size of the ultrafine mode increased, probably due to increased metal vaporization and subsequent increased rate of coagulation at the higher flame temperatures.

Similar results were obtained by Sheng et al. [11] who showed that, when compared to air combustion, oxy-combustion with the same O_2 concentration shifted the peak of ultrafine mode aerosol to a smaller size and decreased the fraction of ultrafine mode aerosol. However, this difference diminished as the O_2 ratio increased. Jia et al. [12] studied ash particulate formation during oxy-coal combustion in a DTF operated at oxygen concentrations of 21% and 31.5% and with three coals. They found three particle modes below 20 μm and the mass concentrations of ultrafine mode aerosol (<0.1 μm) increased with increased temperature. In general, the bench-scale experimental results [10-12] were comparatively consistent with each other. However, pilot-scale studies [13-14] on ash aerosol formation during oxy-coal combustion showed inconsistent results. Yu et al. [13] investigated ash aerosol formation in a self-sustained oxy-fuel combustor, investigating air combustion, as well as oxy-combustion with 27% and 32% O_2/CO_2 oxy-coal combustion. Their results suggested that oxy-coal combustion had no significant effects on either the trimodal particle size distribution (PSD) or the size segregated particle compositions. However, the study of Li and co-workers [14] on a self-sustained one-dimensional down-fired coal combustor suggested the production of increased amounts of fine ash aerosol under oxy-coal combustion conditions compared to under air combustion conditions with similar furnace temperature profiles. Differences between bench-scale and pilot-scale studies [10-14] may be attributed to many factors, such as differences in coal types, furnace temperatures, combustion conditions, and, especially, particle concentrations.

As far as ash deposition is concerned, some studies [13-19] for oxy-coal combustion have raised disparate conclusions, due to variations in experimental equipment, deposition probe conditions, combustion conditions, and coal types. Required is an experimental system in which both combustion conditions and collection devices for deposits are

systematically controlled. To this end, the deposit collection system developed and tested in previous work [9] was applied to the present work.

One would expect that deposit chemistry would be related to the size segregated composition of the ash aerosol. Yet, even though multiple discrepancies exist in ash aerosol studies and in deposit studies [10-19] for oxy-coal combustion conditions, and there have been no attempts to directly relate particle size resolved details of the ash aerosol to temporal details of how the ash deposits were formed. Therefore, in this study size segregated aerosol composition data, PSD data and temporally resolved deposit composition data were obtained, and connections between all of these factors were inferred. To the best of the authors' knowledge, this study is among the first to ascertain the relationship between the detailed ash aerosol chemistry and the ash deposit chemistry in oxy-coal combustion.

4.3 Materials and Methods

4.3.1 Experimental Facility

Experiments were conducted on a nominal 100 kW, laboratory down-fired oxy-fuel combustor (OFC). This rig allows combustion to be self-sustaining with temperatures, particle concentrations, and mixing comparable to those of full-scale units. It nevertheless allows for systematic control of inlet flow rates and wall temperatures, and of other experimental conditions. As shown in Figure 4.1, the OFC contains nine pairs of sampling and observation ports along its vertical section, denoted as P1-P9 in Figure 4.1. In this research, the ash aerosol was sampled at Port 9 and deposits were collected at Port 6, using a unique wall temperature controlled deposit sampling probe described in detail in previous work [9]. It is hypothesized that not much happens to the ash aerosol composition between

Port 6 (1200 K), where the deposits are collected, and Port 9 (960 K - 1060 K), where the ash aerosol sample is withdrawn, and this is supported by (HSC) equilibrium calculations that showed negligible differences in the equilibrium condensed mineral concentrations between these ports. Additional details about OFC can be found elsewhere [9,20]. The burner for this study was the swirl burner used previously [20]. Oxy-fuel combustion with 50% inlet O_2 and once through CO_2, to simulate the fully cleaned RFG, was compared to results from air firing. Although the combustion temperature in the ignition zone was higher in OXY50 than in air, temperatures were almost the same at Port 6 where deposits were collected.

4.3.2 Ash Deposition Collection System

A novel temperature-controlled ash deposition probe system was used for collection of ash deposits [9]. This system allows the probe surface temperature to be controlled. The laminar flow in the OFC at Port 6 allows thermophoretic deposition on the probe vertical surface to be isolated without complications caused by inertial impaction. It has been shown [9] that this vertical layer is similar to the sticky inner deposits on the horizontal surface of the probe. “Outer” and “inner” deposits on the horizontal surface (see Figure 3.3) of deposit probe are separated manually through judicious tapping of the probe. For the present work, the major focus is to determine the relationship between ash aerosol chemistry and the chemistry of the “inside” or sticky ash deposits, and how these vary between air and oxy-combustion. Future work will explore the effects on the “outside” ash deposits. The rate and mechanisms of deposition of the vertical deposits are reported in Reference [9].

4.3.3 Ash Aerosol Sampling Systems

For detailed ash aerosol information, two groups of instruments were utilized: a Berner low pressure impactor (BLPI) [13] and a scanning mobility particle sizer (SMPS, TSI model 3080) coupled with an aerodynamic particle sizer (APS, TSI model 3321, hereafter referred to as SMPS/APS). The working principle for BLPI is inertial impaction, while electron mobility and light scattering are the working principle for SMPS and APS, respectively.

BLPI has a 50% aerodynamic cutoff diameters of 15.7, 7.33, 3.77, 1.98, 0.973, 0.535, 0.337, 0.168, 0.0926, 0.0636, and 0.0324 μm. Cellulose acetate membranes were used to collect ash aerosol samples for subsequent composition and morphology analyses. Aluminum filters coated with Apiezon grease were used for gravimetric PSDs, together with a high-quality Mettler Toledo balance with a precision of 0.1 μg. The raw material for cellulose acetate membranes (Advantec) and aluminum substrates (Reynolds Wrap, heavy duty) were first purchased in sheet, and then cut into O-rings with 33 mm of inside diameter and 70 mm of outside diameter at Pioneer Gasket Company INC., Salt Lake City. The cellulose acetate membranes could be used directly, while the aluminum substrates have to be prepared according to the following procedure: 1) wash the cut aluminum filters with common ethanol, and then dry the filters in oven for one night at 70 ℃; 2) take filters out and put them in clean sandwich bags for future use; 3) prepare the grease/hexane solution with 10-15 grams of grease per liter of hexane (Fischer Scientific brand HPLC grade hexane); 4) use the spray gun or brush to coat the solution to the shiny side of the filters, evenly along the center of the O-ring (about 8 mm away from the border); 5) dry the filters in the oven, laying on aluminum foil sheet, at 55 ℃ for about 10 hours; 6) take them out and keep each substrate in a 90 mm glass petri dish to prevent polluting and static

electricity; 7) install the substrates in the BLPI. The aluminum substrate could be easily charged with static electricity, which affects the weight of the substrate remarkably. Therefore, lay antistatic sheet underneath the working area when necessary.

The SMPS produces PSD's in real time, in the size ranges of 0.0143 μm to 0.6732 μm, with the APS measuring in the size ranges of 0.532 μm to 20 μm. The SMPS and APS data are combined and shown in the same figure. As shown in Figure 4.1, the BLPI sampling system includes a water-cooled, nitrogen-quenched isokinetic sampling probe, a cyclone, a BLPI, a vacuum pump, a nitrogen gas cylinder, and a flow meter. The SMPS/APS sampling system includes the same water-cooled, nitrogen-quenched isokinetic sampling probe, a nitrogen gas cylinder, a flow meter, clean compressed air, an orifice, SMPS, APS, and a dilution manifold. The SMPS/APS sampling system, with a total dilution ratio of about 200 to 400 to 1, uses two-stage dilutions to prevent further interactions between particles.

Sampling was as isokinetic as possible for both air and oxy cases, based on calculated furnace flue gas rates and measured sampling flow rates, which were adjusted for air and oxy conditions through changes in the dilution N_2 flow rate.

4.3.4 Experimental Conditions and Analysis Methods

A Powder River Basin (PRB) coal was used in this research, and its composition is shown in Table 3.1 and Table 3.2.

To identify PRB coal ash formation characteristics in oxy-coal combustion and ascertain the relationship between ash aerosol chemistry and ash deposit chemistry, experiments on air and OXY50 combustion were conducted on the OFC. Details about combustion conditions can be found elsewhere [9].

Ash aerosol PSDs were obtained by both BLPI (gravimetric) and SMPS/APS (electric mobility and light scattering). The ash aerosol particles on cellulose acetate membranes were analyzed by scanning electron microscopy–energy-dispersive X-ray spectrometry (SEM–EDS) for elemental composition analysis. The collected deposits, on the other hand, were analyzed using computer-controlled scanning electron microscopy (CCSEM) and SEM. In this work, the chemistry of the deposits rather than their deposition rate are of interest.

We did not report an overall ash balance because deposits on the wall and large bottom ash particles that are not collected make this impossible for equipment of this scale.

4.4 Results and Discussion

4.4.1 Ash Aerosol PSD

For comparison and validation purposes, both the BLPI and the SMPS/APS were used to measure the PSD of the ash aerosol. The ash aerosol PSDs of both air and OXY50 combustion are shown in Figure 4.2. The BLPI and the SMPS/APS PSD's showed excellent agreement, with the latter instruments providing greater resolution. The flue gas flow rate of the OXY50 case (13.36 Nm^3/h) is significantly less than that of the air fired case (30.65 Nm^3/h). Gas volume-based PSD's are shown on Figure 4.2a, whereas PSD's based on the input ash amount (Figure 4.2b) account for different dilutions between the air and oxy-firing case. Figure 4.2a shows higher ash aerosol concentration in OXY50 for all measured size ranges; these differences are much diminished once dilution effects are taken into account (Figure 4.2b).

As shown in Figure 4.2, the ash aerosol PSD's contain (at least) three modes for both air and OXY50 combustion. Two of these modes lie within the particle size regime caused

by ash vaporization, with one mode less than 0.1 μm most probably caused by nucleation of ash constituents in the dilution sampling probe, and the other one, lying between 0.1 μm to 1 μm, being the accumulation mode of coagulated nuclei formed in the combustor. Dilution at the tip of the sampling probe is designed to inhibit subsequent coagulation there. The modes for particles larger than 1 μm are fragmentation modes, and, following Linak et al. [21], may be divided into a fine fragmentation mode (<2.5 μm) and a coarse fragmentation mode (~10 μm). Switching from air firing to oxy-firing (OXY50) moves the peak of the first vaporization mode from 0.06 μm to 0.17 μm most probably because of increased vaporization at the higher flame temperatures [22], increased nucleation and subsequent coagulation [23], either before or after the sample probe intake. Taking dilution into account, Figure 4.2b shows that for the same amount of input-ash, OXY50 also produces a greater amount of particles in that size range than did air firing. This will be shown below to have implications on deposition of the first, inner layer of deposits. Jia et al. [12] obtained a similar result for the PRB coal, where combustion in a 31.5% oxygen O_2/CO_2 environment yielded smaller amounts of nuclei (< 0.1 μm) particles than for either air or 20% oxygen O_2/CO_2 environments. The fine resolution data from the SMPS/APS on Figure 4.2b showed that OXY50 also yielded a lower mass of particles in the fine fragmentation mode, with the peak in that mode shifted somewhat to the smaller size. The coarse fragmentation mode was essentially unchanged.

4.4.2 Elemental Compositions of Ash Aerosol

The ash aerosol collected on cellulose acetate membranes on the BLPI plates was analyzed for elemental compositions by EDS. Given the very small amounts of samples on stages 10 and 11, only the ash aerosol on stages 1 to 9 (size ranges of 0.0324 μm to 3.77

μm) were analyzed. The size segregated distributions of the main elements Na, S, Si, and Fe are shown in Figure 4.3. These elements comprise a subset of those that were analyzed, and are highlighted here because they show significant differences in their size segregated concentrations between air firing and oxy-firing. It should be noted that the particle aerodynamic diameter used to plot BLPI data is not identical to the visual diameter measured by CCSEM. An aerodynamic diameter of 3.77 μm is equivalent to a geometric visual diameter [24-25] of 2.36 μm, assuming a particle density of 2.56 g/cm^3.

The mass fraction of Na is higher in air combustion than in OXY50 for all impactor stages in the range 0.0324 μm to 3.77 μm. This might be due to increased scavenging of Na vapor by larger alumina-silicate particles at the higher combustion temperature in OXY50. Previous studies [26-27] have shown that increased temperatures actually result in a decrease in the sodium sulfate fume, because of increased reaction with aluminum silicates or silicates to form sodium aluminum silicates or sodium silicates, even though more Na might initially be vaporized [28].

Sulfur is enriched in the vaporization modes, most probably occurring by condensation in the probe. Its mass size distribution is similar in both air and OXY50, although its concentration is ostensibly lower throughout the vaporization modes in OXY50. This is consistent with the decrease in sodium vapor produced under OXY50 conditions, and its propensity to form sodium sulfate. Furthermore, the high CO_2 partial pressure in OXY50 combustion may well restrain sulfate formation [29]. Some sulfates will homogeneously nucleate or condense directly onto a cold surface at 1250 K temperature [30-31]. However, most of the sulfates will condense on the suspended particles, forming sulfate-coated particles. The mixture of the sulfates is molten and sticky between 1157 and 1250 K [31]. Therefore, the sulfur in the vaporization modes may contribute largely to the initial layer

deposition at the deposition collection port temperature of 1200 K.

There is a significant difference in the size segregated silicon concentration distribution in particles formed in air and oxy-combustion. The Si concentrations in the ultrafine vaporization mode are much higher under OXY50 conditions, either because of the higher combustion temperature in OXY50 [22] or possibly because of increased CO levels near the particle surface. The size segregated composition of Fe presents the converse picture compared to silicon. Fe concentrations in the ultrafine vaporization mode are lower for OXY50 conditions than for air firing. This is consistent with Sheng [32] who found increased iron present in glass (presumably in larger particles) under oxy-firing conditions. It is unclear whether this is a temperature effect or a CO_2 chemistry effect or both.

4.4.3 Relationship between Ash Aerosol and Ash Deposition

Figures 4.4a and b show the composition and morphology of the inside deposits, for all particles observed to be less than 4.6 μm in diameter. Inside deposits after 1 hour exposure and after 7 hours exposure to the flue gas were analyzed. Inside deposits constitute those not easily removed by tapping the deposit probe, and have been shown to be similar to deposits laid down by thermophoresis rather than by impaction [9]. The deposit probe wall temperature was held constant at 923 K. Differences between 1 hour and 7 hours holding times might be due to increasing “dilution” of the early deposit constituents by the bulk ash that arrives later by impaction and sticks. Note that the high Si content of the 1 hour deposit under OXY50 conditions is double that under air firing conditions. This is consistent with the increased ultrafine vaporized silicon rich particles produced under OXY50 conditions (see Figure 4.3). Note also how the 1-hour deposits have lower S and lower Na under oxy-firing than under air firing. This also is consistent with the differences

in the vaporized ultrafine aerosol data shown on Figure 4.3. It is also noteworthy that the S content in the deposits increases from 1 hour through 7 hours for both air and oxy-firing. This suggests that sulfated ash continues to be impacted and to stick on the deposit surface as time proceeds.

It is appropriate to address the issue of particle sizes found by CCSEM in the deposits. The inside deposits appear mainly to consist of particles with geometric sizes less than 4.6 μm [9]. However, the geometric size of the original ash aerosol forming the inside ash deposits is actually much smaller than 4.6 μm. The SEM photograph of the inside deposits, shown in Figure 4.4b, suggests that some larger particles are formed by agglomeration of groups of small particles with geometric sizes less than 2.5 μm. Therefore, the ash aerosol with particle geometric sizes of less than 2.5 μm (equals to about 3.77 μm in aerodynamic size) is the original source of the inside deposits.

Sodium exhibited a straightforward relationship between ash aerosol and inside deposition, that is, compared with OXY50, higher sodium in the ash aerosol of air combustion results in higher sodium in the inside ash deposition of air combustion. Furthermore, the sodium mass fractions in ash aerosol matched those in inside ash deposition, which are around 5% in air and 3% in OXY50. The results imply that the sodium concentration in the initial layer deposition may be predicted by merely examining ash aerosols. However, the contribution of S and Si to inside deposits seems to be more particle size selective.

Sulfates and sulfate-coated particles are molten and sticky at between 1157 and 1250 K, and thus, could be easily captured on a cooled surface. The flue gas temperature at the deposition collection port is about 1200 K. Therefore, during air combustion, the higher S concentration in the ultrafine and fine vaporization mode ash aerosol indicated more

sulfates than under oxy-coal conditions. Consequently deposits contain more sulfur during air combustion than for the OXY50 case. Alternatively, sulfur in the deposits might be replaced by carbon, or sulfate formation might be otherwise diminished, in the high CO_2 partial pressure environment occurring in OXY50, as hypothesized by some studies [29,33]. Chen et al. [29] noticed that the high CO_2 partial pressure in oxy-fuel furnace had an inhibitory effect on limestone calcination and Zhan et al. [33] reported higher CO_3/SO_4 ratios (measured by XPS) in the bulk ash and deposits from oxy-coal combustion than those from air combustion.

4.5 Conclusions

Ash aerosol particle size distributions measured by SMPS/APS were consistent with BLPI. The high resolution PSD's measured by the SMPS/APS showed two modes within the vaporization regime and two modes within the fragmentation regime. Oxy-combustion with 50% O_2 in the inlet oxidant (OXY50) increased the size and location of the first vaporization mode, most probably through increased vaporization of silicon at the higher flame temperatures experienced there. Conversely, the fine fragmentation mode decreased under OXY50 conditions, for reasons that are unclear.

The chemistry of the ash deposits collected on a specially designed, controlled deposit probe, were related to the ash aerosol data. The composition of the inside deposits was consistent with the composition of the vaporization mode aerosol. Under OXY50 conditions, the higher Si concentrations in vaporization mode led to increased concentrations of Si in the early deposits. However, air combustion produced increased S in both the ultrafine aerosol and in the early deposits, compared to OXY50.

In order to elucidate mechanisms of deposit formation two types of data appear to be

useful. First, it is important to separate the early deposits that are bound more tightly to the cooled surface from the bulk deposits. Their composition differs from the bulk deposits, and contributes to adhesion mechanisms allowing the bulk deposits to accumulate. Second, one needs the size segregated composition of the ash aerosol, with emphasis on particle sizes in the submicron vaporization mode. It is the fine and ultrafine particles that dominate the early stages of ash deposition.

4.6 References

[1] IPCC. *Contribution of Working Groups I, II and III to The Fourth Assessment Report of The Intergovernmental Panel on Climate Change*, 2007.

[2] IEA. *Energy Technology Perspectives 2010*, 2010.

[3] Chen, L.; Yong, S. Z.; Ghoniem, A. F. *Progress in Energy and Combustion Science* **2012**, *38*, 156-214.

[4] Toftegaard, M. B.; Brix, J.; Jensen, P. A.; Glarborg, P.; Jensen, A. D. *Progress in Energy and Combustion Science* **2010**, *36*, 581-625.

[5] Buhre, B. J. P.; Elliott, L. K.; Sheng, C. D.; Gupta, R. P.; Wall, T. F. *Progress in Energy and Combustion Science* **2005**, *31*, 283-307.

[6] Lighty, J. S.; Veranth, J. M.; Sarofim, A. F. *Journal of the Air & Waste Management Association* **2000**, *50*, 1565-1618.

[7] Baxter, L. L. *Ash Deposit Formation and Deposit Properties: A Comprehensive Summary of Research Conducted at Sandia's Combustion Research Facility*, 2000.

[8] Bryers, R. W. *Progress in Energy and Combustion Science* **1996**, *22*, 29-120.

[9] Zhan, Z.; Bool, L. E.; Fry, A.; Fan, W.; Xu, M.; Yu, D.; Wendt, J. O. L. *Energy & Fuels* **2014**.

[10] Suriyawong, A.; Gamble, M.; Lee, M. H.; Axelbaum, R.; Biswas, P. *Energy & Fuels* **2006**, *20*, 2357-2363.

[11] Sheng, C.; Li, Y.; Liu, X.; Yao, H.; Xu, M. *Fuel Processing Technology* **2007**, *88*, 1021-1028.

[12] Jia, Y.; Lighty, J. S. *Environmental Science & Technology* **2012**, *46*, 5214-5221.

[13] Yu, D.; Morris, W. J.; Erickson, R.; Wendt, J. O. L.; Fry, A.; Senior, C. L. *International Journal of Greenhouse Gas Control* **2011**, *5, Supplement 1*, S159-S167.

[14] Li, G.; Li, S.; Dong, M.; Yao, Q.; Guo, C. Y.; Axelbaum, R. L. *Fuel* **2013**, *106*, 544-551.

[15] Wigley, F.; Goh, B. In *1st Oxyfuel Combustion Conference* Cottbus, Germany, 2009.

[16] Weller, A. E.; Rising, B. W.; Boiarski, A. A.; Nordstrom, R. J.; Barrett, R. E.; Luce, R. G. *Experimental Evaluation of Firing Pulverized Coal in A CO_2/O_2 Atmosphere*, 1985.

[17] Jones, M.; Pavlish, B.; Kay, J.; Laumb, J.; Downs, J. In *Air Quality VII Conference* Arlington, Virginia, USA, 2009.

[18] Fryda, L.; Sobrino, C.; Glazer, M.; Bertrand, C.; Cieplik, M. *Fuel* **2012**, *92*, 308-317.

[19] Fryda, L.; Sobrino, C.; Cieplik, M.; van de Kamp, W. L. *Fuel* **2010**, *89*, 1889-1902.

[20] Morris, W. J. *An Examination of Pulverized Coal Combustion Aerosols in Air and in Oxyfuel Combustion Environments*. University of Utah, 2011.

[21] Linak, W. P.; Miller, C. A.; Seames, W. S.; Wendt, J. O. L.; Ishinomori, T.; Endo, Y.; Miyamae, S. *Proceedings of the Combustion Institute* **2002**, *29*, 441-447.

[22] Quann, R. J.; Sarofim, A. F. *Symposium (International) on Combustion* **1982**, *19*, 1429-1440.

[23] Somasundaran, P. *Encyclopedia of Surface and Colloid Science*; CRC Press: Boca Raton, 2006.

[24] Casuccio, G. S.; Janocko, P. B.; Lee, R. J.; Kelly, J. F.; Dattner, S. L.; Mgebroff, J. S. *Journal of the Air Pollution Control Association* **1983**, *33*, 937-943.

[25] Chen, W.; Fryrear, D. W. *Journal of Sedimentary Research* **2001**, *71*, 365-371.

[26] Gallagher, N. B.; Bool, L. E.; Wendt, J. O. L.; Peterson, T. W. *Combustion Science and Technology* **1990**, *74*, 211-221.

[27] Gallagher, N. B.; Peterson, T. W.; Wendt, J. O. L. *Symposium (International) on Combustion* **1996**, *26*, 3197-3204.

[28] Neville, M.; Sarofim, A. F. *Fuel* **1985**, *64*, 384-390.

[29] Chen, J.; Yao, H.; Zhang, L. *Fuel* **2012**, *102*, 386-395.

[30] Raask, E. *Mineral Impurities in Coal Combustion: Behavior, Problems, and Remedial Measures*; Hemisphere Publishing Corporation: New York, 1985.

[31] Walsh, P. M.; Sarofim, A. F.; Beer, J. M. *Energy & Fuels* **1992**, *6*, 709-715.

[32] Sheng, C.; Li, Y. *Fuel* **2008**, *87*, 1297-1305.

[33] Zhan, Z.; Wendt, J. O. L. In *3rd Oxyfuel Combustion Conference* Ponferrada, Spain, 2013.

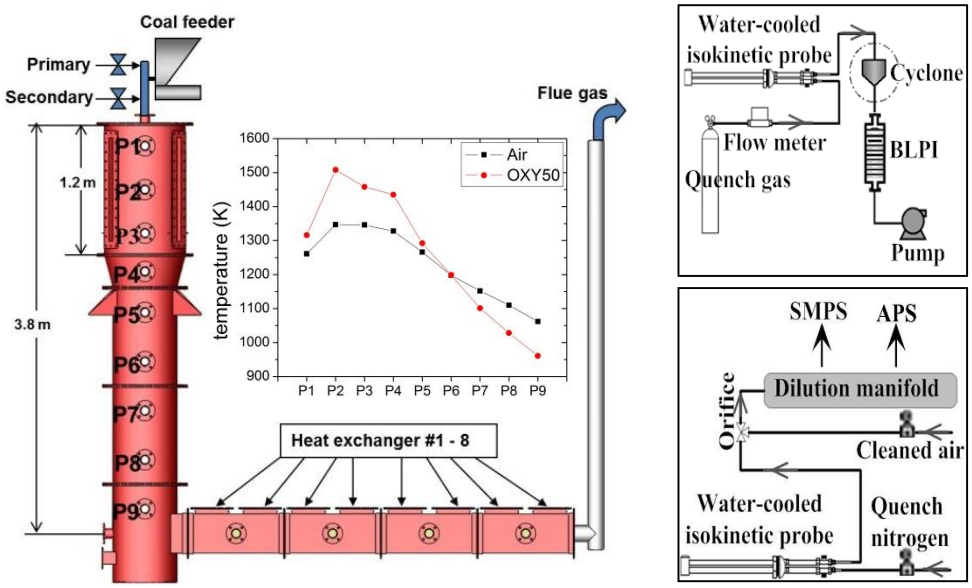

Figure 4.1 Oxy-fuel combustor (OFC) structure, temperature profiles and ash aerosol sampling systems.

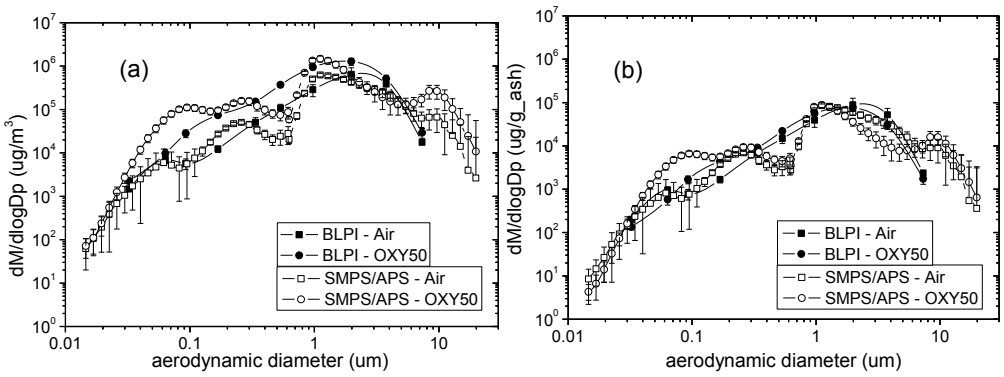

Figure 4.2 Ash aerosol PSD measurements by BLPI and SMPS/APS from air and OXY50 combustion: (a) volume-based; (b) input-ash based.

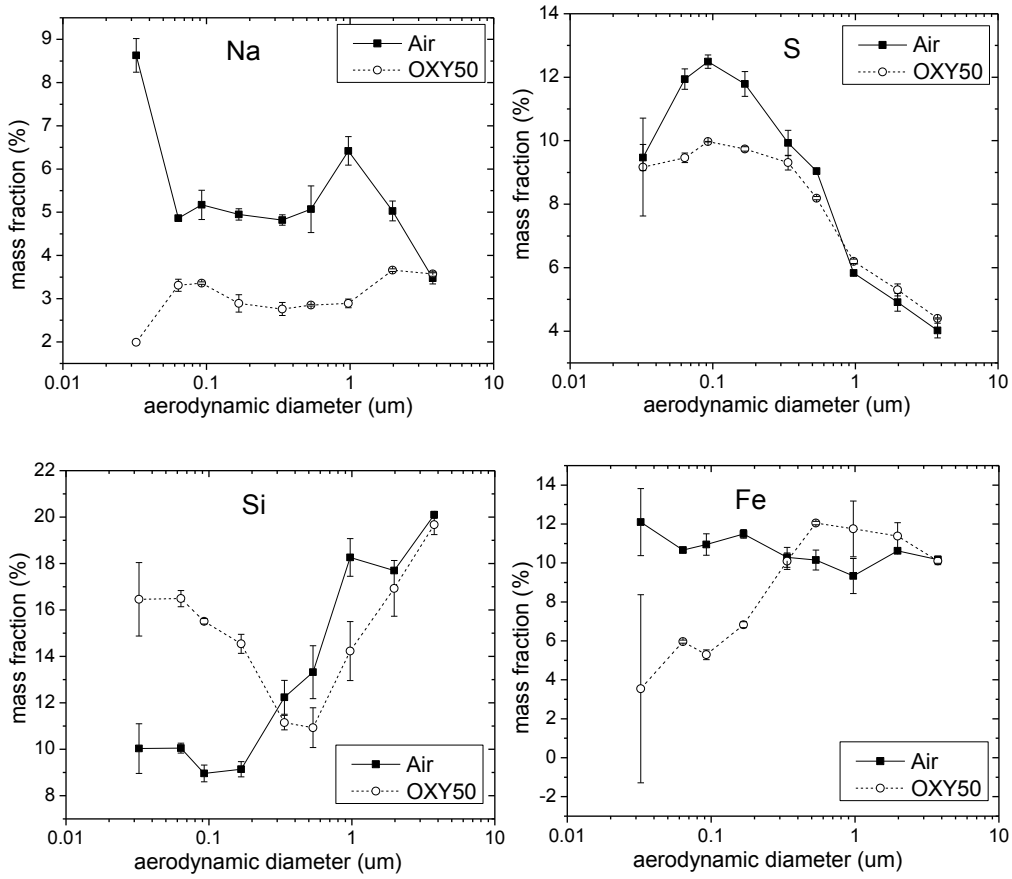

Figure 4.3 Size segregated concentrations of Na, S, Si and Fe in the ash aerosol from air and OXY50 combustion.

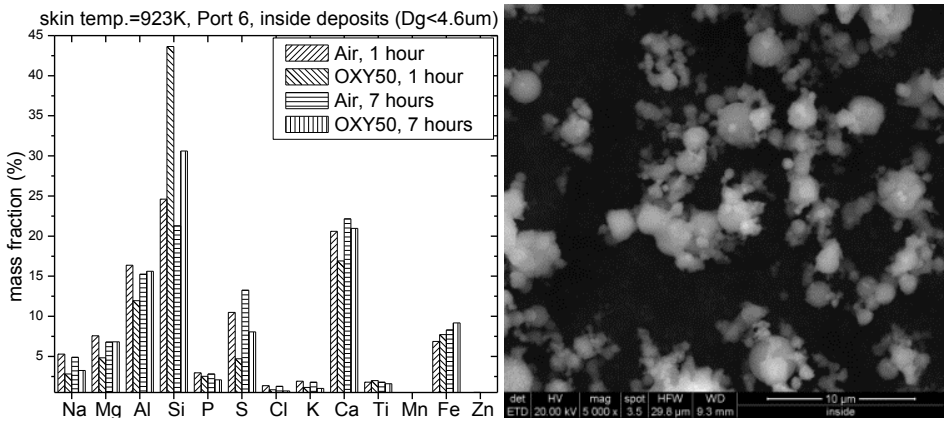

Figure 4.4 Inside deposits: (a) Elemental compositions of inside deposits (geometric size less than 4.6 μm) from air and OXY50 combustion; (b) SEM image of inside deposits.

CHAPTER 5

ASH FORMATION AND DEPOSITION DURING OXY-COAL COMBUSTION IN A 100 KW LABORATORY COMBUSTOR WITH VARIOUS FLUE GAS RECYCLE OPTIONS[1]

5.1 Abstract

Fouling and slagging processes are important in oxy-coal combustion processes because they greatly influence heat transfer and boiler performance. Ash partitioning processes are precursors to deposition processes and so in order to predict the latter one must have a good understanding of the former. This work involves a 100 kW rated down-fired oxy-fuel combustor outfitted with sophisticated ash aerosol and ash deposit sampling equipment. The work differs from that previously published, in that here we focus on the effects of changes in the composition and amounts of actual recycled flue gas (RFG) streams used in oxy-coal combustion, not using once-through CO_2, as before. Conditions examined here included oxy-coal combustion with three different RFG cleanup options

[1] Reprinted with permission from Zhan, Z.; Fry, A.; Yu, D.; Xu, M.; Wendt, J., Ash Formation and Deposition during Oxy-coal Combustion in A 100 kW Laboratory Combustor with Various Flue Gas Recycle Options. To be accepted by *Fuel Processing Technology*.

and two different RFG amounts, and results consist of size segregated compositions of the ash aerosol and spatially resolved compositions within the deposits. In general, results suggested that oxy-combustion conditions did not cause major changes in ash partitioning, fouling and slagging. There are, however, changes in both the compositions of the ultrafine particles and in that of the inner layer of the deposits, and these were due to higher flame temperatures, when these occurred. These results are discussed and interpreted in detail.

5.2 Introduction

CO_2, one of the main contributors to climate change [1], attracts more and more attention. As a major source of CO_2 emissions, the pulverized coal combustion power generation industry is likely to have to confront CO_2 capture and sequestration in the foreseeable future. Oxy-coal combustion, which yields a CO_2 rich exhaust gas suitable for sequestration, burns coal in a mixture of pure oxygen and recycled flue gas (RFG), rather than in air. It is a promising option for retrofit to existing, or slightly modified, coal fired power plants. Numerous studies have been conducted to evaluate this technology and have been summarized in several comprehensive reviews [2-7].

Ash formation is an important concern in coal combustion due to the formation of slagging deposits, fouling deposits and particulate matter emissions [8-9]. Slagging deposition is made up of the fused ash that sticks on the furnace walls in the radiation zone, while fouling deposition is the friable ash that adheres to heat transfer tubes in the convection zone. These ash deposits (slagging and fouling) on furnace walls would produce changes to radiative heat transfer in the radiation zone and increased resistance to heat transfer in the convection zone. They can cause corrosion and even accidents [8]. Particulate matter is the fine ash aerosol, a portion of which can penetrate the ash collection

system, causing a hazardous air pollutant emission into the atmosphere. Therefore, knowledge of ash formation and ash deposition during oxy-coal combustion is required to evaluate the impact of this technology when retrofitting existing units from air to oxy-firing.

Ash formation during coal combustion is a complex process of mineral transformations, which include fragmentation, vaporization, coalescence, condensation, reaction, nucleation and coagulation [9]. The ash aerosol will then deposit to form slagging, fouling deposits and airborne particulate matter. Information on the ash aerosol is, therefore, essential to help understand and alleviate deposition consequences.

Currently, few studies are reported on both ash aerosol and ash deposit formation during oxy-coal combustion. As far as ash aerosol research is concerned, tests [10-12] conducted on bench-scale facilities show consistent results, namely, compared to air combustion, oxy-coal combustion with the same input O_2 concentration shifts the peak of ultrafine vaporization mode ash aerosol to a smaller size. Increasing the inlet O_2 concentration moves the peak of the ultrafine vaporization mode to a larger size. Its concentration also increases. The effect of inlet O_2 concentration on ash aerosol formation is due largely to the effect of differences in combustion temperature. Higher combustion temperature from the higher inlet O_2 concentration case vaporizes more ash in the ultrafine vaporization mode, increasing coagulation rates and moving the peak of the ultrafine vaporization mode to a larger size. However, the research [13-14] performed on pilot-scale facilities exhibits inconsistent results. Under a similar furnace temperature profile for air and oxy-coal combustion, Yu [14] suggests insignificant differences in both ash aerosol particle size distribution (PSD) and chemical composition, while Li [13] shows that oxy-coal combustion produces more fine ash aerosol. For ash deposition, contradictions also

exist in the literature for both ash deposition rates [13-18] and deposit chemistries [14,16,18-19]. These have been summarized in our previous study [20] and might be due to variations in coals, combustion conditions, sampling parameters, as well as insufficient spatial resolution of mineral concentrations within the deposits [20].

Using a novel deposition probe we demonstrated that it was important to spatially segregate ash deposits into initial and outer deposit layers [20]. Then, the size segregated composition of the ash aerosol was related to that of initial layer of the deposits [21]. The results suggested that initial layer deposits consisted of the vaporization mode ash aerosol transported to the surface by thermophoresis. The previous work, however, focused on oxy-coal combustion experiments with pure once through CO_2 as the diluent for oxygen. This did not allow for variations in SO_2, water, and ash content in the recycle stream. The current work reported here builds on the previous work [20-21] but extends it to oxy-coal combustion with actual recycled flue gases, of various compositions and in various amounts. The objective was to explore the impact of various practically realizable RFG cleanup options on the resulting ash aerosol and deposit. Other work from our laboratory dealt with total (not spatially resolved) ash deposits on uncooled ceramic surfaces, also with once through CO_2 [14]. Other published work [22] using actual RFG focused only on the ash aerosol, and not simultaneously on the ash deposit, as did this work. The relationship between the size segregated composition of the ash aerosol from a given coal and the composition of the segregated inside fouling deposits is an important feature of this work. Additional focus here is also on the uncooled slagging deposits obtained in the radiation zone, where all experiments described below were performed using actual RFG, not once through CO_2 as the diluent.

5.3 Materials and Methods

5.3.1 Experimental Facility

A pilot-scale Oxy-Fuel Combustor (OFC) with an FGR system was used in this work. The OFC allows systematic controlled tests, but still represents combustion conditions of commercial-scale units, especially in terms of temperatures, particle concentration and mixing. More details about OFC can be found elsewhere [20,23].

A bag house system, installed after convection zone, was used for fly ash removal [24], as shown in Figure 5.1(a). It utilizes six fabric filters [0.14 × 0.79 m (diameter × length)], which are made of nomex cloth and could operate at temperatures as high as 473 K. A gas-injected pulse system is designed to prevent ash particle buildup on the filters. Either CO_2 from a CO_2 tank donated by Praxair (for oxy-coal combustion) or compressed air (for air combustion) could be injected into the bag house to shake off the ash particles. The pulse interval is set at 300 seconds and each pulse lasts for 999 milliseconds. The filters could be removed for experiments employing FGR without particle removal (dirty recycle).

A condenser, as shown in Figure 5.1(b), was used to remove the moisture in the flue gas [24]. To reduce air leaking in as much as possible in oxy-coal combustion with RFG, pressure resistance in the RFG stream needs to be minimized. Therefore, the condenser is designed to be a two-stage direct contact heat exchanger, with water as the cooling medium. The first stage is that flue gas enters from the bottom of the condenser and bubbles up through the water. The second stage is the spray of cold water from the top of the condenser, while the flue gas flows up and exits from the top of the condenser. This process could help cool down the flue gas to below 43 ℃ with little pressure drop. When the cooling water contains dissolved (and suspended) lime (CaO), the condenser acts as both condenser and scrubber to remove both H_2O and SO_2 from the flue gas. The condenser is

located downstream of the bag house and could be bypassed by manually disconnecting it.

Two blowers, as shown in Figure 5.2, were used for the RFG stream [24]. One is a small size blower, which could produce high pressure (25 kPa) recycle, but is functional only for clean low temperature flue gas. The other is a very much oversized blower, which produces only low pressures (5 kPa) and could work for high temperature (505 K) and particle laden flue gas. The large oversized blower is used only for particle laden recycle (dirty recycle) case, and only 5% of the gas recycled in that blower is drawn off for the dirty RFG stream. The remaining 95% is recycled through the blower, in order to allow it to operate at its design capacity, which is necessary in order for it to handle particle laden gases. This facet of the design had ramifications as noted in the results section below. The oversized blower with "internal" 95% recycle is used for RFG of dirty flue gas, while the small blower is used for all the other FGR cases.

5.3.2 Sampling Systems

A Berner low pressure impactor (BLPI), a scanning mobility particle sizer (SMPS, model 3080; with Model 3081 long differential mobility analyzer (DMA)) and an aerodynamic particle sizer (APS, model 3321) were used for size segregated ash aerosol samples and PSD measurements extracted from port 9. The BLPI has a 50% aerodynamic cutoff diameters of 15.7, 7.33, 3.77, 1.98, 0.973, 0.535, 0.337, 0.168, 0.0926, 0.0636, and 0.0324 μm. Cellulose acetate membranes were used as substrates to collect ash aerosol samples for subsequent chemistry analysis. Aluminum substrates coated with Apiezon grease were used to determine gravimetric PSD's, together with a high-quality Mettler Toledo balance with a precision of 0.1 μg. The SMPS and APS provided PSD's in the size ranges of 0.0143 μm ~ 0.6732 μm and 0.532 μm ~ 20 μm, respectively. The SMPS and

APS data were merged and plotted together. Details of the aerosol sampling systems can be found elsewhere [21]. Collection of fouling deposit samples was achieved using a novel surface temperature controlled ash deposition probe system that allowed the separation of fouling deposits into inside, outside, vertical and side deposits, as described in a previous paper [20]. The probe surface temperature was kept at 923 K with a holding time of 1 hour and location of port 6 [20], where the flue gas temperature is similar to those around the superheaters in full scale units. In addition to this, an uncooled ceramics tube [0.03×0.12 m (diameter $\times$ length)], attached to the end of a water-cooled stainless probe, was used to collect slagging deposits. The slagging deposits on the ceramics tube were scraped off for further analysis. The slagging deposits were collected at port 4 [20] right off the flame in the radiation zone, with a holding time of 2 hours.

5.3.3 Experimental Conditions and Analysis Methods

Ash aerosols and ash deposition data were obtained from cases of oxy-coal combustion with three different RFG cleanup options and two different RFG amounts. The three different RFG cleanup options are:

1) RFG with ash removed, which means recycling the flue gas right after the bag house.
2) RFG with ash and moisture removed, which means recycling the flue gas right after the condenser.
3) RFG with ash, moisture and sulfur removed, which means recycling the flue gas right after the scrubber.

The two different RFG amounts are:

1) 27 vol. % O_2 / 73 vol. % RFG (overall) in oxy-coal combustion.

2) 50 vol. % O_2 / 50 vol. % RFG (overall) in oxy-coal combustion.

The first condition represents that in which radiant heat fluxes between oxy and air firing are matched [7]. Previous data [14] have shown no significant difference between 27% inlet O_2 and 32% inlet O_2, which matches adiabatic flame temperatures. The second condition allows large changes in RFG amount to be investigated. The flame temperatures are 1334 ± 20 K and 1441 ± 10 K for OXY27 cases and OXY50 cases, respectively (measured by K-type unshielded thermocouple. Therefore the measured temperatures are lower than actual temperatures but offer a relative value.).

All these cases are labelled as shown in Table 5.1. A dirty recycle case (RFG with nothing removed) was also attempted for the OXY27 case. However, the operation did not yield reasonable results in that the data obtained suggested that recycling dirty flue gases without particulate removal yielded lower particle concentrations in the exhaust, rather than higher, as would be expected. We now believe that the internal recycle around the oversized blower that was used for RFG in these tests, removed these particles with condensed water within the piping. Therefore, the dirty recycle case with the oversized blower and internal recycle and no baghouse is not further discussed in this work. It might be noted that this newly uncovered problem calls into question some of the results of Morris et al. [22], who showed, using a similar system, that dirty recycle appeared to remove exhaust soot, a process that was then attributed to reburning, but might in fact have removed the soot physically in the internal recycle loop.

A Powder River Basin (PRB) coal was the only coal used in the research presented here. Future work will present results from other coals. PRB coal is a subbituminous coal, with high moisture content (23.69 wt. %), low ash and low sulfur. Its proximate analysis, ultimate analysis and ash composition data are shown in Table 3.1 and Table 3.2 [21].

O_2 and CO_2 (for baghouse pulse) needed in the combustion were supplied by the Praxair O_2 and CO_2 storage tanks. No pure CO_2 was injected into the combustion system for oxy-coal combustion cases with RFG. The furnace wall temperature at the ignition zone was set at 1283 K (1850 F). The coal feed rate was set at 4.54 kg/h (10 lb/h). Excess oxygen in the exhaust was fixed at 3 vol. % (dry). CO_2 concentrations in flue gas for all these cases were between 88-95 vol.% (dry). The OFC was always at a slightly positive inside pressure to prevent air leakage.

We experienced some problems due to limitations of the OFC during actual furnace operation under these conditions. First, it is difficult to prevent some moisture condensation in the recirculated flue gas. That is because the RFG temperature is limited by the maximum working temperature (377 K) of the smaller FGR blower. At the OFC scale the high surface to volume ratio in the pipe downstream of the blower exacerbates the flue gas cooling rate. Furthermore the moisture removal system did not remove the moisture completely (for this high moisture PRB coal) and so the flue gas leaving the scrubber is saturated at temperatures of about 316 K for OXY27 cases and 303 K for OXY50 cases. The saturated vapor pressures of water removed cases are 11.7 kPa and 6.6 kPa for OXY27 and OXY50 respectively, while those of water contained cases are 20 kPa and 17.3 kPa for OXY27 and OXY50, respectively.

5.4 Results and Discussion

5.4.1 Ash Aerosol PSD

Ash aerosol PSD's were measured gravimetrically by BLPI and through electric mobility and light scattering through SMPS/APS. Results are shown in Figure 5.3 (gravimetric PSD's) and Figure 5.4 (electric mobility and light scattering PSD's) for all the

runs listed on Table 5.1. Figure 5.3(a) is volume based ash aerosol PSD, that is, aerosol mass per unit volume of flue gas ($\mu g/m^3$) versus particle size (μm). It contains the information on ash aerosol concentrations, showing that ash aerosol concentrations in the OXY50 cases are higher in all size ranges, when compared to the OXY27 cases. Figure 5.3(b) is based on the aerosol mass per unit input ash (μg/g) versus particle size (μm). It accounts for the changes in flue gas volume, and shows that the OXY50 cases actually produce more ash aerosol in the submicron particle size range. Figure 5.4 compares the BLPI data of Figure 5.3 to the analogous SMPS/APS data. The latter has a finer particle size resolution and potentially can uncover finer detail regarding PSD modes and consequently different particle formation mechanisms. In general, the two PSD measuring technologies show consistent results even though there is an apparent discrepancy at around 0.6 μm which is at the upper limit of accuracy of the SMPS and the lower limit of accuracy of the APS. Nevertheless, both the gravimetric and the electric mobility/light scattering technique show two PSD modes in the submicron region, at the same locations. The SMPS data show them more clearly because of the increased resolution.

The BLPI offers a fairly narrow size range PSD (0.0324 μm ~ 7.33 μm), and is able to show three modes over its entire particle size range (Figure 5.3): a distinct ultrafine vaporization mode at ~0.06 μm for OXY27 and air conditions and a fine vaporization mode at ~0.17 μm for OXY50 conditions, followed by a fragmentation mode at ~2 μm. The SMPS/APS combination offers a wider size range PSD (0.0143 μm ~ 20 μm), and exhibits four modes, where the first three modes roughly overlap the three modes uncovered by the BLPI, and the largest particle mode lies at ~10 μm. One can identify modes at a particle size smaller than 0.1 μm as an ultrafine particle vaporization mode (probably due to nucleation in the probe), whereas the mode centered at a particle diameter of 0.5 μm is the

typical accumulation mode resulting from nucleation and significant coagulation prior to sampling. It is also a vaporization mode. A fine fragmentation mode is centered at around 2.5 μm and the coarse fragmentation mode centered at around 10 μm [25]. The similar PSD's between the air case and all the OXY27 cases suggest that switching from air combustion to oxy-coal combustion at 27% inlet O_2 to match radiant heat flux [7] may not greatly affect the ash aerosol formation mechanisms, even with different RFG cleanup options applied. However, decreasing the RFG amounts (50% O_2 in the inlet oxidant versus 27% O_2) leads to an increased load of ultrafine particulates, most probably due to the increased flame temperature. The shift of the vaporization mode from 0.06 μm (for OXY27) to 0.17 μm (for OXY50) is likely due to the increased concentration of ultrafines in the OXY50 case to allow more rapid coagulation and hence cause the ultrafine mode to shift to the right [26-27]. This change in ultrafine and fine particle concentrations may impact deposition rates, since the ultrafine and fine particles are the ones that form the initial sticky layer, which is critical to the ultimate rate of fouling [21]. Although different RFG amounts have an apparent effect on vaporization mode particle formation, the RFG's with different cleanup options seem to have insignificant effect on ash aerosol formation, at least in the pilot combustor used here. This is discussed in more detail below.

5.4.2 Ash Aerosol Elemental Compositions

Size-segregated ash composition data are shown in Figure 5.5, for S, Si, Na and Ca respectively. Figures 5.5(a) (c) (e) (g) are the elemental composition for OXY27 and air cases under various RFG cleanup options. Figures 5.5(b) (d) (f) (h) are the elemental composition for OXY50 cases under various RFG cleanup options.

The partitioning of sulfur is shown in the top panel (Figure 5.5(a) (b)). For both OXY27

and OXY50 cases sulfur is concentrated in the vaporization mode particles. However, in order to interpret the sulfur, and to some extent the Na, data, one must consider removal of sulfur (and Na_2SO_4) by water within the piping downstream of the baghouse, which was kept at approximately a constant temperature for all cases. Results for these recycle options are therefore unique to the cooling rates experienced in this equipment, and may not be valid for all full scale systems. Data show that with no water or sulfur removed, but only ash removed, there is less sulfur in the particles for the OXY50 case than in the OXY27 case. This is because, in the OXY50 case, more sulfur is removed in the piping downstream of the baghouse, at the lower RFG flow rates and longer (post baghouse) residence times. Therefore, when the water in the RFG is removed for the OXY50 case, there is a large increase of S in the ultrafines. Removal of sulfur by SO_2 scrubbing from the RFG lowers the concentration of S in the vaporization mode particles for both OXY27 and OXY50, as is to be expected. The higher sulfur content in the ultrafines for OXY27 compared to OXY50 (except for ash and water removed case) is consistent with the results also reported by Sheng [11] who shows higher S concentration in OXY20 compared to OXY40 case. This is associated with the fate of Na, the reaction between Na and Si and the reaction between Na and S, as discussed in greater detail below.

Comparison of Figure 5.5(c) and (d) suggests that with only ash removed in the FGR, the partitioning of Na in the ultrafines is higher for OXY27 cases than for OXY50. This is maybe due to the effect of increasing temperature on increasing the reaction rate of the scavenging reaction between Na and silica or alumina-silicate particles [28]. Note that for OXY50 the Na (Figure 5.5d) very roughly tracks the Si (Figure 5.5f), whereas for OXY27 it does not (Figure 5.5c, e). The effect of different RFG cleanup options on Na for the OXY50 cases is consistent with the hypothesis that Na_2SO_4 is removed by condensing

water in the piping downstream of the baghouse. The highest Na content is found in all particle sizes when water and ash but not sulfur are removed. Without sulfur, there can be no formation of sulfate in the pipe, and without water any sulfate particles formed are not removed. Most of the sodium, however is bound with the silicon, which it tracks. Only a small fraction of Na is sulfated in the piping, leading to the trend observed in Figure 5.5d).

Si is rich in both ultrafine vaporization mode and fine fragmentation mode for OXY50 cases, while merely rich in fine fragmentation mode for OXY27 cases. It roughly tracks Na for OXY50 but not for OXY27. Both effects can be explained by the higher temperatures for OXY50, which vaporize more silicon and enhance the reaction rate of silicon and sodium in the combustor. Quantitative conclusions based on correlations between elements are reached with difficulty because interactions between Na and Si (in the combustor) and Na and S (in the cool flue gas), and the effect of condensed water in the pipe downstream of the baghouse all complicate interpretations of apparent correlations between the size segregated concentrations of Si, Na, and S. Comparison of the size segregated distribution of Ca in OXY27 (Figure 5.5g) to that in OXY50 (Figure 5.5h) suggests that increased temperature (in the OXY50 case) yields increased amounts of Ca in the smaller particles. The effect of various RFG cleanup options (H_2O and S) on Si and Ca transformation is negligible suggesting that Ca and Si did not interact with S or H_2O in the piping downstream of the baghouse, and this respect differed from Na.

5.4.3 Relationship among Ash Aerosol, Fouling and Slagging Deposition Chemistry

Elemental mass fraction of inside fouling deposits is shown in Figure 5.6, for S, Si, Na and Ca, respectively. According to previous research [21], vaporization mode ash aerosol

is the main contributor to inside layer deposits. Here, the effects of higher concentration of S in vaporization mode ash aerosol for OXY27 cases and higher concentration of Si in vaporization mode ash aerosol for OXY50 cases are to produce higher concentration of S in inside deposits for OXY27 cases and higher concentration of Si in inside deposits for OXY50 cases, correspondingly. The relationship of Na in ash aerosol and inside fouling deposits is not clear, possibly due to low concentration of Na. The story of Ca is not clear and needs further analysis.

Figure 5.7 shows the elemental mass fraction of slagging deposits, for S, Ca, Na and Si respectively. It can be seen that OXY27 cases have more S and Ca in slagging deposition, compared to OXY50 cases. This is most likely due to the decreased stability of sulfur containing compounds at higher combustion temperature for OXY50 cases. Furthermore, the chemical form of S and Ca in slagging deposition in OXY27 cases is presumed to be $CaSO_4$. The results also show that concentration of Na and Si in slagging deposition in OXY50 cases is twice as much as in OXY27 cases. These are expected because of higher combustion temperature in OXY50 cases and the scavenging reaction between Na and Si. Higher combustion temperature will increase the vaporization of Si, which then helps increase the scavenging reaction rate [28]. The sodium-silicates or sodium-aluminum-silicate formed from the scavenging reaction normally are sticky and could be easily captured as slagging deposition.

It is further found that, compared to OXY27 cases, the concentrations of S are always less in OXY50 cases for all three different categories of ash (aerosols, fouling and slagging deposits). It is likely that OXY50 cases have higher S retention in the bulk ash than OXY27 cases due to higher combustion temperature, as reported in previous research [14], while OXY27 cases have higher S deposition (fouling and slagging) tendency.

5.5 Conclusions

Size segregated ash aerosols and ash deposition (fouling and slagging) data were obtained from oxy-coal combustion conditions, with various RFG cleanup options and RFG amounts. The ash aerosols measured by BLPI and SMPS/APS show similar PSD results, which suggest switching from air combustion to oxy-coal combustion with different RFG cleanup options and RFG amounts may not greatly affect the ash aerosol formation mechanisms. However, the vaporization mode peak shifts from 0.06 μm to 0.17 μm when switching from OXY27 to OXY50 due to higher combustion temperature in OXY50 cases. In addition, compared with OXY27 cases, OXY50 cases also increase the formation of vaporization mode particles. That change might lead to a higher ash deposition propensity for OXY50 cases than OXY27 cases.

Sulfur is concentrated in vaporization mode. Removal of sulfur by water within the RFG piping stream effects the mass size distribution of sulfur, and simultaneously effects that of sodium. The mass fraction of Na in ash aerosols is slightly higher in OXY27 cases than in OXY50 cases for vaporization modes. This is likely due to the increased reaction rate for the scavenging reaction between Na and silicate or alumina-silicate particles in OXY50 cases because of higher combustion temperature and higher vaporized Si concentrations. Vaporization mode ash aerosol is the main contributor to inside layer deposits.

In the respect of slagging deposits, OXY27 cases produce more S and Ca, and less Na and Si in slagging deposition, compared to OXY50 cases. This is most likely due to the decreased stability of sulfur containing compounds and increased scavenging reaction between Na and Si at higher combustion temperature for OXY50 cases.

RFG's with different cleanup options seem to have an insignificant effect on ash

transformation in oxy-coal combustion. The realistic limitations during RFG operation might diminish the difference of expectation. In addition, it could be inferred that OXY50 cases have higher S retention in the bulk ash than OXY27 cases due to higher combustion temperature, while OXY27 cases have higher S deposition (fouling and slagging) tendency.

5.6 References

[1] IPCC *Contribution of Working Groups I, II and III to The Fourth Assessment Report of The Intergovernmental Panel on Climate Change*, 2007.

[2] Buhre, B. J. P.; Elliott, L. K.; Sheng, C. D.; Gupta, R. P.; Wall, T. F. *Progress in Energy and Combustion Science* **2005**, *31*, 283-307.

[3] Chen, L.; Yong, S. Z.; Ghoniem, A. F. *Progress in Energy and Combustion Science* **2012**, *38*, 156-214.

[4] Scheffknecht, G.; Al-Makhadmeh, L.; Schnell, U.; Maier, J. *International Journal of Greenhouse Gas Control* **2011**, *5, Supplement 1*, S16-S35.

[5] Toftegaard, M. B.; Brix, J.; Jensen, P. A.; Glarborg, P.; Jensen, A. D. *Progress in Energy and Combustion Science* **2010**, *36*, 581-625.

[6] Wall, T.; Liu, Y.; Spero, C.; Elliott, L.; Khare, S.; Rathnam, R.; Zeenathal, F.; Moghtaderi, B.; Buhre, B.; Sheng, C.; Gupta, R.; Yamada, T.; Makino, K.; Yu, J. *Chemical Engineering Research and Design* **2009**, *87*, 1003-1016.

[7] Wall, T. F. *Proceedings of the Combustion Institute* **2007**, *31*, 31-47.

[8] Bryers, R. W. *Progress in Energy and Combustion Science* **1996**, *22*, 29-120.

[9] Xu, M.; Yu, D.; Yao, H.; Liu, X.; Qiao, Y. *Proceedings of the Combustion Institute* **2011**, *33*, 1681-1697.

[10] Jia, Y.; Lighty, J. S. *Environmental Science & Technology* **2012**, *46*, 5214-5221.

[11] Sheng, C.; Li, Y.; Liu, X.; Yao, H.; Xu, M. *Fuel Processing Technology* **2007**, *88*, 1021-1028.

[12] Suriyawong, A.; Gamble, M.; Lee, M. H.; Axelbaum, R.; Biswas, P. *Energy & Fuels* **2006**, *20*, 2357-2363.

[13] Li, G.; Li, S.; Dong, M.; Yao, Q.; Guo, Y.; Axelbaum, R. L. *Fuel* **2013,** *106*, 544-551.

[14] Yu, D.; Morris, W. J.; Erickson, R.; Wendt, J. O. L.; Fry, A.; Senior, C. L. *International Journal of Greenhouse Gas Control* **2011**, *5, Supplement 1*, S159-S167.

[15] Jones, M.; Pavlish, B.; Kay, J.; Laumb, J.; Downs, J. In *Air Quality VII Conference* Arlington, Virginia, USA, 2009.

[16] Fryda, L.; Sobrino, C.; Glazer, M.; Bertrand, C.; Cieplik, M. *Fuel* **2012**, *92*, 308-317.

[17] Weller, A. E.; Rising, B. W.; Boiarski, A. A.; Nordstrom, R. J.; Barrett, R. E.; Luce, R. G. *Experimental Evaluation of Firing Pulverized Coal in A CO_2/O_2 Atmosphere*, 1985.

[18] Fryda, L.; Sobrino, C.; Cieplik, M.; van de Kamp, W. L. *Fuel* **2010**, *89*, 1889-1902.

[19] Wigley, F.; Goh, B. In *1st Oxyfuel Combustion Conference* Cottbus, Germany, 2009.

[20] Zhan, Z.; Bool, L. E.; Fry, A.; Fan, W.; Xu, M.; Yu, D.; Wendt, J. O. L. *Energy & Fuels* **2014**, *28*, 146-154.

[21] Zhan, Z.; Fry, A.; Zhang, Y.; Wendt, J. O. L. *Proceedings of the Combustion Institute* **2015**, *35*, 2373-2380.

[22] Morris, W. J.; Yu, D.; Wendt, J. O. L. *Proceedings of the Combustion Institute* **2013**, *34*, 3453-3461.

[23] Zhang, J. *Oxy-coal Combustion: Stability of Coaxial Pulverized Coal Flames in O_2/CO_2 Environments*. University of Utah, 2010.

[24] Morris, W. J. *An Examination of Pulverized Coal Combustion Aerosols in Air and in Oxyfuel Combustion Environments*. University of Utah, 2011.

[25] Linak, W. P.; Miller, C. A.; Seames, W. S.; Wendt, J. O. L.; Ishinomori, T.; Endo, Y.; Miyamae, S. *Proceedings of the Combustion Institute* **2002**, *29*, 441-447.

[26] Quann, R. J.; Sarofim, A. F. *Symposium (International) on Combustion* **1982**, *19*, 1429-1440.

[27] Somasundaran, P. *Encyclopedia of Surface and Colloid Science*; CRC Press: Boca Raton, 2006.

[28] Gallagher, N. B.; Peterson, T. W.; Wendt, J. O. L. *Symposium (International) on Combustion* **1996**, *26*, 3197-3204.

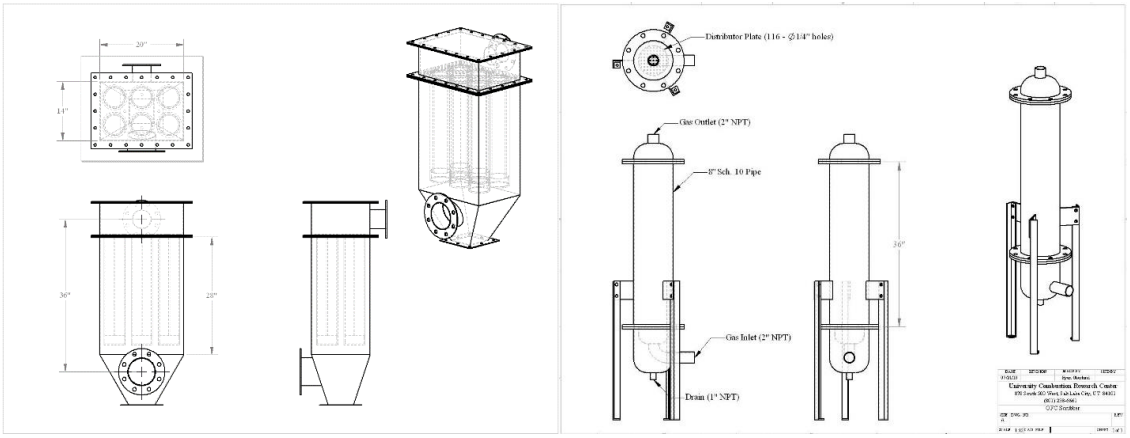

Figure 5.1 RFG system: (a) bag house system and (b) moisture/sulphur removal system.

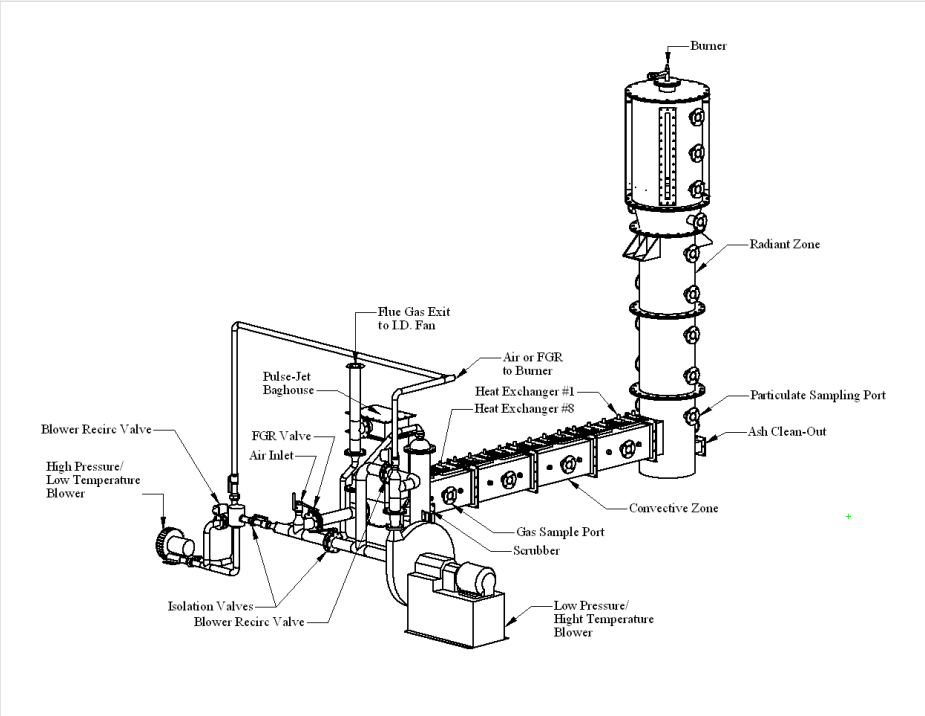

Figure 5.2 OFC with RFG system.

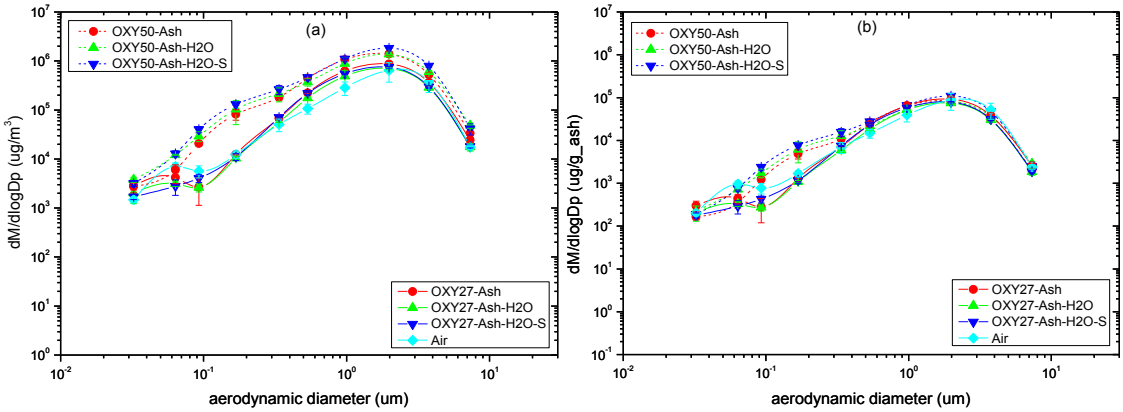

Figure 5.3 PSD from BLPI: (a) volume based; (b) input ash based.

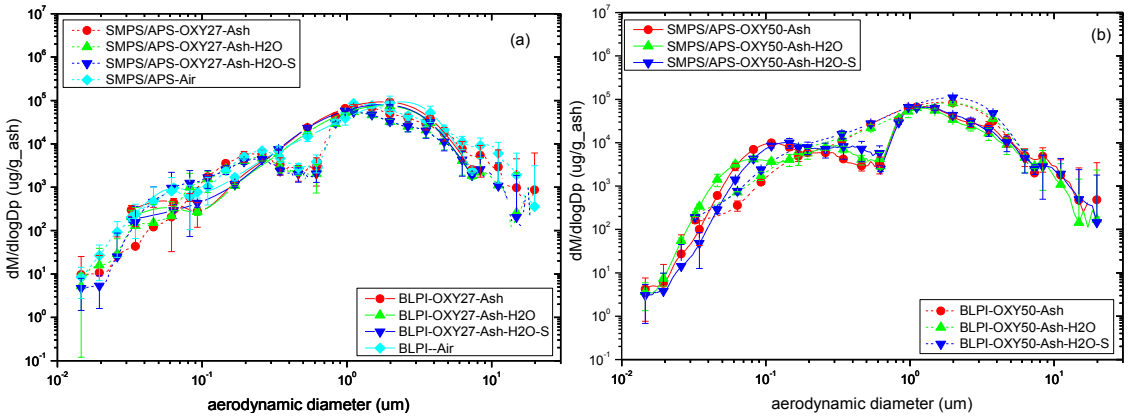

Figure 5.4 Ash based PSD from SMPS/APS and BLPI: (a) Air and OXY27 cases; (b) OXY50 cases.

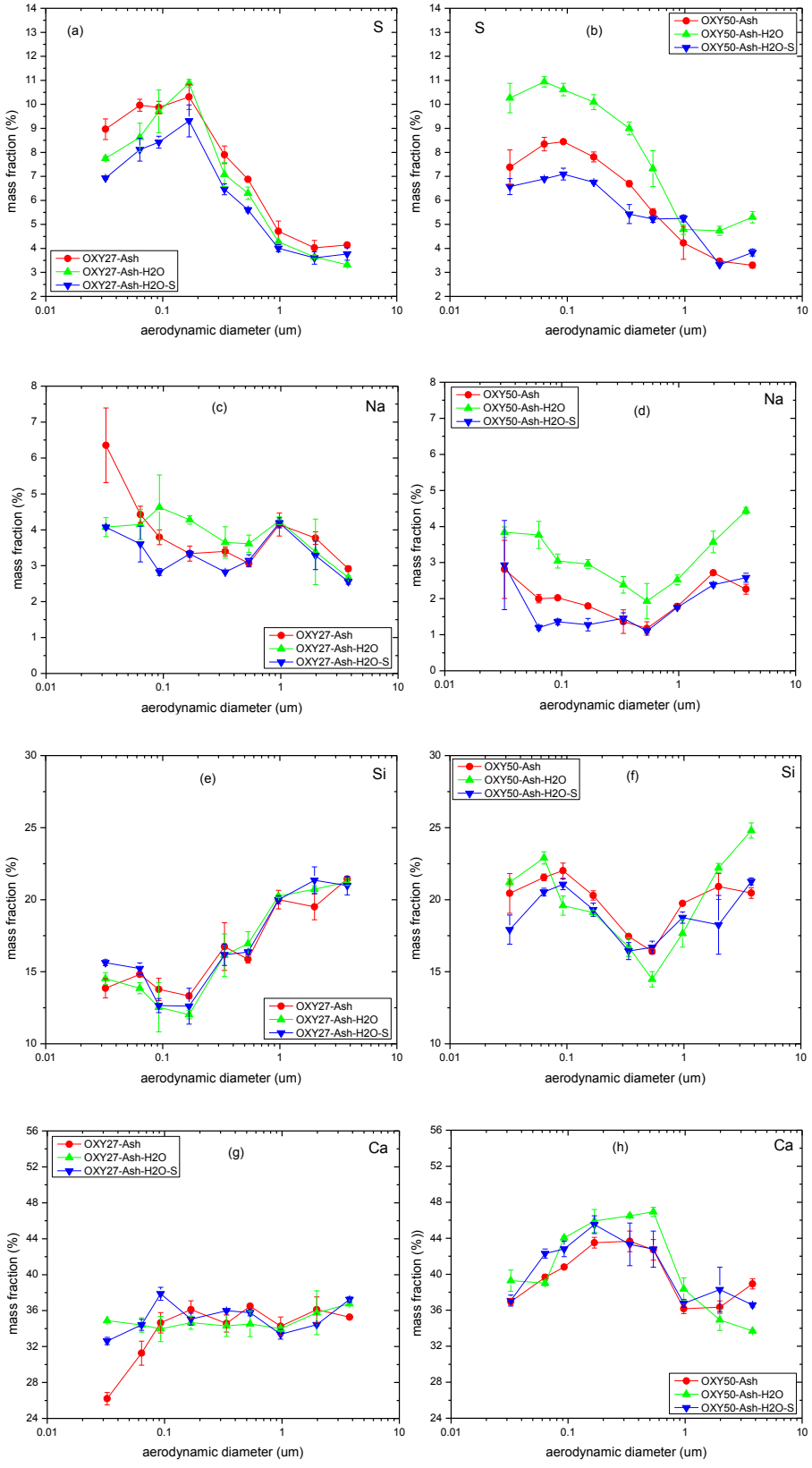

Figure 5.5 Elemental mass PSD of ash aerosols from BLPI: Na, S, Si and Ca.

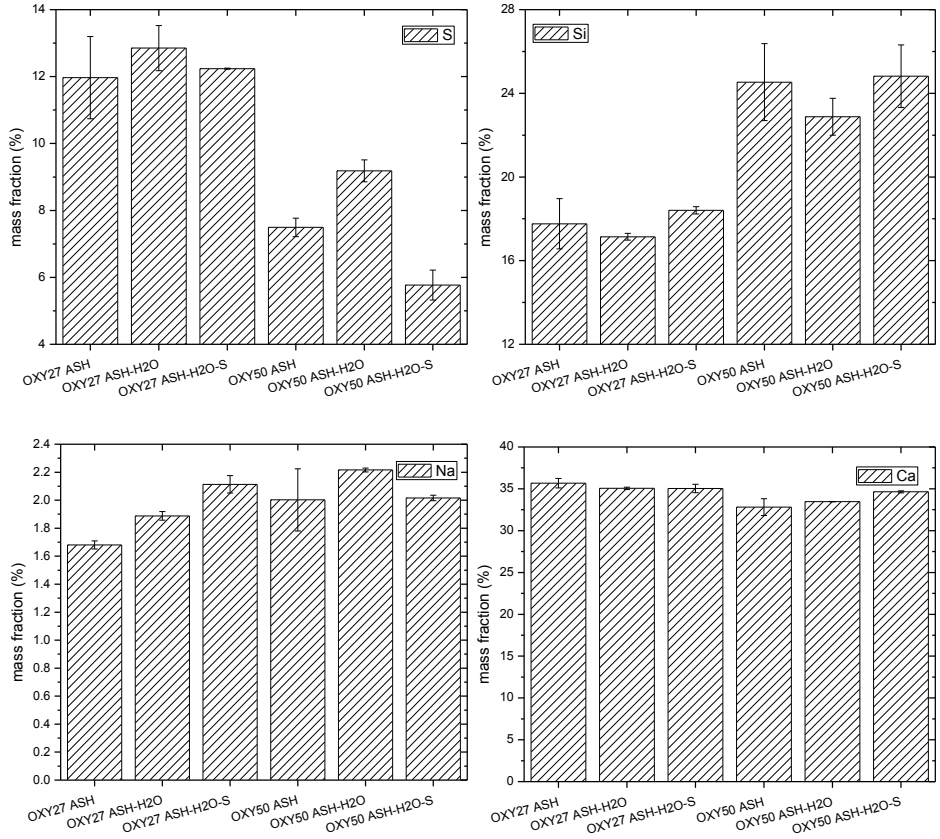

Figure 5.6 Elemental mass fraction of inside deposit from RFG cases: S, Si, Na and Ca.

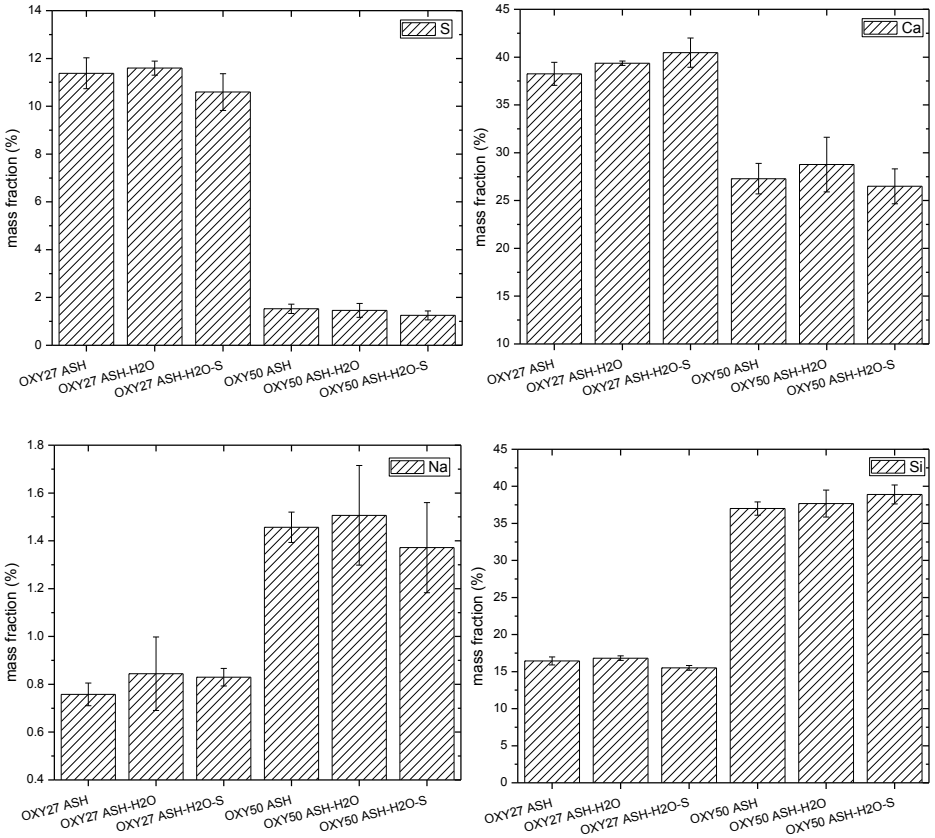

Figure 5.7 Elemental mass fraction of slagging deposits from RFG cases: S, Ca, Na and Si.

Table 5.1 Experimental cases abbreviation and description.

Case abbreviation	Description
OXY50-Ash	oxy-coal combustion with 50% inlet O_2 and 50% RFG after bag house
OXY27-Ash	oxy-coal combustion with 27% inlet O_2 and 73% RFG after bag house
OXY50-Ash-H_2O	oxy-coal combustion with 50% inlet O_2 and 50% RFG after condenser
OXY27-Ash-H_2O	oxy-coal combustion with 27% inlet O_2 and 73% RFG after condenser
OXY50-Ash-H_2O-S	oxy-coal combustion with 50% inlet O_2 and 50% RFG after scrubber
OXY27-Ash-H_2O-S	oxy-coal combustion with 27% inlet O_2 and 73% RFG after scrubber

CHAPTER 6

DEPOSITION OF COAL ASH ON A VERTICAL SURFACE IN A 100 KW DOWNFLOW LABORATORY COMBUSTOR: A COMPARISON OF THEORY AND EXPERIMENT[1]

6.1 Abstract

This paper is concerned with deposition rates of coal ash on a vertical surface in a 100 kW rated down-flow laboratory coal combustor. At that scale, flow in the post flame where deposition occurs is laminar, and the deposits on a vertical surface are similar to the early, sticky, inner deposits on horizontal surfaces. Therefore the problem addressed has relevance to understanding mechanisms of deposit formation in general. Experimental data presented here consist of particle size distributions of the ash aerosol, and time resolved measurements of the vertical deposit mass, for various controlled surface temperatures, one coal, and two combustion conditions: air-firing and oxy-firing with 50% inlet O_2. Theory consisted of a transport model in which the criterion on whether an ash particle was captured, depended on a newly introduced "Thermophoresis Number," Tp, which is the ratio of the time taken for the particle to contact the (cold) surface through thermophoresis

[1] Reproduced by permission from Zhan, Z.; Zhou, M.; Fry, A.; Wendt, J. O. L., Deposition of Coal Ash on A Vertical Surface in A 100 kW Downflow Laboratory Combustor: A Comparison of Theory and Experiment. *To be submitted to Energy & Fuels*.

to that for the particle to pass by the surface. If Tp < 1 the particle is captured; otherwise it escapes. It is assumed that only those particles in the submicron vaporization mode are both subject to thermophoresis and will stick to the surface. Equilibrium calculations showed that the ash aerosol in the vaporization mode had condensed just upstream of the thermal boundary layer next to the cold surface and later calculations showed that additional ultrafines condensed within the thermal boundary layer had insufficient mass to account for the deposition rates measured. Using calculated velocity and temperature fields in the fluid next to the vertical surface, and the Tp < 1 criterion alluded to above, it was possible to calculate a two-dimensional cross-sectional area that defined the area through which all particles that will contact the vertical surface must pass. Ash deposition rates so calculated were compared to experimental data. Quantitative agreement between theory and experiment was good, considering the difficulties in accurately measuring deposition rates and in view of simplifications contained in the model.

6.2 Introduction

Pulverized coal combustion will still be one of the most important power supplies worldwide, even though some alternative energy sources have started growing in recent decades [1]. This situation, however, requires the development of clean coal technology as well as reducing the cost. Ash deposition on heat exchanger surface during coal combustion has been a problematic issue that affects heat transfer efficiency, decreases the lifetime of the boiler tubes and reduces plant profit since the utilization of coal [2]. Therefore, it is essential to have a comprehensive understanding of ash deposition in coal combustion to help develop technology avoiding or reducing ash deposition.

There are typically two types of ash deposition, slagging deposition formed at the

radiation section and fouling deposition formed at the convection section of the furnace. Slagging deposition is normally molten and sintered, while fouling deposition is normally dry and porous [3]. As being widely recognized, the formation mechanisms for ash deposition include inertial impaction, chemical reaction, condensation and thermophoresis [4]. The dominant formation mechanism for ash deposition varies with locations within the furnace, because of different flow field, temperature and aerosol particle characteristics.

Inertial impaction is a deposition process by which bulk deposits are transported to the heat exchanger surface by the fluid gas. This process is affected by target geometry, particle size and density, as well as gas flow field [5-8]. Typically, it is important for particles with a size larger than 10 μm [4], because they have sufficient inertia to traverse the gas streamlines and impact onto the heat exchanger surface. The inertial impaction rate is controlled by Stokes number [4], which is defined as the ratio of the characteristic time of a particle to come to rest when injected into a stagnant fluid to a characteristic time of the flow to pass over a distance equal to the tube radius. The impaction rates are normally the highest at the cylinder stagnation point, and are decreasing fast with angular position measured from this stagnation point [4]. However, not all the impacted particles could be captured by the surface because some may bounce off. This is related to capture efficiency, which strongly depends on target geometry, particle size and density, gas flow properties, particle composition and viscosity, as well as deposit surface composition, morphology and viscosity [5-8]. Most of the existing impacting models define the capture efficiency as a function of ash viscosity [9-10], which could be calculated through different methods [11-16]. Condensation is a process in which mineral vapor deposits at a cooler probe surface, which is significant for low rank fuel because they will produce a large amount of condensable materials during combustion [17-19]. Deposits formed through condensation

have a profound influence in the bulk strength and thermal conductivity, as well as capture efficiency, for inertially impacted particles. Chemical reaction is another principal mechanism for accumulating deposits from the gas phase vapor, where the important reactions include sulfation, alkali absorption and oxidation on the tube surface. Thermophoresis is a process of particle transportation due to temperature gradient in the gas where the particle is suspended or the temperature gradient in the particle itself, which is an important formation mechanism for particles with a diameter less than 5 μm [20-24]. However, the role of thermophoresis would be weakened with the accumulation of the deposits, due to the decreasing of the temperature gradient in the thermal boundary layer.

Numerous theoretical studies have been conducted to help predict ash deposition during coal combustion, including traditional indices [25-26] and modern modeling [7,27-42]. The traditional indices are based on chemical composition and fusion temperature of the ash, while the modern modeling considers the fluid dynamics of the ash particles as well. Most of the existing models are developed for the prediction of slagging deposition [7,31,33-34,36,38-41], with an emphasis on inertial impaction and capture efficiency. Very few studies attempt to predict fouling deposition during coal combustion [28-29,32,35], possibly due the complexity of that process. Typically, a thin initial sticky layer of fouling deposits were first formed on heat exchanger surface through condensation, chemical reaction and thermophoresis [3-4]. Then the heat exchanger surface would have the capability of capturing the subsequent impacted particles. The formation of the initial layer deposits, therefore, is an important process in fouling deposits formation. Thermophoresis, an important phenomenon that transports small size particles to the cold surface, plays an important role in initial layer deposits formation [43-45]. Costen et al. [43] developed a three-dimensional CFD model to simulate ash deposition in pulverized coal combustion.

Cases with and without thermophoretic force were tested, and the results showed that thermophoresis had an important impact on finer particle deposition, and thermophoretic force was 5 to 10 times larger than the drag force, depending upon the size of the particle and temperature gradient.

However, there is no such research that investigates ash deposition on a vertical surface both experimentally and theoretically, with a focus on the role of thermophoresis. Previous work [46-47] from this research group has experimentally demonstrated that initial layer deposits mainly consist of vaporization mode ash aerosols transported by thermophoresis from boundary layer to the probe surface. This work is to demonstrate the importance of thermophoresis through both experimental work and theoretical modeling.

6.3 Materials and Methods

6.3.1 Experimental Conditions

Cases of air combustion and oxy-coal combustion with 50% inlet O_2 and 50% once through CO_2 (OXY50) were conducted, firing a Powder River Basin (PRB) coal. The experimental work was conducted on a 100 kW rated pilot-scale down-fired self-sustained oxy-fuel combustor (OFC), which could be operated to have a similar combustion condition as full-scale units in terms of temperatures, particle concentration and mixing. Details about OFC could be found elsewhere [46-47]. Coal feeding rate was 4.54 kg/hour; and excess oxygen in the exhaust was fixed at 3 vol. % in dry basis. Details about PRB coal and combustion conditions can be found elsewhere [46-47]. Although the combustion zone was filled with a turbulent diffusion flame, the flow laminarized downstream, especially at the location where the fouling deposits were collected. The Reynolds number at the fouling deposits collection port was 743 for OXY50 case and 1153 for air

combustion. The flue gas temperatures at the collection port reached the same (1199 K) for both OXY50 and air combustion cases. A novel surface temperature-controlled ash deposition probe system, which allowed us to separate the deposits into inside, outside, vertical and side deposits, was used to collect ash deposits [47]. To investigate the effect of probe surface temperature on ash deposition rate on vertical surface, fouling deposits were collected at three different probe surface temperatures, which were 723 K, 823 K and 923 K. To obtain high quality ash aerosol data, two groups of instruments were utilized: a Berner low pressure impactor (BLPI) and a scanning mobility particle sizer (SMPS) coupled with an aerodynamic particle sizer (APS) [46]. Ash deposition rates on vertical surface from some other combustion conditions are also presented for model demonstration purposes, in which the combustion conditions are explained in the caption of corresponding figure.

6.3.2 Thermophoresis

Thermophoresis is the diffusion of mass caused by temperature gradient. Particles suspended in the gas phase encounter collisions by surrounding gas molecules. Molecules on the high temperature side collide with increased energy, because of higher kinetic energy at the high temperature side compared to that on the low temperature side. Therefore, the mechanically unbalanced particle will move towards the low temperature side when it is placed in an environment with a temperature gradient. The temperature gradient can inherently exist in the gas phase, or it can be produced by the suspended particle itself if its surface temperature is not uniform [27]. The phenomenon of thermophoresis was discovered experimentally in 1870 [48]. The relationship between the flow field of particle and the surrounded gas temperature was first proposed

theoretically by Maxwell [49] and demonstrated experimentally by Reynolds [50]. Those relationships were then further developed and modified by other scientists as summarized by Bakanov [51]. Later, thermophoresis was also considered in the process of ash deposition during coal combustion [4,45].

6.4 Results and Discussion

6.4.1 Ash Aerosol Formation

Particle size distributions (PSD's) of the ash aerosols were obtained by BLPI and SMPS/APS, for both air and OXY50 combustion, as shown in Figure 6.1. It shows four modes: an ultrafine vaporization mode centered at ~0.06 μm, a fine vaporization mode at ~1 μm, a fine fragmentation mode at ~2.5 μm and a coarse fragmentation mode at ~10 μm. The ash aerosol PSD's measured by different technologies (gravimetric for BLPI, electric mobility for SMPS and light scattering for APS) show high consistence, which implies high quality aerosol data. Previous research [46-47] has shown that deposits on a vertical surface are formed by vaporization mode aerosols through thermophoresis. In this work it is assumed that all particles less than 1 μm are subject to thermophoresis. Therefore, the mass fluxes of vaporization mode particles (submicron particles) are used in the theoretical modeling discussed below. The fractions of submicron size aerosols are $1.82 \pm 0.52\%$ and $2.68 \pm 0.30\%$ of the input coal ash for air and OXY50 combustion, respectively.

Particles subject to thermophoresis may be formed by nucleation outside the thermal boundary next to the heat transfer surface, or within that thermal boundary layer. To address this issue, multicomponent equilibrium calculations were performed using HSC software. Mineral equilibrium was calculated on HSC, as shown in Figure 6.2, which only shows the abundant species of solid and gas phase minerals. The results showed that, at the

deposit collection location (flue gas temperature is 1199 K), the concentrations of the mineral species in vapor phase are ignorable compared to those of minerals in solid phase, implying that most of the ash aerosols in the vaporization mode had condensed upstream of the thermal boundary layer next to the cold surface. In addition, based on the concentrations of mineral species in vapor phase provided by HSC, and the concentration of the ultrafine vaporization mode aerosols measured by SMPS/APS, which is typically formed from nucleation of the mineral vapor, the additional ultrafines condensed within the thermal boundary layer had insufficient mass to account for the deposition rates measured.

6.4.2 Definition of Thermophoresis Number

According to previous research [46-47], the formation mechanism of ash deposition on vertical surface is vaporization mode particles (~1 μm) transported by thermophoresis, where temperature gradient is the key driving force and happens merely within an area extremely close to the vertical surface (within boundary layer). Therefore, that process could be treated as laminar flow passing a plane surface, as illustrated in Figure 6.3. According to HSC mineral equilibrium calculations discussed above, almost all of the ash particles have been formed before arriving at the deposition probe collection location, where the gas temperature is about 1199 K. For a particle to be captured onto the vertical surface, it has to be located within the boundary layer where temperature gradient exists. Then the criterion that whether a particle will be captured by the vertical surface or not is dependent on the ratio of travel time caused by thermophoretic force and drag force, defined as thermophoresis number, Tp, a dimensionless number given in equation (6.1).

$$Tp = \frac{travel\ time\ caused\ by\ thermophoretic\ force}{travel\ time\ caused\ by\ drag\ force} = \frac{\frac{d1}{V_t - V_y}}{\frac{d2}{V_x}} \tag{6.1}$$

where V_x, V_y, V_t are vertical velocity, horizontal velocity and thermophoresis velocity inside of the boundary layer, respectively; average velocities of V_x, V_y and V_t based on the shaded area are used in this work, as shown in Figure 6.3. d1 is the perpendicular distance of the particle to probe surface, and d2 is the tangential distance of the particle to the downstream edge of the surface.

With the integral approach [52], an approximate analytical solution for V_x and V_y could be derived from the boundary layer equations, which are

$$V_x = \left[\frac{3}{2}\frac{y}{\delta} - \frac{1}{2}\left(\frac{y}{\delta}\right)^3\right] * U_\infty \ \ for\ y < \delta \tag{6.2}$$

$$V_y = \left(\frac{3}{4}\frac{y^2}{\delta * x} - \frac{3}{8}\frac{y^4}{\delta^3 * x}\right) * U_\infty \ \ for\ y < \delta \tag{6.3}$$

where U_∞ is the upstream velocity, δ is the thickness of the hydrodynamic boundary layer, which is given as

$$\delta = \frac{4.64x}{\sqrt{Re_x}} \tag{6.4}$$

where $Re_x = \frac{U_\infty x}{\upsilon}$ is Reynolds number.

Equation (6.2) and (6.3) are a proper approximation for a laminar flow close to the plate, especially when $y \ll \delta$. This assumption will be verified afterwards.

A simplified equation for terminal velocity of a particle caused by thermophoresis was derived by Rosenblatt and LaMer [53]. In this work, the average velocity V_t is approximated to be a half of the terminal velocity and is given by equation (6.5).

$$V_t = \frac{K1}{2T}\frac{dT}{dy} \tag{6.5}$$

where K1 is a constant, which is a function of environmental pressure and particle size [53]. Based on experimental results, K1 is estimated to be 4e-6 for particles in the size range of 0.28 to 1.3 μm at one atmosphere [53]. Effect of the value of K1 on ash deposition rate will be discussed afterwards. T is gas temperature, $\frac{dT}{dy}$ is temperature gradient of the gas surrounding the particle in the y-axis direction.

In this study, the temperature of the vertical surface is controlled at a constant value for each case. Therefore, the Prandtl number here is larger than 0.928, thus it is reasonable to assume that the thermal boundary layer equals the hydrodynamic boundary layer [52]. This work also assumes that the gas temperature beyond the outer border of the boundary layer equals to upstream temperature T_{gas}, the probe surface temperature stays constant at T_{probe} and particle temperature equals the local gas temperature. Therefore, the temperature profile within that thermal boundary layer could be solved as in equation (6.6).

$$T = T_{probe} + \left[\frac{3}{2}\frac{y}{\delta} - \frac{1}{2}\left(\frac{y}{\delta}\right)^3\right] * (T_{gas} - T_{probe}) \tag{6.6}$$

Then the temperature gradient could be derived as in equation (6.7).

$$\frac{dT}{dy} = (\frac{3}{2\delta} - \frac{3y^2}{2\delta^3}) * (T_{gas} - T_{probe}) \quad (6.7)$$

If a particle is assumed to be captured by the probe vertical surface, then the Tp number should be smaller than one. Otherwise the particle will go off downstream. In that way, a two-dimensional capture zone for each chord of the round surface along the flow direction could be calculated; then a three-dimensional capture zone (Cz) could be obtained by integrating the two-dimensional capture zone through all the chords, as shown in Figure 6.4(a) with left, top and front view. Submicron size particles within that zone will be captured onto the probe surface by thermophoresis. That criterion could be written as in equation (6.8).

$$Cz = f(x, z) \rightarrow Tp < 1 \quad (6.8)$$

If you project the capture zone Cz onto the y-z coordinate plane, then a two-dimensional deposition region (S) could be obtained, as shown in Figure 6.4(b). The two-dimensional deposition region is perpendicular to the flow, through which any submicron size particles flowing will deposit onto the vertical surface.

With this information, the ash deposition rate (dr) on the vertical surface could be predicted by equation (6.9).

$$dr = \dot{q}_{PM1} * \frac{S}{S_{OFC}} * \frac{1}{S_{probe}} * \eta_c \tag{6.9}$$

where S, S_{OFC} and S_{probe} are the area of two-dimensional deposition region, OFC cross section at sampling location and probe vertical surface, respectively. $\dot{q}_{PM1}$ is the mass flux of the submicron ash particles, which is measured experimentally by SMPS/APS and BLPI. η_c is capture efficiency of the impacted particles, which is assumed to be one for submicron particles. This is reasonable because the submicron particles are normally formed through vaporization-condensation process, through which a sticky outer layer would form on a particle [54]. In addition, the submicron size particles are too light to have excess kinetic energy to bounce off.

6.4.3 Ash Deposition Rate on Vertical Surface

The ash deposition rates from both prediction and experiments are shown in Figure 6.5, which investigates the effect of probe surface temperature and combustion conditions on ash deposition on vertical surface. The results show that ash deposition rate on vertical surface increases linearly as temperature difference between gas and probe surface increases, and OXY50 case has a higher deposition rate comparing to that of AIR case. The predicted ash deposition rates agree reasonably well with experimental data, which implies a well-interpreted formation mechanism and a well-proposed deposition model.

The difference of the ash deposition rate between prediction and experiments is most possibly due to the chosen of value of the constant K1. It is widely recognized that terminal velocity of particles caused by thermophoresis is proportional to $\frac{1}{\mathrm{T}}\frac{dT}{dy}$. However, the definition of the coefficient before this part differs among existing research [53,55-56].

Hettner's [55] formula shows that the coefficient is a function of viscosity and density of gas, as shown in equation (6.10), while Waldmann [56] suggests that the coefficient is related to thermal conductivity of gas and particle, as well as density and viscosity of gas, as shown in equation (6.11). In this work, a value of 4e-6 is chosen for the coefficient K1, which is measured experimentally and is said to be a function of pressure and particle size by Philip [53]. Ash deposition rates on vertical surface were also calculated under different values of K1. As shown in Figure 6.5, the predicted ash deposition rates increased for both cases when increasing the value of K1. For case of various probe surface temperature, the slopes of the predicted lines also increased when increasing K1. To further evaluate the effect of the coefficient K1 on ash deposition rate on vertical surface, the slope of predicted ash deposition rates under different value of K1 are shown in Figure 6.6. It shows that the slope of the predicted ash deposition rate increases with increasing of K1. Therefore, to improve the precision of this model, it is essential to find out the best value of K1.

$$\mathrm{Vt} = \frac{3\eta\Gamma_{\mathrm{i}}}{4\gamma_g T} \tag{6.10}$$

where γ_g is density of gas, η is viscosity of gas, Γ_{i} is temperature gradient inside of the particle, T is temperature [55].

$$\mathrm{Vt} = -\frac{3\chi_{\mathrm{a}}\eta\Gamma_a}{2(2\chi_{\mathrm{a}} + \chi_i)\gamma_g T} \tag{6.11}$$

where γ_g is density of gas, η is viscosity of gas, χ_{a} is thermal conductivity of gas, χ_i is

thermal conductivity of particle, Γ_a is temperature gradient in gas phase, T is temperature [56].

For the cases of varying probe surface temperature, the area of the two-dimensional deposition region is the only variable that made the difference of deposition rate. For the cases of AIR and OXY50, both the area of the two-dimensional deposition region and the concentration of the submicron size ash aerosol will contribute to the ash deposition rate. The deposition regions for all cases are shown in Figure 6.7. It shows that the area of the two-dimensional deposition region increases as the difference of gas-probe temperature increases. The AIR case has a smallest ash deposition region, which is because of shorter travel time caused by drag force due to higher gas velocity comparing to OXY50 case. However, lower concentration of the submicron size ash aerosol is another equally important reason that reduces the ash deposition rate in AIR case, as shown in the previous section that the fraction of submicron size aerosols is 1.82±0.52% of the input coal ash for air combustion, while 2.68±0.30% for OXY50 combustion.

The analytical solution of the flow field near the plate is a critical step in this model, which is well valid if $y \ll \delta$. To verify this, y/δ as a function of probe diameter for all the cases are plotted in Figure 6.8. It shows that y/δ is always smaller than 0.1; for most of the locations, it is smaller than 0.06, which is small enough so that the near plate assumption is reasonable.

To further demonstrate this model, prediction of ash deposition rates on vertical surface for some other combustion conditions are also calculated, with a comparison to experimental data, as shown in Figure 6.9. The modeling is calculated under three different values of K1. The combustion cases includes three different coals (PRB, Illinois and blend) and various combustion conditions (both air and oxy-coal combustion with various

recycled flue gas options), as shown in Table 6.1. Considering the difficulties in measuring ash deposition rates, the predicted ash deposition rates agree well with data from experiments, especially when K1 equals to 4e-5. However, there are relatively big gaps for case 12 and 13 (filled points in Figure 6.9 (b)), in which the coals are different from the other cases. Different coals imply different properties of the aerosols, which suggests that the value of K1 might be related to the properties of aerosol particles.

6.5 Conclusions

To investigate ash deposition on vertical surface during coal combustion, experiments were conducted on a 100 kW rated down-fired self-sustained combustor. Data of the ash aerosol PSD's and deposition rates on the vertical surface were obtained from experiments for various combustion conditions. A model was also developed to predict ash deposition rate on vertical surface within a laminar flow field. A dimensionless number, Thermophoresis number (Tp), was defined, which is the ratio of travel time caused by thermophoresis force and travel time caused by drag force. The criterion that a particle will be captured onto the vertical surface is $Tp < 1$. Based on this criterion, a three-dimensional capture zone and a two-dimensional deposition region, in which particles will be captured onto the vertical surface, were calculated. The predicted ash deposition rates showed high consistence with the experimental data. That is, ash deposition rates on vertical surface increased linearly as the gas-probe temperature difference increased. This is because the area of the deposition region increased as the difference of gas-probe temperature increased. Comparing to air combustion, a larger area of deposition region and a higher concentration of submicron size ash aerosols in OXY50 case contributed equally to the higher deposition rate on vertical surface of OXY50 case.

6.6 References

[1] IEA. *Energy Technology Perspectives 2010*, 2010.

[2] Raask, E. *Mineral Impurities in Coal Combustion: Behavior, Problems, and Remedial Measures*; Hemisphere Publishing Corporation: New York, 1985.

[3] Bryers, R. W. *Progress in Energy and Combustion Science* **1996**, *22*, 29-120.

[4] Baxter, L. L. *Ash Deposit Formation and Deposit Properties: A Comprehensive Summary of Research Conducted at Sandia's Combustion Research Facility*, 2000.

[5] Smouse, S. M.; Wagoner, C. L. In *Conference on Inorganic Transformations and Ash Deposition During Combustion* Palm Coast, Florida, ASME, 1991.

[6] Srinivasachar, S.; Helble, J. J.; Boni, A. A. *Symposium (International) on Combustion* **1991**, *23*, 1305-1312.

[7] Srinivasachar, S.; Senior, C. L.; Helble, J. J.; Moore, J. W. *Symposium (International) on Combustion* **1992**, *24*, 1179-1187.

[8] Wagoner, C. L.; Yan, X. X. In *Conference on Inorganic Transformations and Ash Deposition During Combustion* Palm Coast, Florida, ASME, 1991.

[9] Huang, L. Y.; Norman, J. S.; Pourkashanian, M.; Williams, A. *Fuel* **1996**, *75*, 271-279.

[10] Walsh, P. M.; Sayre, A. N.; Loehden, D. O.; Monroe, L. S.; Beér, J. M.; Sarofim, A. F. *Progress in Energy and Combustion Science* **1990**, *16*, 327-345.

[11] Browning, G. J.; Bryant, G. W.; Hurst, H. J.; Lucas, J. A.; Wall, T. F. *Energy & Fuels* **2003**, *17*, 731-737.

[12] Vorres, K. S.; Greenberg, S. A. *Viscosity of Synthetic and Natural Coal Slags*; Argonne National Laboratory, 1984.

[13] Kalmanovitch, D. P.; Frank, M. *An Effective Model of Viscosity for Ash Deposition Phenomena*; New York: United Engineering Trustees, Inc. , 1988.

[14] Streeter, R. C.; Diehl, E. K.; Schobert, H. H. In *The Chemistry of Low-Rank Coals* Washington, USA, 1984.

[15] Urbain, G.; Cambier, F.; Deletter, M.; Anseau, M. R. *Transactions and Journal of the British Ceramic Society* **1981**, *80*, 139-141.

[16] Watt, J. D.; Fereday, F. *Journal Institute Fuel* **1969**, *42*, 99-103.

[17] Castillo, J. L.; Mackowski, D. W.; Rosner, D. E. *Progress in Energy and Combustion Science* **1990**, *16*, 253-260.

[18] Helble, J.; Neville, M.; Sarofim, A. F. *Symposium (International) on Combustion* **1988**, *21*, 411-417.

[19] Rosner, D. E.; Nagarajan, R. *Chemical Engineering Science* **1985**, *40*, 177-186.

[20] Beck, J. V.; Murio, D. A. *AIAA Journal* **1986**, *24*, 172-179.

[21] Byers, R. L.; Calvert, S. *Industrial & Engineering Chemistry Fundamentals* **1969**, *8*, 646-655.

[22] Fuchs, N. A. *The Mechanics of Aerosols*; Oxford: Pergamon Press, 1964.

[23] Gokoglu, S. A.; Rosner, D. E. *Industrial & Engineering Chemistry Fundamentals* **1985**, *24*, 208-214.

[24] GökoĞlu, S. A.; Rosner, D. E. *International Journal of Heat and Mass Transfer* **1984**, *27*, 639-646.

[25] Benson, S. A. *Inorganic Transformations and Ash Deposition during Combustion;* Engineering Foundation Press: New York, 1992.

[26] Couch, G. *Understanding Slagging and Fouling in pf Combustion*; IEA Coal Research: London, 1994.

[27] Baxter, L. L.; DeSollar, R. W. *Fuel* **1993**, *72*, 1411-1418.

[28] Beer, J. M.; Sarofim, A. F.; Barta, L. E. *From Coal Mineral Matter Properties to Fly Ash Deposition Tendencies: A Modeling Route*; Engineering Foundation Press: New York, 1992.

[29] Benson, S. A.; Hurley, J. P.; Zygarlicke, C. J.; Steadman, E. N.; Erickson, T. A. *Energy & Fuels* **1993**, *7*, 746-754.

[30] Bryers, R. W.; Harding, N. S. *Coal-blending and Switching of Low-sulfur Western Coals;* Engineering Foundation Press: New York, 1994.

[31] Degereji, M.; Ingham, D.; Ma, L.; Pourkashanian, M.; Williams, A. *Fuel* **2012**, *101*, 171-178.

[32] Erickson, T.; Allan, S.; McCollor, D.; Hurley, J.; Srinivasachar, S.; Kang, S.; Baker, J.; Morgan, M.; Johnson, S.; Borio, R. *Fuel Processing Technology* **1995**, *44*, 155-171.

[33] Fan, J.; Zha, X.; Sun, P.; Cen, K. *Fuel* **2001**, *80*, 645-654.

[34] Garba, M.; Ingham, D.; Ma, L.; Degereji, M.; Pourkashanian, M.; Williams, A. *Fuel* **2013**, *113*, 863-872.

[35] Lee, B. E.; Fletcher, C. A.; Shin, S. H.; Kwon, S. B. *Fuel* **2002**, *81*, 2001-2008.

[36] Lee, F.; Lockwood, F. *Progress in Energy and Combustion Science* **1999**, *25*, 117-132.

[37] Losurdo, M.; Spliethoff, H.; Kiel, J. *Fuel* **2012**, *102*, 145-155.

[38] Mueller, C.; Selenius, M.; Theis, M.; Skrifvars, B. J.; Backman, R.; Hupa, M.; Tran, H. *Proceedings of the Combustion Institute* **2005**, *30*, 2991-2998.

[39] Rushdi, A.; Gupta, R.; Sharma, A.; Holcombe, D. *Fuel* **2005**, *84*, 1246-1258.

[40] Wang, H.; Harb, J. N. *Progress in Energy and Combustion Science* **1997**, *23*, 267-282.

[41] Wang, X.; Zhao, D.; He, L.; Jiang, L.; He, Q.; Chen, Y. *Combustion and Flame* **2007**, *149*, 249-260.

[42] Williamson, J. *The Impact Of Ash Deposition On Coal Fired Plants;* Engineering Foundation Press: New York, 1994.

[43] Costen, P. G.; Lockwood, F. C.; Siddique, M. M. *Proceedings of the Combustion Institute* **2000**, *28*, 2243-2250.

[44] Khodier, A. H. *Co-firing Fossil Fuels and Biomass: Combustion, Deposition and Modelling*. Cranfield University, 2011.

[45] Li, B. *Modeling of Fireside Deposit Formation in Two Industrial Furnaces.* Abo Akademi University, 2013.

[46] Zhan, Z.; Fry, A.; Zhang, Y.; Wendt, J. O. L. *Proceedings of the Combustion Institute* **2015**, *35*, 2373-2380.

[47] Zhan, Z.; Bool, L. E.; Fry, A.; Fan, W.; Xu, M.; Yu, D.; Wendt, J. O. L. *Energy & Fuels* **2014**, *28*, 146-154.

[48] Tyndall, J. *Journal and Proceedings of the Royal Institute of Chemistry of Great Britain and Ireland* **1870**, 189-199.

[49] Maxwell, J. C. *Philosophical Transactions of the Royal Society of London* **1879**, 170-231.

[50] Reynolds, O. *Philosophical Transactions of the Royal Society* **1880**, *170*, 727.

[51] Bakanov, S. P. *Soviet Physics Uspekhi* **1992**, *35*, 783.

[52] Thomas, L. C. *Heat Transfer*; Prentice Hall Books: New Jersey, 1993.

[53] Rosenblatt, P.; Lamer, V. K. *Physical Review* **1946**, *70*, 385-395.

[54] Xu, M.; Yu, D.; Yao, H.; Liu, X.; Qiao, Y. *Proceedings of the Combustion Institute*

2011, *33*, 1681-1697.

[55] Hettner, G. *Zeitschrift Fur Physik* **1924**, *27*, 12-22.

[56] Waldmann, L. *Z. Naturforsch* **1959**, *14a*, 589-599.

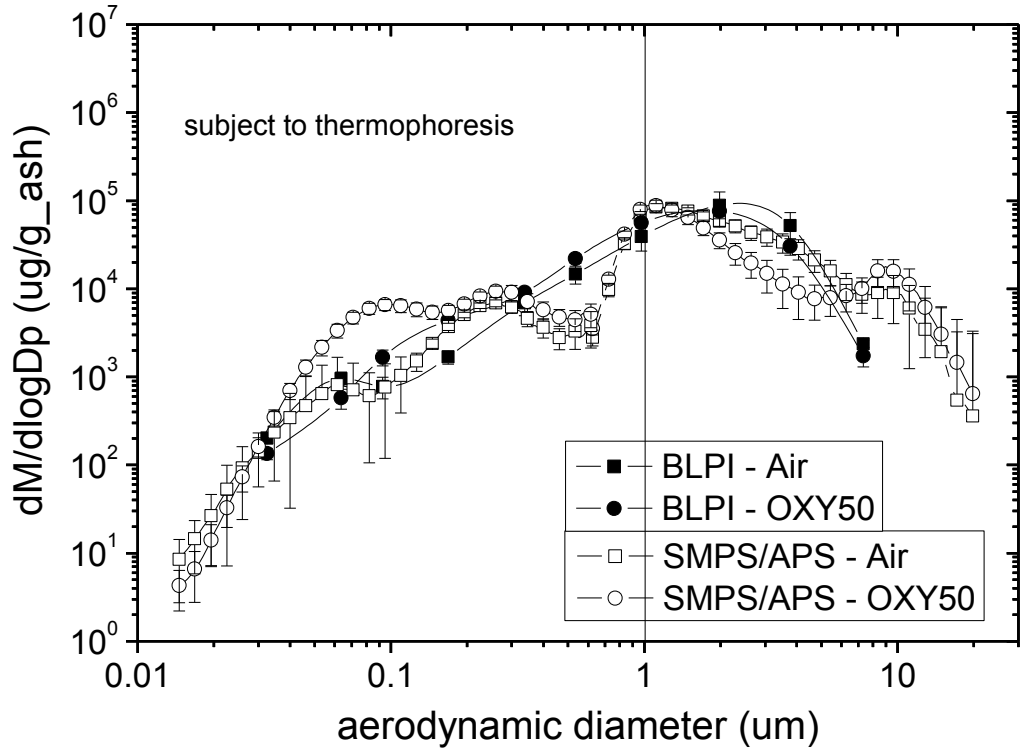

Figure 6.1 Particle size distributions of the ash aerosols for both air and OXY50 combustion conditions.

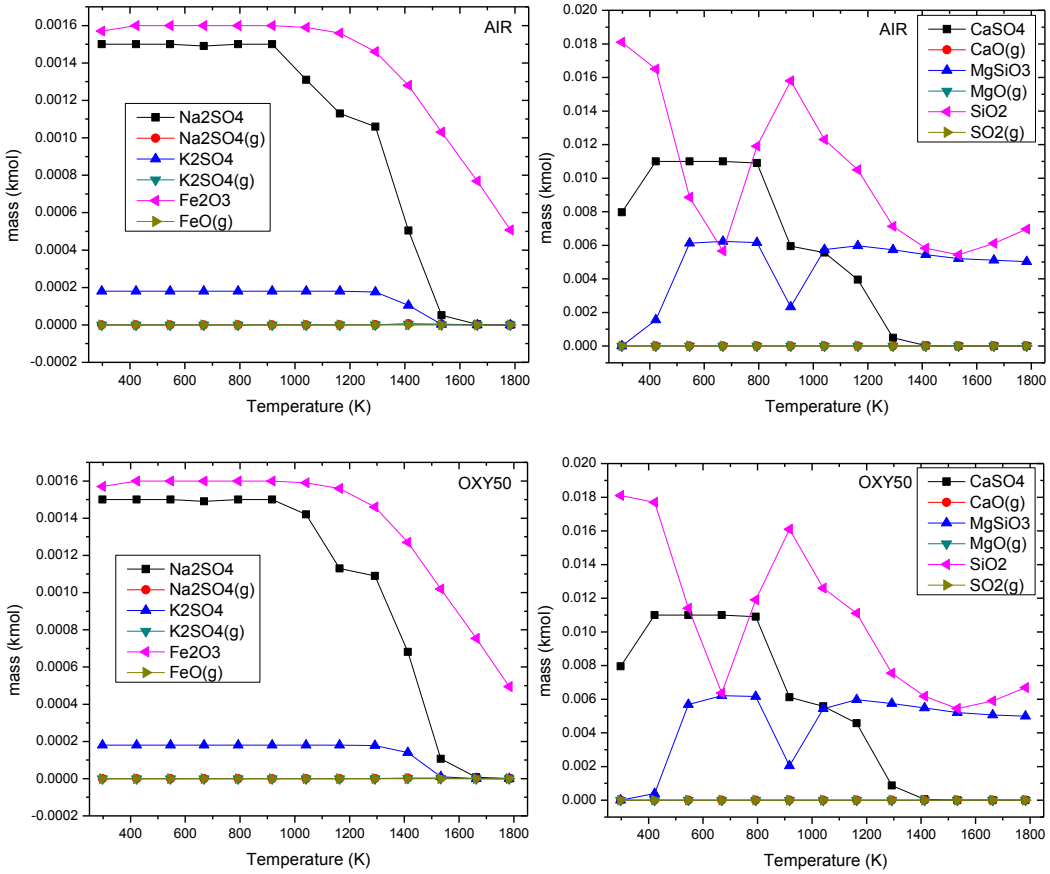

Figure 6.2 HSC equilibrium calculation of the mineral species for both air and OXY50 combustion conditions (only abundant species of solid and gas phase minerals are plotted).

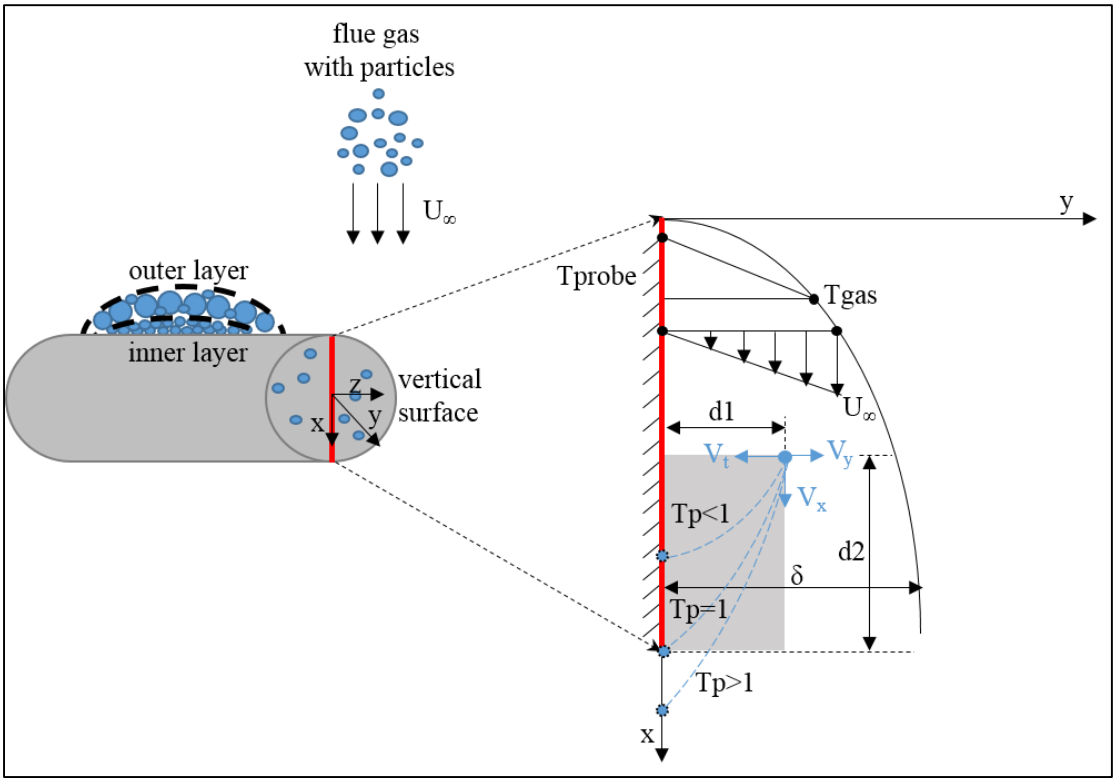

Figure 6.3 Model for ash deposition on vertical surface in a laminar flow.

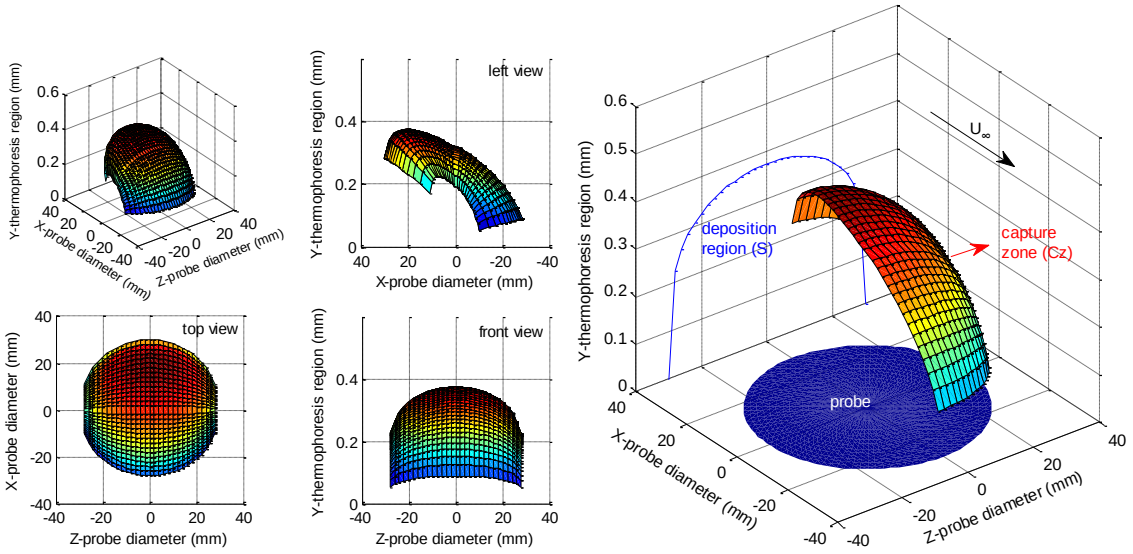

Figure 6.4 Capture zone: (a) Three-dimensional capture zone with left, top and front view; (b) crossing view of the three-dimensional capture zone and two-dimensional deposition region (this is OXY50 case with probe surface temperature at 923 K).

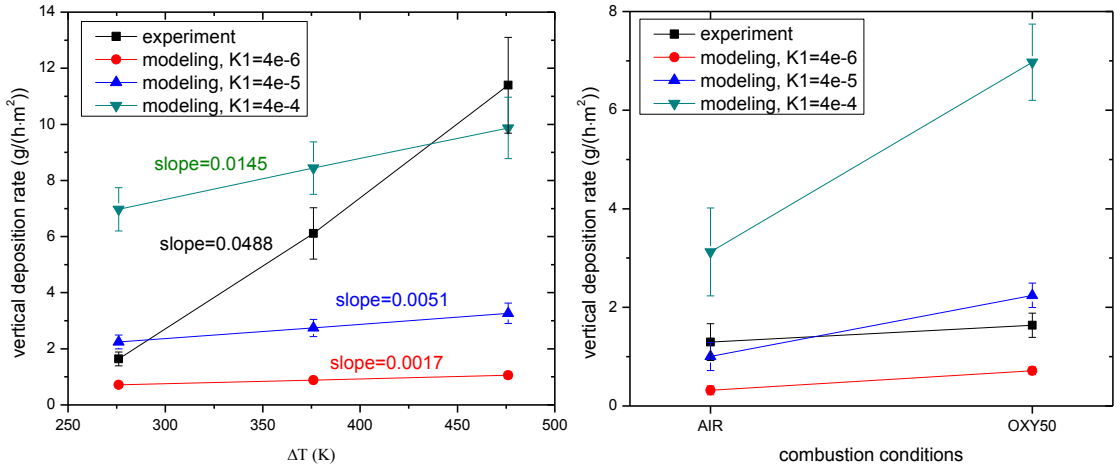

Figure 6.5 Ash deposition rates on vertical surface from both experiment and modeling: (a) effect of probe surface temperature; (b) different combustion condition: AIR and OXY50 (the predictions are calculated under three different values of K1).

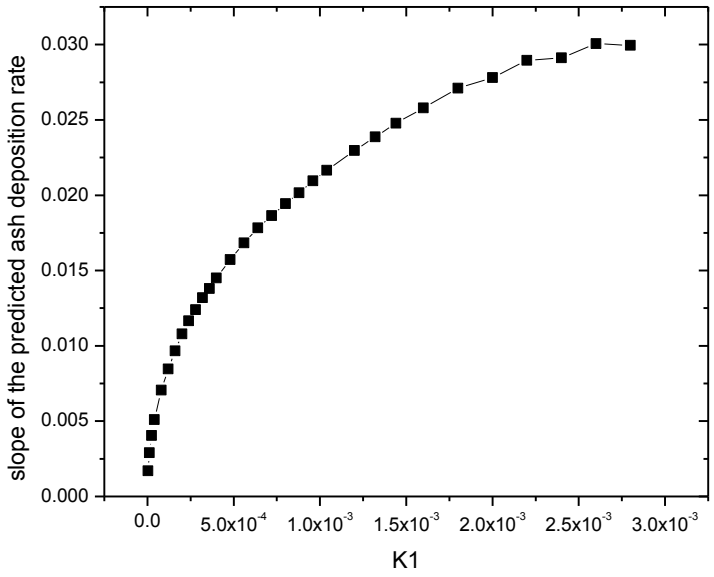

Figure 6.6 Effect of the value of K1 on the slope of ash deposition rate for the various probe surface temperature case.

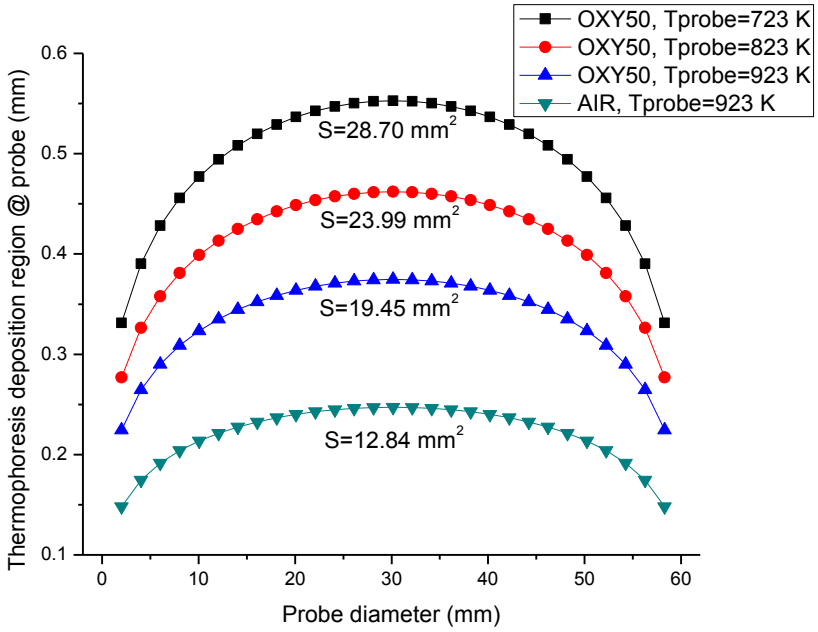

Figure 6.7 Projected two-dimensional deposition region and areas of the deposition region (S).

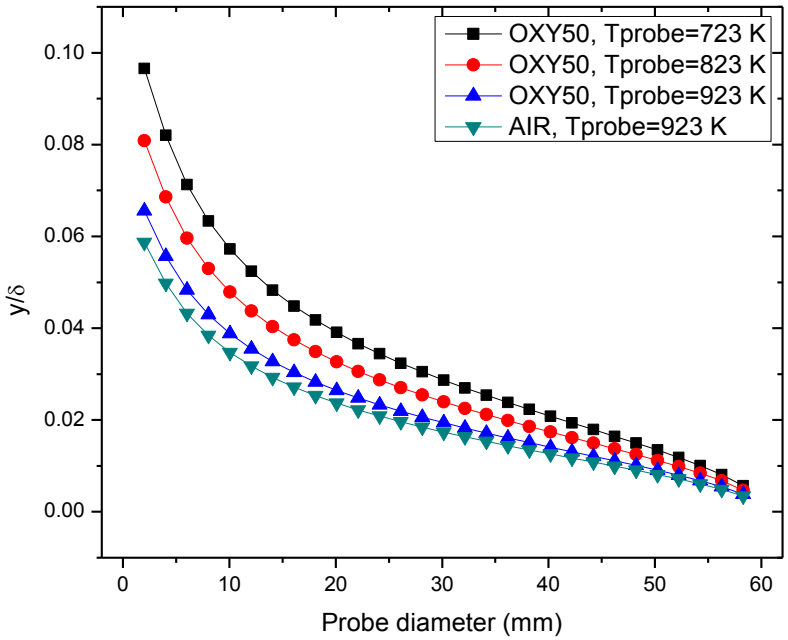

Figure 6.8 Verification for the near plate assumption.

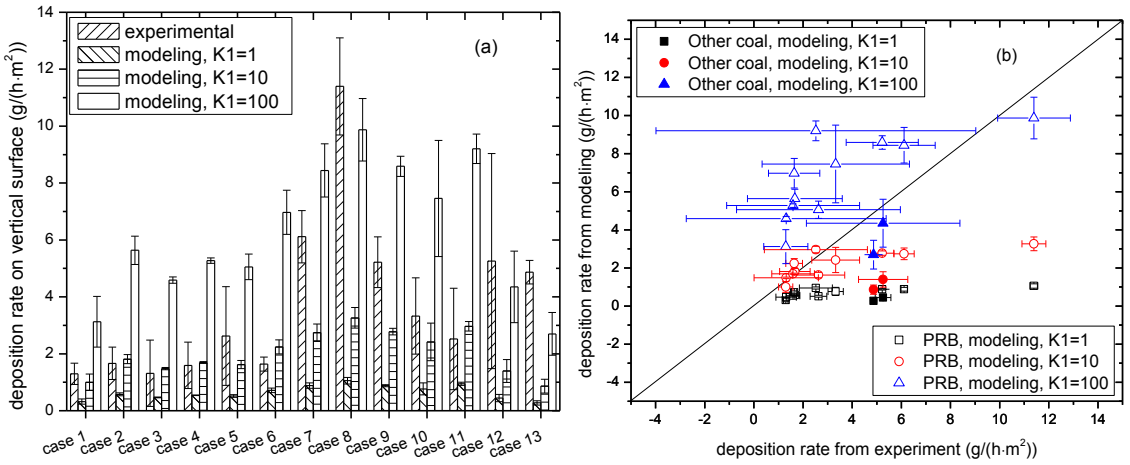

Figure 6.9 Ash deposition rates on vertical surface obtained from experiment and modeling with three different values of K1 under various combustion conditions. The combustion conditions (case 1 to case 13) are listed and interpreted in Table 6.1. Figure (b) differs from figure (a) only in the way it is plotted. The corresponding combustion conditions of the points in figure (b) are the same as in figure (a).

Table 6.1 Case description for Figure 6.9.

	Case description
case 1	air combustion of PRB coal, probe surface temperature is 923 K
case 2	oxy-coal combustion of PRB coal with 27% inlet O_2 and 73% recycled flue gas (denoted as OXY27) with ash removed, probe surface temperature is 923 K
case 3	OXY27with ash and H_2O removed, probe surface temperature is 923 K
case 4	OXY27 with ash, H_2O and S removed, probe surface temperature is 923 K
case 5	OXY27 with nothing removed, probe surface temperature is 923 K
case 6	oxy-coal combustion of PRB coal with 50% inlet O_2 and 50% CO_2 (denoted as OXY50 Once), probe surface temperature is 923 K
case 7	OXY50 Once, probe surface temperature is 823 K
case 8	OXY50 Once, probe surface temperature is 723 K
case 9	oxy-coal combustion of PRB coal with 50% inlet O_2 and 50% recycled flue gas (denoted as OXY50) with ash removed, probe surface temperature is 923 K
case 10	OXY50 with ash and H_2O removed, probe surface temperature is 923 K
case 11	OXY50 with ash, H_2O and S removed, probe surface temperature is 923 K
case 12	air combustion of Illinois coal, probe surface temperature is 923 K
case 13	air combustion of Illinois and PRB blended coal, probe surface temperature is 923 K

CHAPTER 7

DISSERTATION CONCLUSIONS AND PROPOSED FUTURE WORK

7.1 Dissertation Conclusions

Research on ash aerosol and ash deposition formation mechanism during oxy-coal combustion was conducted on a 100 kW rated down-fired self-sustained combustor. First, a novel surface temperature controlled ash deposition probe system and deposit sample processing method were developed. These were demonstrated to be a success because they helped identify the importance of treating the deposits separately instead of in bulk. Then, these methods and procedure were applied to OXY50 and air combustion cases, where ash aerosol chemistry was successfully related to that of the initial layer deposits. After that, these methods and procedure were further applied to cases of oxy-coal combustion with various RFG cleanup options and RFG amounts. Finally, a model for predicting ash deposition rate on vertical surface was developed. The detailed conclusions could be summarized as follows.

1) A novel surface temperature controlled ash deposition probe system was developed and used to collect the fouling deposits. To have a better understanding of the formation mechanism of the ash deposition, the deposits on the probe were separated into vertical, side, inside and outside deposits depending on their physical

location. The results showed that deposits from different locations of the probe showed different characteristics in both composition and PSD. Deposits from the vertical and side surfaces were more similar to the inside deposits on the horizontal surface than they were to the bulk deposits. They were rich in sulfur, alkali and alkaline earth metallic species, while depleted in Si and Fe, compared to the outside deposits on the horizontal surface, and consisted chiefly of fine particles. The main formation mechanism for vertical (inside) deposits was thermophoresis because its deposition rate was found to be proportional to the temperature gradient.

2) With the application of this deposit collection system and sample processing method to OXY50 and air combustion, this work found that the inside deposits from OXY50 have higher Si and Fe and lower S and Na for the OXY50 case than for the air combustion case. To reveal the reason behind this, high quality ash aerosol data were obtained by BLPI and SMPS/APS. The results showed that the composition of the inside deposits was consistent with the composition of the vaporization mode aerosol. This implied that the main formation mechanism of the inside (initial) layer deposits is transportation of the vaporization mode ash aerosol through thermophoresis. Therefore, in order to elucidate mechanisms of deposit formation two types of data appear to be useful. First, it is important to separate the early deposits that are bound more tightly to the cooled surface from the bulk deposits. Their composition differs from the bulk deposit and contributes to adhesion mechanisms allowing the bulk deposits to accumulate. Second, one needs the size segregated composition of the ash aerosol, with emphasis on particle sizes in the submicron vaporization mode. It is the fine and ultrafine particles that dominate the early stages of ash deposition.

3) Those methods were then used to identify ash aerosol and ash deposit formation characteristics during oxy-coal combustion under various RFG stream cleanup options and various RFG amounts. Similar ash aerosol PSD between air combustion and oxy-coal combustion implied that the oxy-coal combustion with different RFG cleanup options and RFG amounts may not greatly affect ash aerosol formation mechanism. However, OXY50 cases produced more vaporization mode particles due to higher combustion temperature. OXY27 cases had more S in vaporization mode ash aerosol than OXY50, possibly due to decreased stability of sulfur containing compounds at higher combustion temperature. OXY50 increased the vaporization of Si; this then enhanced the scavenging reaction, diminishing more Na vapor in OXY50 cases. The formed sticky sodium-silicates or sodium-aluminum-silicate could be easily captured as slagging deposition. OXY50 are supposed to have higher S retention in the bulk ash than OXY27.
4) Finally, a model was built to predict ash deposition rate on vertical surface within a laminar flow field to evaluate the role of thermophoresis in ash deposition on vertical surface. A dimensionless number, Thermophoresis number (Tp), was defined, which was the ratio of travel time by thermophoresis force and travel time by drag force. The criterion that a particle would be captured onto the vertical surface was $Tp < 1$. Based on this criterion, a three-dimensional capture zone and a two-dimensional deposition region, in which a particle would be captured onto the vertical surface, were calculated. The predicted ash deposition rates showed high consistence with the experimental data. That was, ash deposition rates on vertical surface increased linearly as gas-probe temperature difference increased, and this was because the deposition region increased while the difference of gas-

probe temperature increased. Compared to air combustion, a larger deposition region and a higher ash aerosol concentration in OXY50 case contributed equally to the higher deposition rate on vertical surface of OXY50 case.

7.2 Suggestions for Future Work

The following suggestions are recommended for continuing research on ash aerosol and ash deposition during oxy-coal combustion:

1) To improve the OFC recycle system. To have a further insight into the effect of oxy-coal combustion with various RFG stream cleanup options on ash aerosol and ash deposition formation, it is essential to have a more precise control on the flue gas stream cleanup process. For example, to investigate the effect of moisture on ash aerosol and ash deposition formation, cases of moisture removed and moisture contained were explored. However, for the moisture removed case, the moisture condenser we used was merely able to decrease the flue gas temperature to about 40 ℃, which was still saturated gas with a vapor concentration of 7.4%. For the moisture contained case, the flue gas temperature was only able to be kept as high as about 60 ℃, with a vapor concentration of 20%. Although there existed a relative difference in vapor concentration for the desired two cases, it would be more helpful if the vapor concentration (flue gas temperature) could be controlled precisely and randomly.
2) To better understand the function of thermophoresis force in transporting ash particles formed during coal combustion. Thermophoresis force is caused by temperature gradient, where gaseous molecules have different kinetic energy at different temperatures. The gaseous molecules on the hot side of the particles push

harder than the molecules on the cold side. Therefore, if an ash particle has high heat conductivity, it will reach homogeneous temperature environment quickly and sustain little thermophoresis force. However, if an ash particle has low heat conductivity, it will not change the temperature field around itself apparently. Therefore, fundamental research is needed to help find out which groups of particles suffer from thermophoresis, that is, what kind of particles have a low heat conductive coefficient.

3) To develop technology for ash aerosol and ash deposition formation control. It is already widely known that both vaporization mode ash aerosol and initial layer deposits are very harmful. Vaporization mode ash aerosol could escape easily from the dust removal system causing an air pollution problem. Initial layer deposits are the essential condition required for deposits growing. Based on the knowledge we gained in this work, ash aerosol and ash deposition are closely related, that is, vaporization mode ash aerosols are the main contributor to initial layer deposits. Therefore, if there is a method capable of controlling the formation of vaporization mode ash aerosols, the deposition problem will also be reduced. The main formation mechanism for vaporization mode ash aerosol is vaporization and condensation, which is greatly affected by combustion temperature and mineral state. Therefore, the recommendation here is to decrease the combustion temperature and/or increase mineral reaction. The method of mineral reaction includes blended fuel combustion (coal-coal, coal-biomass) or combustion with additive.
4) To develop a three-dimensional thermophoresis model and plug into a computational fluid dynamics (CFD) model. This work only developed a two-

dimensional thermophoresis model for a laminar flow field. However, the actual situation is normally three-dimensional turbulent flow. Therefore, a three-dimensional thermophoresis model is necessary to help predict ash deposition rate through thermophoresis.

APPENDIX A

CARBONATION OF FLY ASH AND ASH DEPOSITS DURING OXY-COAL COMBUSTION

A.1 Abstract

Ash formation is always a troublesome problem during coal combustion due to operation, safety, environmental and health issues. In oxy-coal combustion, the CO_2 partial pressure is higher than that in air combustion, and has been hypothesized to enhance the mineral carbonation [1]. In this work, PRB coal was combusted in a 100 kW down-fired Oxy-Fuel Combustor (OFC), under oxy-firing at inlet O_2 concentrations of 50% and 27% and also under air-firing. Deposits and bulk fly ash samples were analyzed by X-ray photoelectron spectroscopy (XPS) for carbonate (CO_3^{2-}) and sulfate (SO_4^{2-}). Theoretical calculations for mineral equilibrium are conducted by HSC. Both theoretical calculations and experimental results show higher carbonation in oxy-coal combustion than in air combustion.

A.2 Objectives

To determine whether oxy-coal combustion enhances CO_3^{2-} formation in bulk fly ash and deposit ash.

A.3 Background

Oxy-coal combustion (95 vol.%) has a higher CO_2 partial pressure than air combustion (17 vol.%), and this might enhance carbonation of mineral matter and, thereby affecting the characterization of either bulk fly ash or deposits or both.

A.4 Theoretical Equilibrium Calculation by HSC

HSC calculations show higher carbonate (Na_2CO_3 and $CaCO_3$) under oxy-coal conditions in the temperature range of 1000-1500 °C (similar combustion temperature as in OFC), as shown in Figure A.1.

A.5 Experimental Results and Discussion

Figure A.2 shows the presence of three types of carbon in the ash sample. One is CO_3 species; the others are organic forms of carbon, e.g., soot, char or even contamination of the sample.

Figure A.3, Figure A.4 and Table A.1 show that carbonates in both bulk fly ash and deposits increase in the order of OXY27>OXY50>Air, this might be because oxy-coal combustion has higher CO_2 partial pressure than air combustion, and the higher combustion temperature in OXY50 case limits the formation of carbonate. Table A.1 also shows significant non-CO_3, non-SO_4 amounts of C and S.

Figure A.4 shows that inside and vertical deposits have a higher CO_3/SO_4 ratio than outside deposits. Since inside and vertical deposits are rich in alkali and alkaline earth metallic species [2], carbonate might be closely related to these species. In addition, bulk ash has the highest CO_3/SO_4 ratio in all combustion conditions, suggesting (surprisingly) that S displaces C in the deposits, rather than the converse.

A.6 Conclusions

Both theoretical calculation and experimental results show higher carbonation in oxy-coal combustion than in air combustion. Inside and vertical deposits have higher carbonation species than outside deposits. Bulk ash has higher carbonation species than deposit ash. It is not clear why a large amount of organic carbon exists in the deposit ash. If caused by sample contamination, the reported CO_3/SO_4 data and ensuing conclusions should still have validity.

A.7 References

[1] Maier, J. In Seminar Presented at the University of Utah, Utah, USA, 2010.

[2] Zhan, Z.; Bool, L. E.; Fry, A.; Fan, W.; Xu, M.; Yu, D.; Wendt, J. O. L. *Energy & Fuels* **2014**, *28*, 146-154.

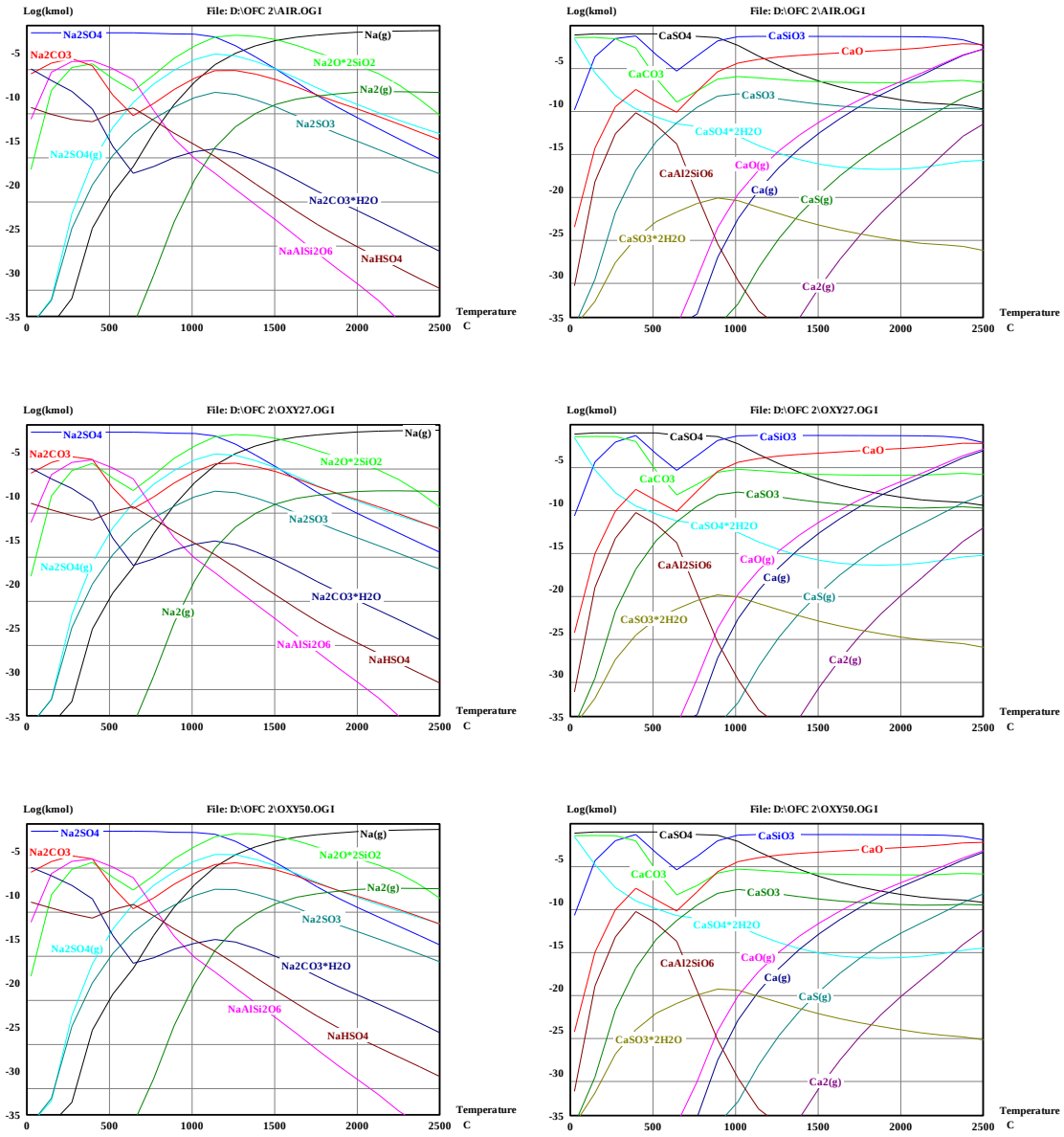

Figure A.1 HSC calculation for Air, OXY27 and OXY50 cases.

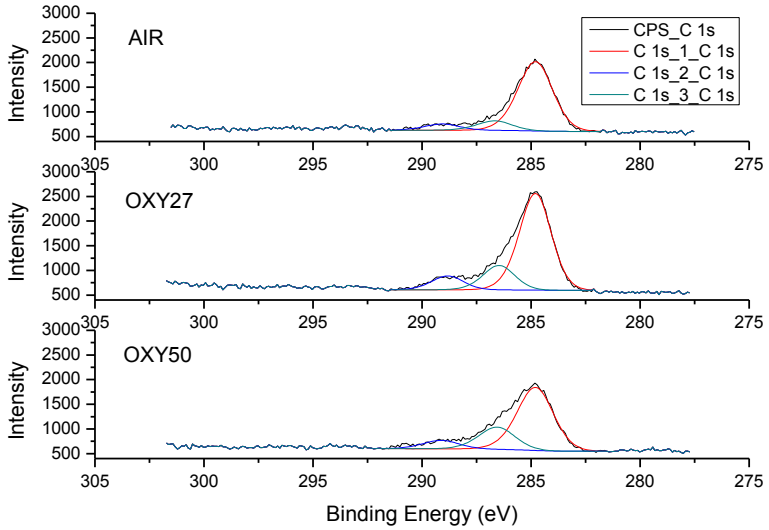

Figure A.2 Representative XPS intensities of carbon related species in bulk ash from different combustion conditions (C 1s_1_C 1s refers to CH_2, CH_3 et al species; C 1s_2_C 1s refers to CO_3; C 1s_3_C 1s refers to C=C et al.).

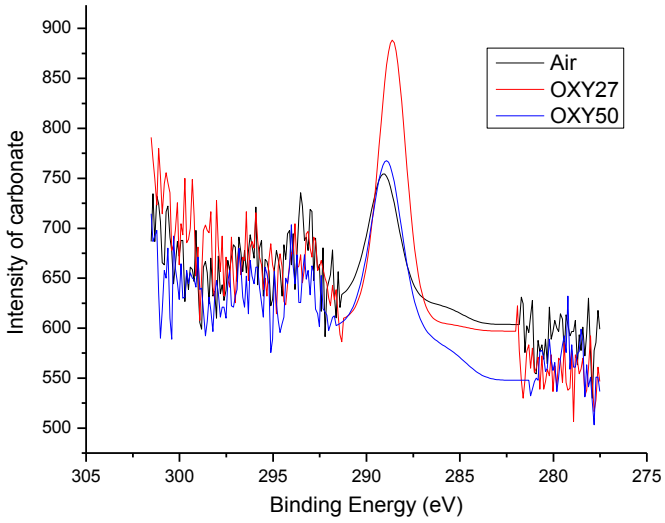

Figure A.3 XPS intensity (subtracted from CO_3 fitting) of carbon in the form of CO_3.

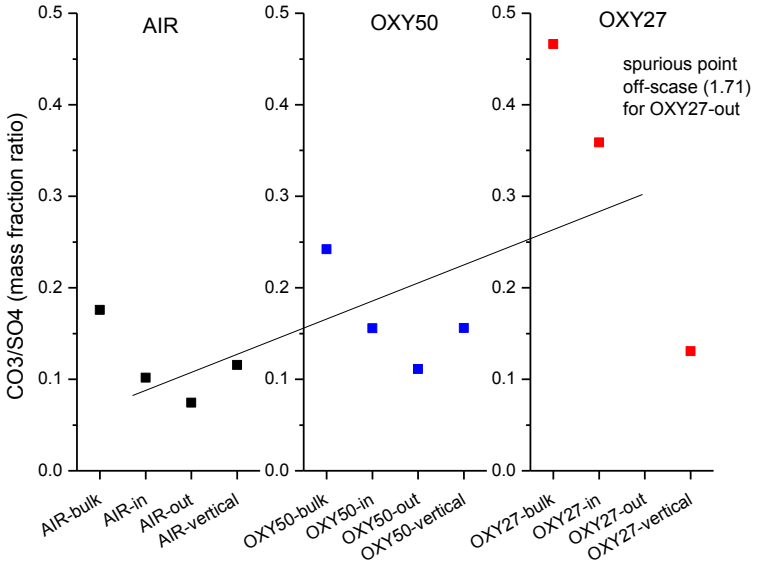

Figure A.4 CO_3/SO_4 of bulk ash and deposits ("in" refers to inside deposits, "out" refers to outside deposits, "vertical" refers to vertical deposits, "bulk" refers to bulk fly ash.).

Table A.1 Mass fraction carbon (sulphur) in the form of CO_3 (SO_4) to all forms of carbon (sulphur).

Case	CO_3 (%)	SO_4 (%)	Case	CO_3 (%)	SO_4 (%)
OXY50-bulk	8.98	66.88	OXY27-outside	8.55	40.02
OXY50-inside	8.15	70.42	OXY27-vertical	6.05	72.13
OXY50-outside	8.52	64.75	AIR-bulk	7.35	75.40
OXY50-vertical	7.99	70.18	AIR-inside	6.96	67.26
OXY27-bulk	10.26	75.67	AIR-outside	3.93	71.83
OXY27-inside	11.6	34.75	AIR-vertical	6.37	69.50

APPENDIX B

DATA OF OXY-COAL COMBUSTION WITH DIRTY RECYCLE

The case of oxy-coal combustion with recycled flue gas of nothing removed (dirty recycle) was also conducted in this research. The results of this case were briefly discussed in Chapter 5 without showing any data. Those data might be a valuable reference for future research in this topic. Therefore, its ash aerosols and deposits data are attached here as an appendix listed as below:

Figure B.1 Particle size distribution of ash aerosols measured by SMPS/APS and BLPI for dirty recycle case: (a) input ash based; (b) value based.

Figure B.2 Elemental compositions of ash aerosols collected by BLPI for dirty recycle case.

Table B.1 Elemental compositions of inside, outside fouling deposits and slagging deposits for dirty recycle case.

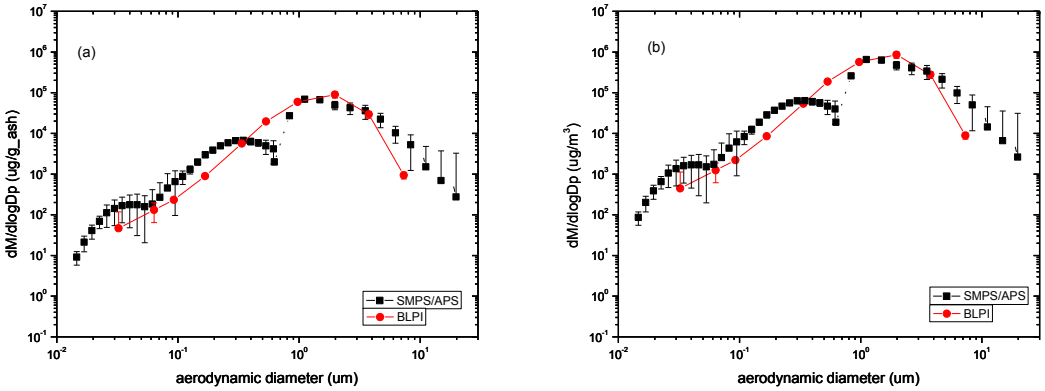

Figure B.1 Particle size distribution of ash aerosols measured by SMPS/APS and BLPI for dirty recycle case: (a) input ash based; (b) value based.

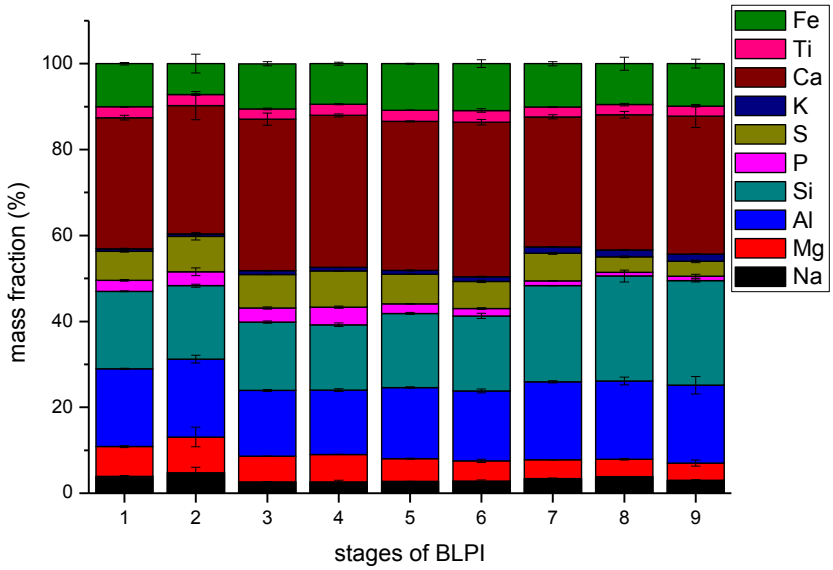

Figure B.2 Elemental compositions of ash aerosols collected by BLPI for dirty recycle case.

Table B.1 Elemental compositions of inside, outside fouling deposits and slagging deposits for dirty recycle case.

Element	Inside deposits (%)		Outside deposits (%)		Slagging deposits (%)	
	average	error bar	average	error bar	average	error bar
Na	2.73	0.24	1.73	0.31	0.93	0.10
Mg	4.23	0.25	4.51	0.10	4.16	0.12
Al	15.84	0.03	13.99	0.18	14.35	0.45
Si	22.00	0.70	18.54	1.20	19.66	0.31
P	0.51	0.22	0.75	0.02	0.66	0.19
S	10.84	0.26	15.65	0.43	9.49	0.07
K	1.26	0.16	0.90	0.04	0.96	0.02
Ca	30.68	0.34	31.72	0.86	34.93	0.20
Ti	2.26	0.02	1.96	0.23	2.13	0.08
Fe	9.62	0.22	10.23	0.28	12.75	0.47

APPENDIX C

ASH DEPOSITION RATES FOR OUTSIDE LAYER DEPOSITS

Ash deposition rates are shown in Figure C.1, for air and oxy-coal combustion cases with different flue gas cleanup options of both 27% and 50% inlet O_2. It can be seen that the deposition rates for total, inside and outside deposits are all higher in OXY50 cases compared to OXY27 and air cases.

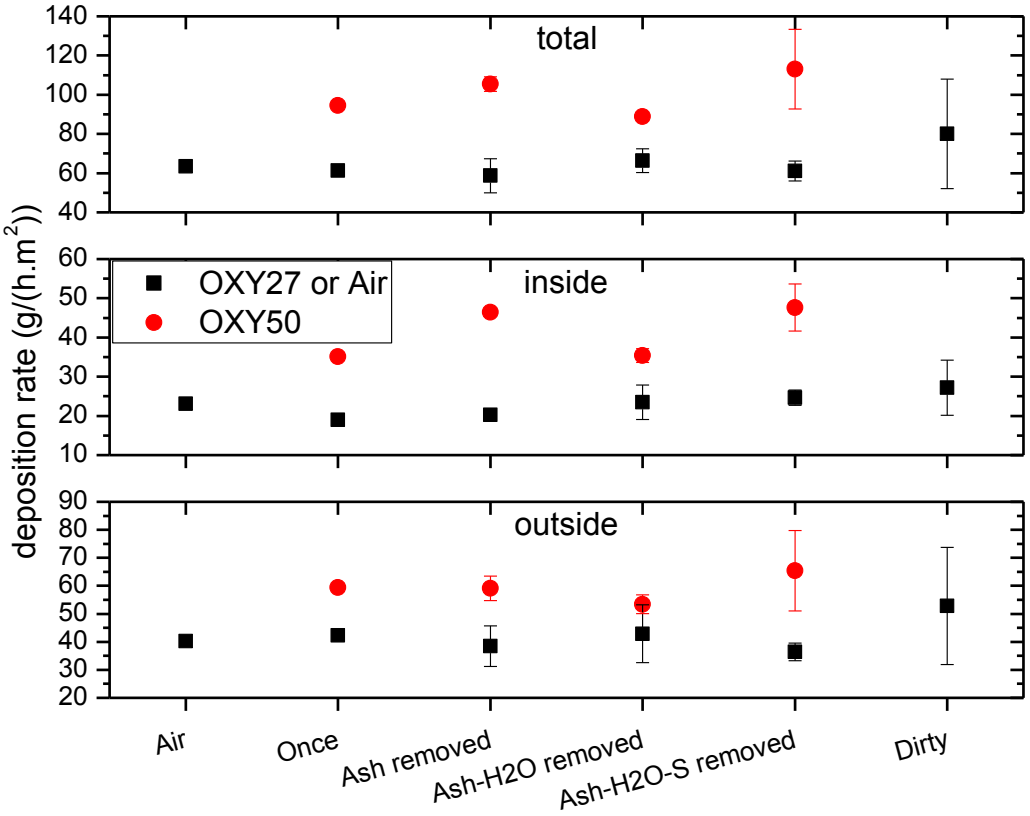

Figure C.1 Ash deposition rates from experiments for total, inside and outside deposits, for air and oxy-coal combustion cases with different flue gas cleanup options of both 27% (OXY27) and 50% (OXY50) inlet O_2. Here the total is the sum of inside and outside deposits.